Philipp A. Schuster, BSc

Characterisation and comparison of process chains for the production of automotive structural parts from EN AW-7xxx aluminium sheets

MASTER THESIS

to be awarded the academic degree

Diplom-Ingenieur (Dipl.-Ing.)

Master program Mechanical Engineering and Business Economics

submitted at

Graz University of Technology

Faculty of Mechanical Engineering and Economic Sciences

Institute of Materials Science, Joining and Forming

Supervisors:
Univ.-Prof. Dipl.-Ing. Dr.techn. Christof Sommitsch
Dr.mont. Josef Domitner

External supervisor:
DI (FH) Georg Kirov MSc, IWE
LKR Leichtmetallkompetenzzentrum Ranshofen GmbH

Graz, December 2017

in cooperation with

LKR Leichtmetallkompetenzzentrum Ranshofen GmbH

Member of AIT Austrian Institute of Technology GmbH
Centre for Low-Emission Transport

Acknowledgement

I want to thank Univ.-Prof. Dipl.-Ing. Dr.techn. Christof Sommitsch and Dr.mont. Josef Domitner for the academic supervision and assessment of this master thesis.

I would further like to express my gratitude to all scientific and workshop staff of LKR Ranshofen GmbH for their help during my thesis time. Special thanks goes to my LKR supervisors Dipl.-Ing. (FH) Georg Kirov MSc, IWE, Dipl.-Ing. (FH) Florian Grabner and Dipl.-Ing. Johannes Österreicher for their competent guidance during the completion of my research tasks.

I would also like to thank Dipl.-Ing. Ermal Mukeli and the CoC Material & Process Engineering department of MAGNA Steyr Fahrzeugtechnik AG & Co KG for their cooperation and support within the project this thesis was conducted in.

Moreover, I want to acknowledge the Austrian Research Promotion Agency (FFG), the Federal Ministry for Transport, Innovation and Technology (BMVIT) and the State of Upper Austria for sponsoring this research in the framework of the COMET project.

Last but not least, big thanks to my family who have supported me financially and mentally during all of my study time.

EIDESSTATTLICHE ERKLÄRUNG

Ich erkläre an Eides statt, dass ich die vorliegende Arbeit selbstständig verfasst, andere als die angegebenen Quellen/Hilfsmittel nicht benutzt und die den benutzten Quellen wörtlich und inhaltlich entnommene Stellen als solche kenntlich gemacht habe.

………………………..   ……..…………………………
(Datum)   (Unterschrift)

STATUTORY DECLARATION

I declare that I have authored this thesis independently, that I have not used other than the declared sources / resources, and that I have explicitly marked all material which has been quoted either literally or by content from the used sources.

………………………..   ……..…………………………
(date)   (signature)

Abstract

Lightweight engineering is a key topic for automotive manufacturers so as to build resource-efficient vehicles. Due to their high specific strength, EN AW-7xxx aluminium alloys are promising materials for reducing the weight of crash-relevant structural parts. Their formability in the as-delivered industrial condition is poor though, so that alternative forming and processing methods are required.

Within this thesis, the hot forming and W-temper forming process chains have been investigated for the AW-7021 and AW-7075 alloys. During hot forming, the sheets are solution heat treated and subsequently formed at elevated temperatures. Quenching is carried out parallel to forming within the cooled dies. During W-temper forming, the sheets are water quenched outside the dies after having conducted the solution heat treatment. They are formed at room temperature in the thermodynamically unstable W state then. For both variants, the formed sheets are eventually stored until being joined and paint baked. Since AW-7xxx aluminium alloys are age-hardenable alloys and do therefore not show stable material properties after forming, it is challenging to introduce stable, standardised post-forming operations. This holds particularly true for mechanical joining operations such as self-pierce riveting. Therefore, this work has also looked into how the conventional hot forming and W-temper process chains can be supplemented by process modifications with regard to an additional stabilisation heat treatment.

The criteria with respect to which the process chains have been characterised and compared are formability, post-forming material properties and energy absorption behaviour on component level. Examination methods involved amongst others tensile testing, hardness testing, differential scanning calorimetry (DSC) experiments, the preparation of rivet cross sections as well as quasi-static crush testing of formed and joined top-hat profiles. Top-hat profiles were also assessed visually regarding their dimensional accuracy after forming and their folding capability after quasi-static compression respectively. The resource efficiency balance of a selected process route was evaluated through the creation of an energy and material flow based process description.

It was found that especially hot forming is suitable to form failure-free parts with good dimensional accuracy for both alloys, AW-7021 and AW-7075. An additional stabilisation heat treatment might not only enhance process stability and could therefore be a suitable lever to facilitate logistics in the automotive industry, it does at the same time also improve the alloys' suitability for being used within crash-relevant structures. Stabilised parts showed slightly higher yield strength values after paint baking and their crushworthiness was ameliorated considerably compared to non-stabilised parts. Altogether, this could help to increase the resource efficiency balance of crash-relevant structural parts, not only in use but also during production.

Kurzfassung

Leichtbau spielt in der Automobilindustrie eine Schlüsselrolle für die Herstellung von ressourcenschonenden Fahrzeugen. Aufgrund ihrer hohen spezifischen Festigkeitswerte sind EN AW-7xxx Aluminiumlegierungen vielsprechende Materialien, um auch bei crashrelevanten Strukturbauteilen eine Gewichtsreduzierung erreichen zu können. Die Umformbarkeit bei Raumtemperatur von AW-7xxx Legierungen im Lieferzustand ist allerdings begrenzt. Aus diesem Grund wird seit einigen Jahren intensiv an der Entwicklung alternativer Prozess- bzw. Verarbeitungswege geforscht.

Im Rahmen dieser Arbeit wurden die Prozessvarianten "Hot forming" und "W-temper forming" für die beiden Legierungen AW-7021 und AW-7075 untersucht. Beim "Hot forming" werden die umzuformenden Bleche zunächst lösungsgeglüht und unmittelbar anschließend bei erhöhter Temperatur in einem gekühlten Werkzeug umgeformt. Die Prozessschritte Umformen und Abschrecken erfolgen dabei simultan. Beim "W-temper forming" werden die umzuformenden Bleche nach dem Lösungsglühen außerhalb des Werkzeugs mit Wasser abgeschreckt. Die Formgebung erfolgt dann bei Raumtemperatur und sollte ehestmöglich stattfinden, da der sogenannte W-Zustand nach dem Abschrecken ein thermodynamisch instabiler Zustand ist. Nach dem Umformen werden die Bleche bei beiden Prozessvarianten für einen bestimmten Zeitraum gelagert, bevor sie schließlich gefügt und im Rahmen der Lackaushärtung nochmals wärmebehandelt werden. Da AW-7xxx Legierungen aushärtbare Legierungen sind und ihre Materialeigenschaften nach dem Umformschritt somit nicht stabil sind, ist es oft schwierig, standardisierte Nachbearbeitungsprozesse festzulegen. Dies trifft insbesondere auf das mechanische Fügen, beispielsweise durch Stanznieten, zu. Daher wurde im Rahmen dieser Arbeit auch untersucht, inwiefern Prozessvarianten wie "Hot forming" und "W-temper forming" durch Prozessmodifikationen im Hinblick auf eine zusätzliche Stabilisierungswärmebehandlung ergänzt werden können.

Die Beurteilungskriterien, die für die Charakterisierung und den Vergleich der verschiedenen Prozessketten verwendet wurden, sind Umformbarkeit, Entwicklung der Materialeigenschaften nach dem Umformen sowie Energieabsorptionsvermögen auf Bauteilebene. Für die Untersuchungen wurden unter anderem Zugprüfungen, Härtemessungen, dynamische Differenzkalorimetrie (DSC) Messungen sowie Schliffbilder von Nietverbindungen als auch quasistatische Stauchversuche von Demonstratorbauteilen herangezogen. Die Form- und Maßhaltigkeit nach dem Umformen sowie das Faltenbildungsvermögen von Versuchsbauteilen nach dem Stauchen wurden durch optischen Vergleich beurteilt. Darüber hinaus wurde eine ausgewählte Prozesskette im Hinblick auf ihre Ressourceneffizienz durch die Erstellung einer Energie- und Stoffstrom basierten Prozessbeschreibung bewertet.

Ein zentrales Ergebnis der Untersuchungen ist, dass sich besonders die Prozessvariante "Hot forming" zur Herstellung von fehlerfreien Bauteilen mit hoher

Form- und Maßhaltigkeit eignet. Das gilt sowohl für die AW-7021 Legierung als auch für die AW-7075 Legierung. Eine zusätzliche Stabilisierungswärmebehandlung könnte nicht nur ein geeigneter Ansatz sein, um die Prozessstabilität zu erhöhen und dadurch die Logistik im Bereich der automotiven Blechumformung zu vereinfachen, sie verbessert auch aus sicherheitstechnischer Sicht das Einsatzpotential von AW-7xxx Legierungen für crashrelevante Strukturbauteile. So wurde festgestellt, dass stabilisierte Bauteile erhöhte Streckgrenzwerte gegenüber unstabilisierten Bauteilen aufweisen und unter anderem dadurch auch deren Energieabsorptionsvermögen im Stauchversuch steigt. Insgesamt ist aus den Ergebnissen zu erwarten, dass AW-7xxx Legierungen zu einer Verbesserung der Resourceneffizienz von crashrelevanten Strukturbauteilen beitragen können. Besonders für stabilisierte Bauteile trifft dies nicht nur aufgrund von Gewichtseinsparungen im Fahrzeug zu, sondern auch im Sinne von standardisierten, stabileren Produktionsprozessen bei der Herstellung.

Contents

1   Introduction

Most modern mainstream cars have considerably increased in weight compared to their predecessors. On the one hand side, the demand for better safety features, comfort and performance has led to extra components being installed which significantly boost the weight spiral. On the other hand side, more stringent energy-saving and emission standards force carmakers to lower the fuel consumption of their cars. This conflict has pushed development goals in the automotive industry more and more towards using lightweight components in the vehicles.

For decades, aluminium has been an important material when it comes to reducing weight while at the same time maintaining functional integrity. From the beginning of the 70s until today, the aluminium share in new cars has risen from 2.5 kg to approximately 150 kg. Experts project that by 2025, this value could even have risen to 196 kg. Aluminium is commonly used in powertrains, chassis and suspension as well as in the car body [1, 2].
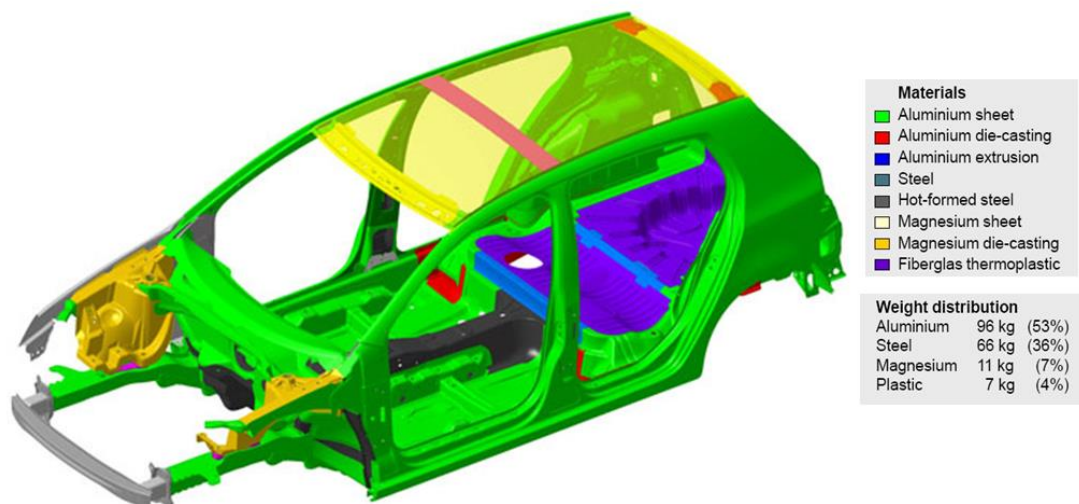
Figure 1-1: *"SuperLIGHT-Car" concept highlighting the importance of aluminium sheets within resource-efficient multi-material approaches* [3]

Especially for the body structure, carmakers increasingly follow a multi-material approach nowadays. This means choosing the right material for every component with respect to end use relevant factors like specific weight, energy absorption behaviour, structural integrity or stiffness but also production relevant factors like cost or processability. Aluminium therefore competes with other materials like high-strength steel, magnesium or fibre-reinforced plastics. Nevertheless, with a weight share of 53 %, aluminium still seems to maintain a leading role in "SuperLIGHT-Car" concepts as an EU-funded study has shown in 2009 (cf. Figure 1-1). This project aimed at developing a lightweight prototype of the VW Golf V body structure that would weigh by 30 % less than the conventional body structure. Besides focusing on a multi-material

design technique, an important project target was improving the overall product life cycle so that the developed body structure would also be capable of saving resources before and after use in traffic [3].

Factors why aluminium alloys often prevail against competing materials are amongst others [2]:

- their large strength spectrum,
- their low specific weight,
- their manifold manufacturing and processing possibilities,
- good corrosion resistance,
- a good recycling capability promoting sustainability in production and use.

Common structural parts made from aluminium are, for instance, the front structure, bumpers, floor panels or roof arches. Three principal processing methods can be distinguished for their production: extrusion, casting and sheet metal forming. The investments required when establishing new process chains are relatively low for extrusions. Therefore, low part cost can already be realised using small-scale production. Castings can efficiently be produced in a medium-scale environment. For sheet metal forming contrarily, the initial investment is very high so that low part cost can only be achieved through mass production [2]. Figure 1-2 illustrates these relationships. Since high volumes are very resource-intensive in terms of material and energy, especially for sheet metal forming highest efforts are required during process planning and improvement. Materials science can make a valuable contribution here.
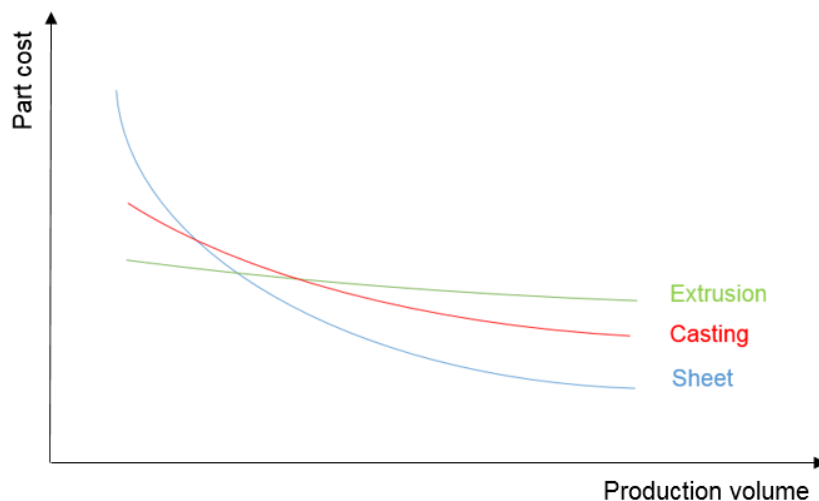
Figure 1-2: *Part cost of different aluminium processing methods as a function of production volume*

Up to now, mostly the medium- to high-strength alloys like the AW-5xxx alloys and the AW-6xxx alloys have been used for aluminium sheet metal forming processes. This is mainly due to their better formability at room temperature. Recently, also high- to ultra-high-strength aluminium alloys of the AW-7xxx series have attracted the interest of automotive manufacturers. As can be seen from Figure 1-3, they are promising candidates for use within crash-relevant structures due to their high specific strength.

However, the formability of these alloys in the as-delivered industrial condition is poor at room temperature, which can amongst others be deduced from their low elongation at fracture values. Therefore, researchers are investigating alternative processing routes for producing quality parts with high- to ultra-high final strength from AW-7xxx alloys. Prior heat treatments and forming at room temperature (retrogression forming, W-temper forming) as well as forming at elevated temperature (warm forming, hot forming) have been proposed as possible process variants to improve formability of AW-7xxx aluminium alloys [4]. Such strategies aim at temporarily lowering strength and increasing ductility of the alloys during the forming operation. A detailed description of the different forming strategies can be found in Section 2.5.
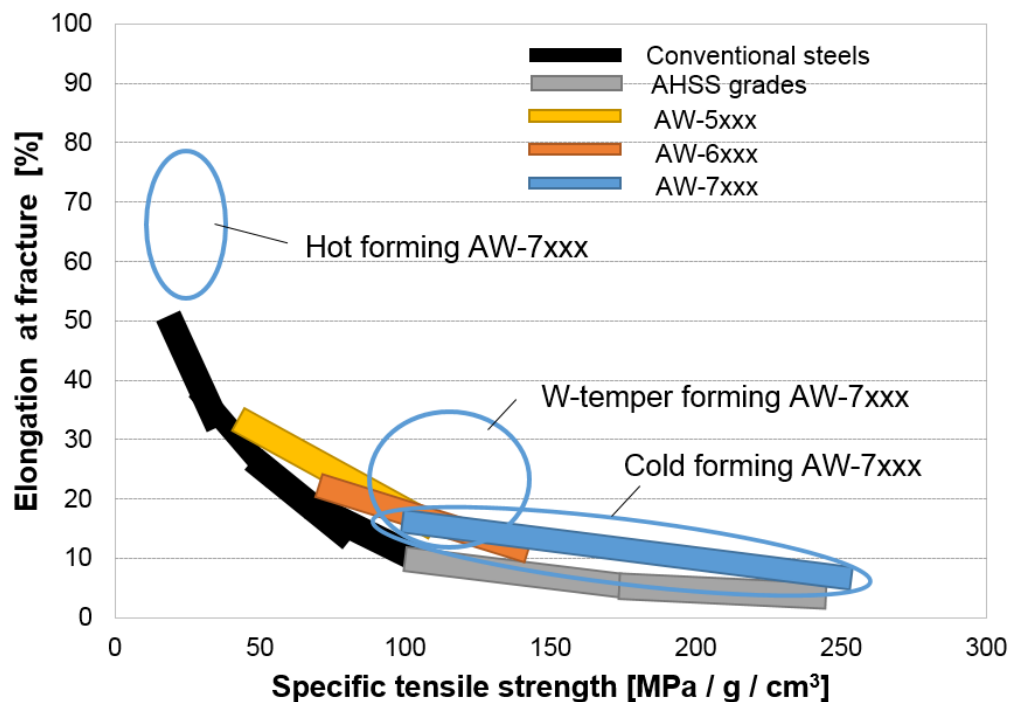
Figure 1-3: *Specific tensile strength plotted against elongation at fracture for different aluminium and steel grades* [5] (*adapted*)

In order to advance with lightweight engineering in mainstream car concepts, investigations into innovative materials, part design and processing technologies are needed. Energy-savings during end use have been the most important driving force for lightweight engineering in the past and will also play an essential role in the future. However, the growing public call for sustainable solutions in a universal sense has shifted priorities to also include resource-efficiency during materials extraction, production and disposal [6]. Due to the predominant use of sheet metal forming technologies in large-scale production environments with high volumes, working sustainably is of vital importance especially for this processing technology. Process chains that produce lightweight parts with excellent final material properties while at the same time not neglecting resource-efficiency during processing must be strived for. Eventually, this two-sided view holds true for process chains potentially suitable for forming structural parts from AW-7xxx aluminium sheets.

2 State of the art

The characterisation of emerging process chains should occur from a broad perspective. The following chapter gives an overview on the theory behind materials and process chains studied within this thesis. Quantitative as well as qualitative methods for the assessment of the process chains will be presented. Directly below, some basic requirements towards automotive structural parts are discussed.

2.1 Automotive structural parts

The body structure is the core element of any car. Requirements towards modern body structures are manifold: They need to be sufficiently rigid so as to support weight, stress and securely tie together all modules and components. They must resist and soften high dynamic loads in crash situations in order to protect passengers. At the same time, they should be as light as possible due to fuel-efficiency and performance reasons. Often, it is difficult to meet all these requirements equally well when developing a new body structure. Multi-material design approaches and lightweight engineering are important means of finding reasonable trade-offs. Besides simple material substitution, these techniques increasingly focus on finding improved solutions in terms of alternative design or fabrication methods [7]. Figure 2-1 exemplarily shows common structural parts within a multi-material body of a modern, mass-produced car.
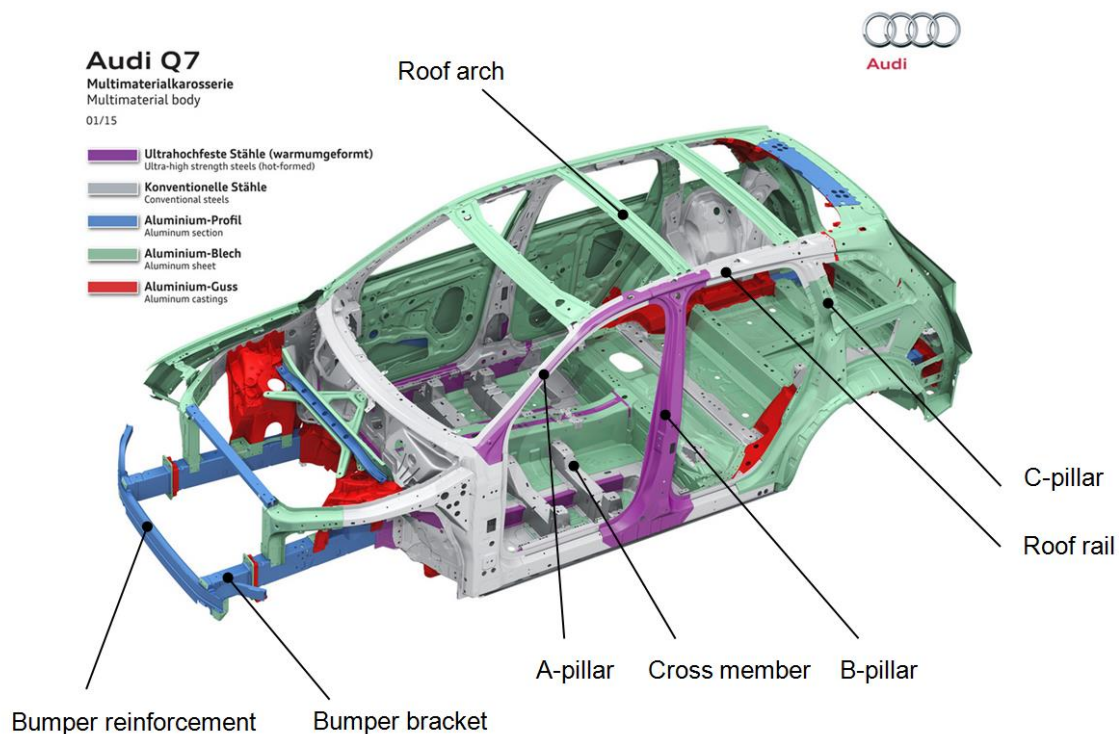

Figure 2-1: *Common structural parts within a mass-produced car* [Image source: Audi]

2.2 Plastic deformation and strengthening of aluminium

Amongst others, aluminium alloys intended to be used for structural parts need to fulfil the following two functional requirements: On the one hand side, their plastic deformation behaviour in the condition they are formed should be high enough to allow for complex shapes. On the other hand side when assembled, they need to perform well in terms of mechanical strength to protect car occupants in the case of a crash situation.

Both properties, plastic deformation behaviour and strength are governed by the phenomenon of dislocation movement on microstructure level. Dislocations are one-dimensional, linear crystal defects and can easiest be envisioned as additional atoms in the middle of an otherwise perfect crystal structure. The additional atoms lead to misalignments within the crystal structure and thus introduce strain into the material. Two different types of dislocations can be distinguished: edge- and screw-dislocations. They most commonly appear together as so-called mixed dislocations though. Figure 2-2 shows visualisations of edge- and screw-dislocations respectively. More detailed information on the theory of dislocation structures is given in [8].
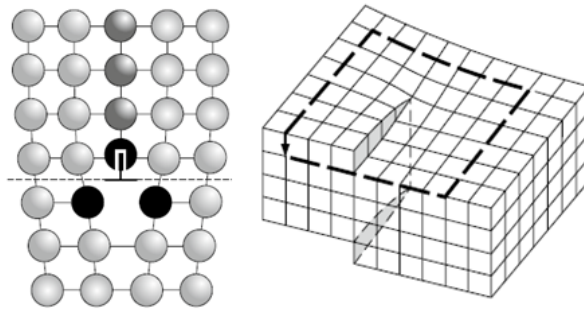
Figure 2-2: *Visualisation of an edge-dislocation (left) and a screw-dislocation (right)* [8]

If dislocations can move easily, the material is low in strength and can be deformed easily. Contrarily, if dislocation movement is blocked, strength increases and plastic deformation gets harder. Four basic mechanisms are believed to prevent dislocations from moving:

- **Solid solution hardening:** Foreign atoms within the aluminium crystals induce strain into their matrix so that dislocation movement is harder.
- **Strain hardening:** Plastic deformation produces and shifts dislocations so that their density within the crystals is raised. Since dislocations block each other, it is more difficult for a single dislocation to move on if their overall density is higher.
- **Grain boundary hardening:** Dislocations can only move within one grain, their movement is hindered at grain boundaries. The finer the grain of the material, the more grain boundaries exist and the harder it gets for dislocations to move.

- **Particle hardening (Precipitation hardening):** Finely dispersed particles (precipitates) make it harder for dislocations to move since they either need to cut the particles or bow around them for passing.

The most important strengthening mechanism for heat-treatable aluminium alloys is the precipitation hardening effect. Finely dispersed precipitates within the aluminium matrix can be achieved by conducting a heat treatment as follows (cf. Figure 2-3):

(1.) Solution heat treatment: The material is heated to an alloy-specific temperature ($\sim$ 500°C for 7xxx series alloys) in order to dissolve the alloying elements into the aluminium crystal.

(2.) Quenching: Rapid cooling to room temperature (RT) freezes the alloying elements within the crystal. A so-called α-supersaturated solid solution (SSS) state emerges. The SSS is a thermodynamically unstable state, high driving forces for decomposition exist.

(3.) Ageing: Storing the solution heat treated and quenched material at room temperature (natural ageing) or heating it once again in the course of an artificial ageing treatment leads to precipitation from the SSS state. Intermetallic phases (precipitates) start to form and the material's strength is increased.

Quenching from solution heat treatment temperature (II) and heating to artificial ageing temperature (III) must occur within critical time frames. Heating to solution heat treatment temperature (I) and cooling from artificial ageing temperature (IV) are uncritical respectively [2].
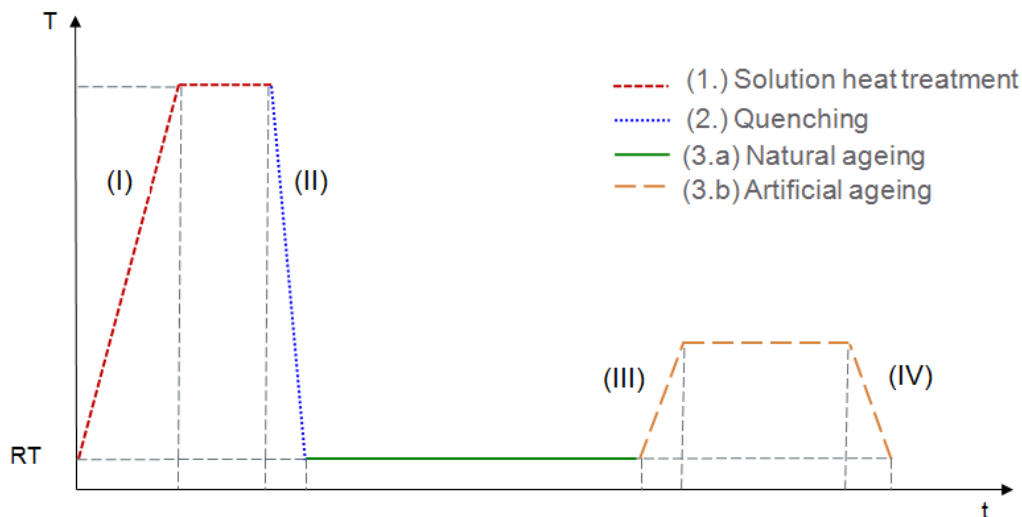
Figure 2-3: Heat treatment for precipitation hardening

The intermetallic phases formed during ageing strongly depend upon whether natural or artificial ageing has been applied. The decomposition of the SSS state is a complex process so that precipitates may vary significantly in type, size and distribution [9]. For every alloy group, a so-called precipitation sequence exists. The precipitation sequence of the EN AW-7xxx alloy group is explained in Section 2.4.4.

2.3 Classification of aluminium alloys

Aluminium alloys are classified according to their processing method: Wrought and cast alloys. Wrought aluminium alloys are designated for forming processes such as extrusion or sheet metal forming. The focus during alloy development lies on achieving good plastic formability in the solid state. Cast alloys contrarily need to meet the requirements of casting processes. Good flow and die filling properties in the liquid state are desired here. Two different designation systems have emerged for wrought and cast aluminium alloys respectively. The alloy group investigated within this thesis belongs to the wrought aluminium alloys.

As shown in Table 2-1, wrought aluminium alloys are divided into eight different alloy groups according to DIN EN 573. A classification is made with respect to the main alloying elements copper (Cu), silicon (Si), manganese (Mn), magnesium (Mg) and zinc (Zn). The amount and combination of the alloying elements strongly influence material properties before and after (thermo-) mechanical processing.

Table 2-1: Classification of wrought aluminium alloys [10]

Alloy group	Main alloying elements	Age hardening potential	Example with corresponding ultimate tensile strength (UTS)	
1xxx	Pure aluminium	non heat-treatable	AW-1050-H18	140 MPa
2xxx	AlCu	heat-treatable	AW-2024-T6	480 MPa
3xxx	AlMn	non heat-treatable	AW-3003-H18	210 MPa
4xxx	AlSi	non heat-treatable	AW-4015-H18	220 MPa
5xxx	AlMg	non heat-treatable	AW-5182-H18	390 MPa
6xxx	AlMgSi	heat treatable	AW-6082-T6	330 MPa
7xxx	AlZnMg	heat treatable	AW-7075-T6	560 MPa
8xxx	others	Mostly non heat-treatable	AW-8011-H18	160 MPa

The strength of some wrought aluminium alloys can be increased through heat treatment, while other alloy groups can only be hardened through introducing further strain into the material. The former are referred to as heat-treatable (age-hardenable), the latter are called non heat-treatable (non age-hardenable) [2]. Examples have been included in Table 2-1 to illustrate typical ultimate tensile strength values of heat-treatable and non heat-treatable alloy groups respectively.

The properties of one and the same wrought aluminium alloy can vary significantly with respect to how it has been processed. For that purpose, a temper designation system specifying their exact condition has been introduced in DIN EN 515. The temper designation is usually added after the alloy number. The basic tempers are as follows:

- **F-temper:** An alloy is in the F-temper, if no specific strength values have been aimed for during its production.

- **O-temper:** An alloy is in the O-temper, if it has been heat-treated (annealed) to obtain lowest strength.
- **H-temper:** An alloy is in the H-temper, if it has been strain hardened to obtain a desired strength level.
- **W-temper:** An alloy is in the W-temper right after solution heat treatment. The W-temper is a soft and unstable temper that does only exist for a short time.
- **T-temper:** An alloy is in the T-temper, if it has been solution heat-treated and naturally or artificially aged to obtain a desired strength level.

For the H-temper and the T-temper, additional digits after the respective letters are used in order to further specify what kind of strain hardening or heat treatment has been applied. The aluminium sheets investigated within this thesis belong to the heat-treatable AW-7xxx alloy group. Their initial tempers were T4 or T6 respectively. In the course of the investigations, they also went through the W-temper and a stabilised condition that will be referred to as the S state in the following.

- **T4:** Solution heat treated, quenched and naturally aged to a substantially stable condition.
- **T6:** Solution heat treated, quenched and artificially aged to obtain maximum strength.
- **S:** Solution heat treated, quenched and artificially aged to obtain a substantially stable condition of reduced strength.

For more comprehensive information on the designation system it is referred to DIN EN 515 at this point.

2.4 EN AW-7xxx aluminium alloys

EN AW-7xxx alloys are heat-treatable and show the highest tensile strength values out of all wrought aluminium alloys. Variants with no significant copper content, such as the EN-AW 7021 alloy, show medium to high tensile strength and can easily be joined through fusion welding. Variants containing copper such as the EN AW-7075 alloy are not suitable for fusion welding, but show high to ultra-high tensile strength values [2].

The materials investigated within this thesis are the EN AW-7021 and EN AW-7075 alloys respectively (cf. Section 4.1). The explanations within the following sections will give special attention to these two alloys.

2.4.1 Alloy composition

The main alloying elements within EN AW-7xxx alloys are Zinc (Zn), magnesium (Mg) and copper (Cu). Zn itself has a good solubility within the aluminium (Al) matrix. Adding Mg drastically reduces the solubility of Zn within the Al matrix, which enhances the artificial ageing potential of the alloy in turn. High Zn/Mg ratios lead to a phase equilibrium of the α-solid solution and the η-phase ($MgZn_2$). For higher Mg contents, a phase equilibrium between the α-solid solution and the so-called T-phase ((Al, $Zn)_{49}Mg_{32}$) emerges. The η-phase and T-phase can also contain Cu, if it is added to the system with more than one weight percent. Adding Cu further reduces the solubility of the alloying elements within the Al matrix and increases the age hardening potential. In that way, ultra-high strength alloys can be achieved [2].

2.4.2 Solution heat treatment

On the one hand side, the solution heat treatment temperature needs to be high enough in order to achieve a complete dissolution of all hardening elements into the Al matrix. On the other hand side, it must not be too high so that the microstructure as a whole remains intact and no local melting occurs. The solution heat treatment time mainly depends upon the material thickness and the furnace used. Determining appropriate solution heat treatment conditions is central to achieving good results during subsequent ageing treatments.

Beck et al. [11] have studied the solution heat treatment conditions of the EN AW-7021 alloy and the EN AW-7075 alloy within a project work previous to this thesis. They identified 515°C (AW-7021) and 480°C (AW-7075) as suitable solution heat treatment temperatures respectively. As for the appropriate heat treatment times, they have conducted differential scanning calorimetry (DSC) tests. The differential scanning calorimetry technique builds upon changes in heat flow that can be related to the extent of diffusion controlled mechanisms within a material (cf. Section 2.6.2). After recording several heat flow-time curves, they found that the curve shape was constant after 5 min (AW-7021) and after 15 min (AW-7075) respectively. This indicates that the dissolution

of alloying elements into the Al matrix has finished, 5 min (AW-7021) and 15 min (AW-7075) are thus sufficient solution heat treatment times.

2.4.3 Quenching

Quenching after the solution heat treatment needs to be sufficiently quick in order to freeze the alloying elements within the solid solution. Too slow cooling can have negative effects on strength, ductility and corrosion resistance during subsequent ageing. The critical temperature range during quenching is generally thought to be between 400°C and 290°C for EN AW-7xxx aluminium alloys. Especially in this temperature range, early and undesired precipitation is likely to occur if the cooling rate falls below a critical value [2].

The determination of the critical cooling rate can be performed by measuring the hardness of differently quenched samples after a defined natural ageing time span. Beck et al. [11] have conducted such tests for the AW-7021 alloy and the AW-7075 alloy. They found that hardness values after 31 days of natural ageing were significantly lower when quenching with cooling rates below 10 K/s (AW-7021) and 100 K/s (AW-7075) respectively. Typical quenching rates reached during water quenching and cold die quenching of AW-7xxx aluminium alloys are given in Section 5.1.2.

2.4.4 Ageing behaviour and precipitation sequence

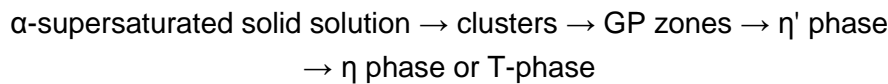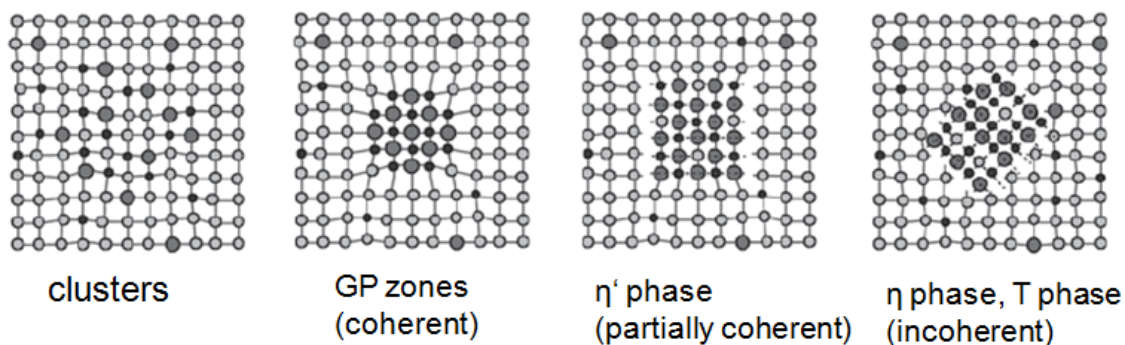The general precipitation sequence of EN AW-7xxx alloys is [2]:

$$\alpha\text{-supersaturated solid solution} \rightarrow \text{clusters} \rightarrow \text{GP zones} \rightarrow \eta' \text{ phase}$$
$$\rightarrow \eta \text{ phase or T-phase}$$

Figure 2-4 illustrates the respective precipitation states.

clusters   GP zones   η' phase   η phase, T phase
   (coherent)   (partially coherent)   (incoherent)

Figure 2-4: *Schematic depiction of the precipitation states* [2]

Natural ageing and early stages of precipitation

The natural ageing process and early stages of precipitation are governed by the formation of clusters and coherent GP zones. Clusters can be envisioned as local accumulations of alloying elements in the Al matrix without any particular structure. Once the clusters have developed an internal structure (e.g. sphere-shaped, plate-

shaped...), they are called GP zones. The temperature range up to which only GP zones are formed may raise up to 100°C depending on the exact alloy composition [2]. It can be distinguished between two types of GP zones. GP(I) zones most commonly form at temperatures below 60°C, while GP(II) zones are generally thought to appear at temperatures above 70°C [2, 12]. Compared to GP(I) zones, GP(II) zones are thermodynamically more stable and can transform directly into the next precipitation state during artificial ageing [2].

Figure 2-5 shows the increase in hardness during natural ageing and early stages of precipitation at different ageing temperatures and times for the EN-AW 7075 alloy. At room temperature (RT), the natural ageing process begins after one hour approximately. For higher temperatures, the start of ageing is moved to earlier times. The process slows down after four to five days. Changes in hardness can still be observed after several years though [2].
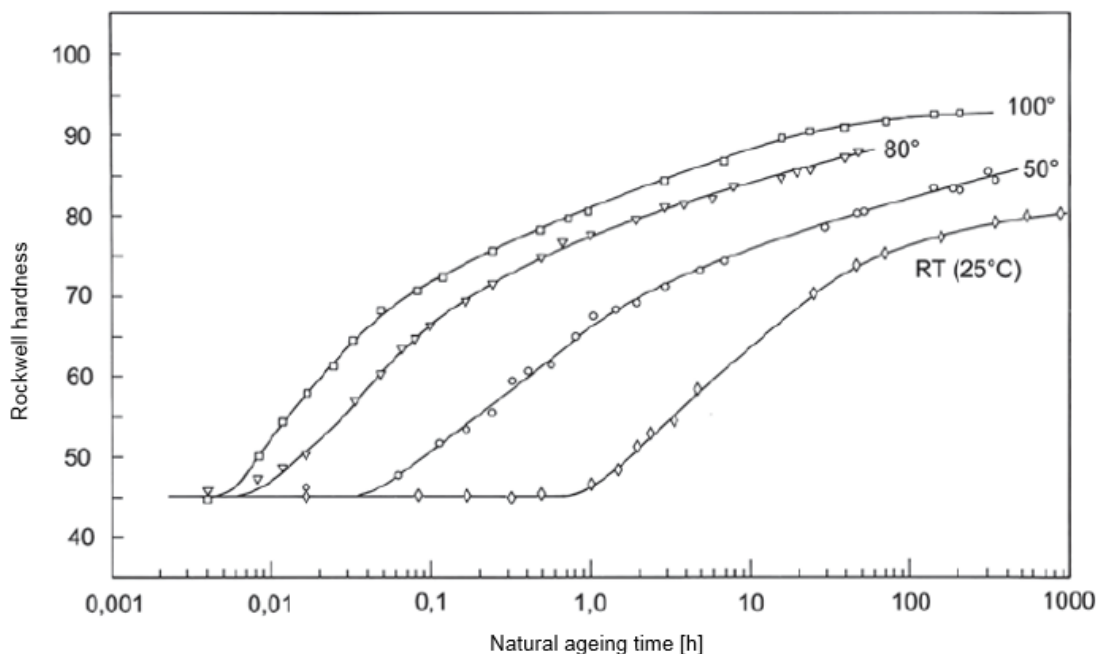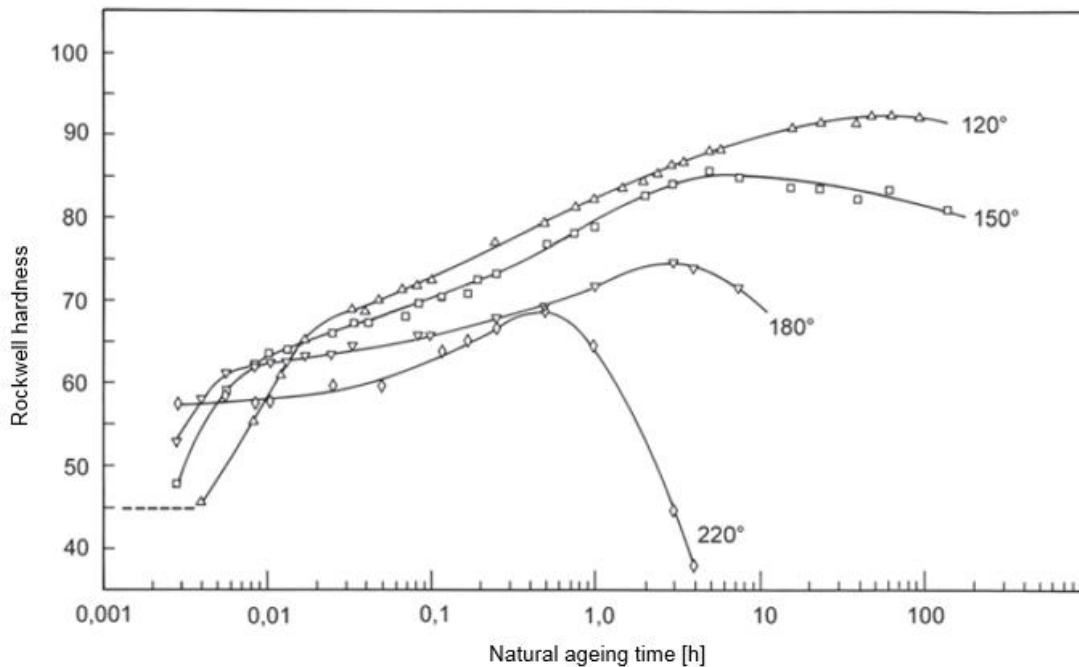

Figure 2-5: *Ageing behaviour of the EN-AW 7075 alloy at different temperatures and times* [2]

Artificial ageing

During artificial ageing, the GP zones first transform into the metastable η' phase and with further ageing into the stable η phase or T-phase. The transition from one precipitation state to the next reduces the coherence of the particles within the Al matrix. The maximum hardness that can be achieved during artificial ageing depends upon the type, size, amount and distribution of the precipitates formed. For the EN AW-7xxx aluminium alloys, it is the partially coherent η' phase that has the highest hardening potential. The time frame between quenching and artificial ageing is critical for achieving highest strength. Solution heat treated and quenched parts from EN AW-7xxx alloys should have been stored at least for 3 days at room temperature in order to achieve good artificial ageing results. Figure 2-6 shows the influence of artificial ageing

time and temperature on hardness for the EN-AW 7075 alloy. Highest hardness values can be achieved at temperatures between 120°C and 130°C. Too long artificial ageing times lead to a so-called over-ageing of the material and hardness drops again [2].
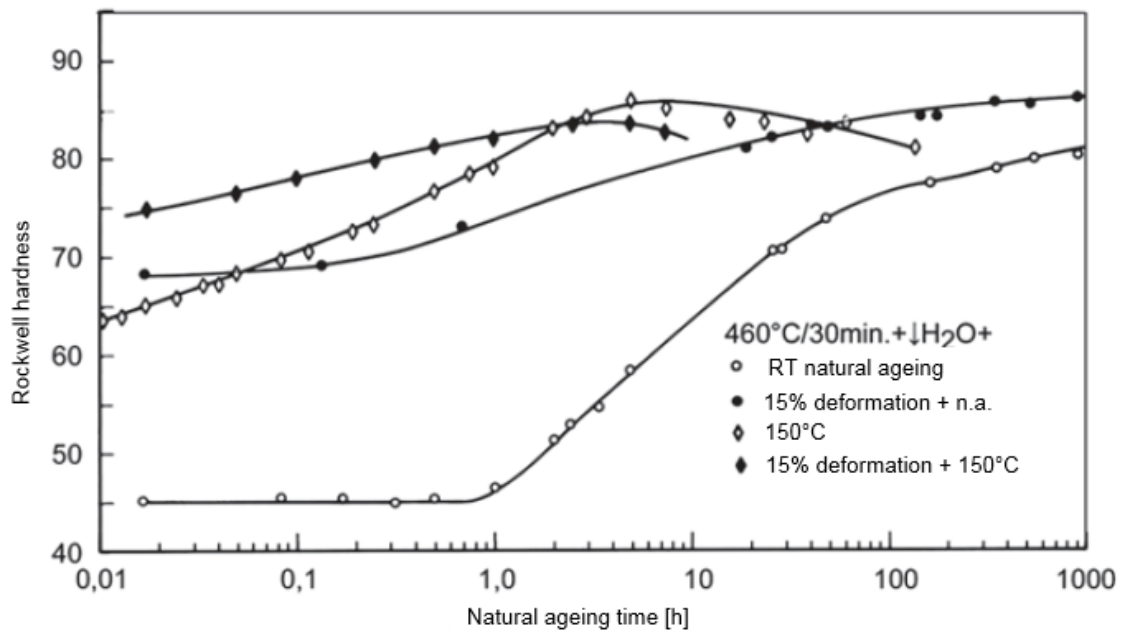

Figure 2-6: *Artificial ageing behaviour of the EN-AW 7075 alloy at different temperatures and times* [2]

The increase in yield strength or hardness after artificial ageing at relatively high temperatures for short times is often called paint bake response in automotive literature. This is due to the fact that automotive structural parts are subjected to elevated temperatures after painting in order to cure the coat. This heat treatment simultaneously acts as an artificial ageing heat treatment for aluminium parts.

Influence of plastic deformation on the ageing behaviour

Sheet metal products from EN AW-7xxx alloys are formed during or after quenching from solution heat treatment temperature (cf. Section 2.5). Introducing plastic deformation into the material prior to natural or artificial ageing changes the ageing behaviour. This relationship is illustrated in Figure 2-7 for the EN AW-7075 alloy subjected to a deformation of 15%. Natural ageing is delayed if the material has been deformed before, however ultimate hardness values are higher. Contrarily, artificial ageing is accelerated if the material has undergone plastic deformation and ultimate hardness values drop compared to the undeformed state. The negative effect of plastic deformation on the artificial ageing behaviour can be reduced though if heating to the respective ageing temperature occurs slowly [2].

Figure 2-7: *Influence of plastic deformation on the natural and artificial ageing behaviour for the EN-AW 7075 alloy* [2]

### *Ageing conditions for EN-AW 7021 and EN-AW 7075*

As for the AW-7021 and AW-7075 alloys investigated within this thesis, a natural ageing interval of 21 days was chosen before conducting the artificial ageing heat treatment. Artificial ageing was carried out in accordance with a typical temperature-time cycle used during paint baking of automotive body structures (185°C, 25 min). An additional reference heat treatment (120°C, 24 h) was performed to achieve the so-called T6 temper (peak hardness) in order to assess the quality of the paint bake cycle. Heating rates were governed by the convection oven used and were at approximately 0.2 K/sec. The recorded temperature-time curves can be found in Appendix 1.

2.4.5 Stabilisation heat treatment

A stabilisation heat treatment can be understood as an additional heat treatment before natural or artificial ageing. Since especially EN-AW 7xxx alloys exhibit a pronounced natural ageing behaviour after quenching, conducting low temperature pre-ageing heat treatments can potentially help keeping mechanical properties on a stable level. In the ideal case, such a stable state should be kept over a time period of several weeks and hardness values should be lower than those occurring due to natural ageing. This is especially important with respect to self-pierce riveting. Self-pierce riveting is a common joining method for structural parts from aluminium and requires definite hardness values in order to achieve a joint of good quality for a given riveting procedure.

Österreicher et al. [13] have investigated the influence of low temperate pre-ageing heat treatments (stabilisation heat treatments) on the EN AW-7021 and EN AW-7075

alloys in a project previous to this thesis. Their core findings are illustrated in Figure 2-8.
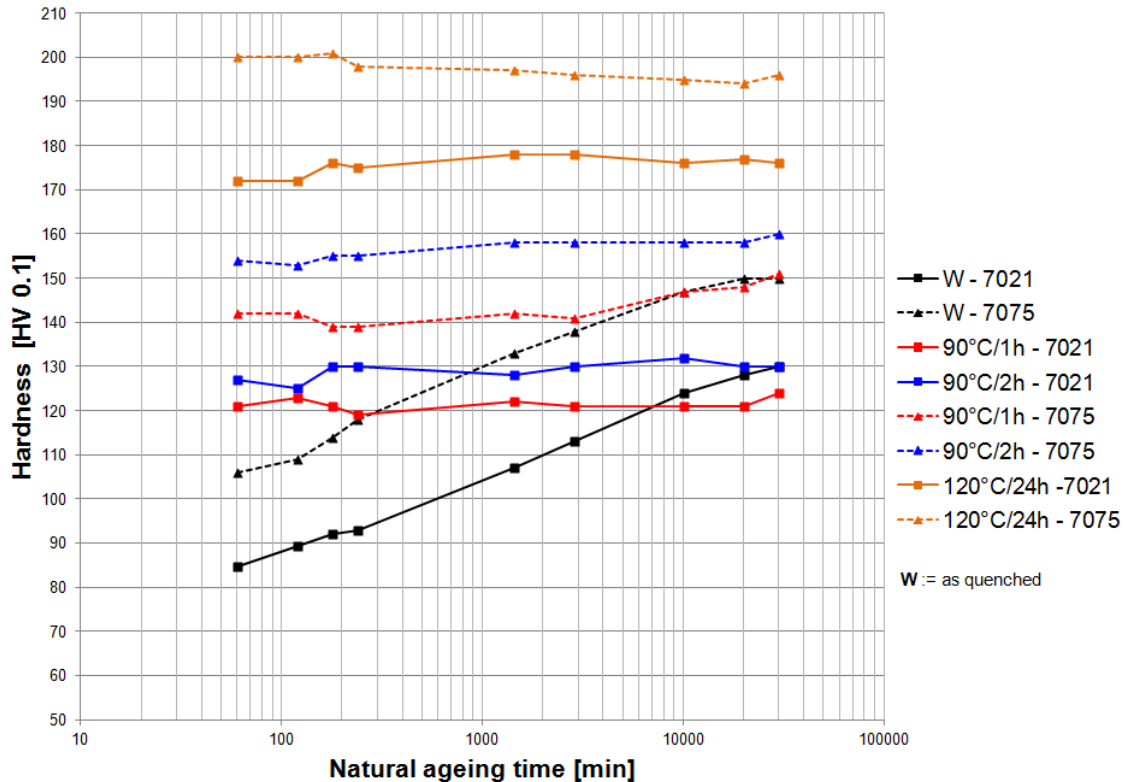
Figure 2-8: *Natural ageing behaviour of peak aged (120°C, 24 h), stabilised and as-quenched (unstabilised) W samples from EN AW-7021 and EN AW-7075* [13]

As can be seen from the diagram, a properly designed stabilisation heat treatment (90°C, 1h) can inhibit the natural ageing process for the AW-7021 alloy. The resulting condition is stable over the course of about 3 weeks and was found to perform well in terms of joinability and formability. Its hardness is lower than the hardness resulting from natural ageing times longer than approximately one week. For the AW-7075 alloy, such a stable condition could not be achieved. However, for the AW-7075 alloy an increase in yield strength after artificial ageing was observed if they had gone through a pre-ageing heat treatment before [13].

A stable condition prior to artificial ageing and improved yield strength values after paint baking are both desired properties when it comes to designing process chains for the production of structural parts. Therefore, this thesis will amongst others investigate how the process chains proposed for forming EN AW-7xxx sheets can be supplemented by an additional pre-ageing heat treatment (cf. Section 2.5.5 and Chapter 3).

2.5 Sheet metal forming processes for EN AW-7xxx aluminium alloys

For decades, EN AW-7xxx aluminium alloys have primarily been used for aircraft construction. Especially the highly-loaded fuselage or the wings are commonly made from high to ultra-high strength aluminium. Recently, also automotive manufactures have been attracted by the high specific strength (yield strength / density) of the AW-7xxx alloy group so as to manufacture crash-relevant body parts. The formability of AW-7xxx alloys at room temperature is limited to simple shapes, though. Therefore, alternative forming strategies are required in order to make the AW-7xxx alloy group suitable for manufacturing complexly shaped sheet products such as B-pillars or side impact beams. Literature has proposed four strategies that could be expedient for improving formability of AW-7xxx alloys: Retrogression forming, W-temper forming, warm forming and hot forming [4].

2.5.1 Retrogression forming (RF)

The retrogression forming (RF) process (cf. Figure 2-9) starts with heat treating the sheets at a temperature below the solution heat treatment conditions. This temperature is only held for a short time (seconds) and leads to a partial dissolution of the hardening precipitates (η' phase) promoting an ameliorated formability compared to the as-delivered condition. Thereafter, the sheet is water quenched and formed. The process chain finishes up with trimming, storing, joining and paint baking respectively. From a resource efficiency perspective, an advantage of the retrogression forming strategy might be seen in short heat treatment cycles with low temperatures. A major drawback is the fact that hardening precipitates are only partially dissolved so that the formability improvement is not sufficient for highly complex geometries [4].
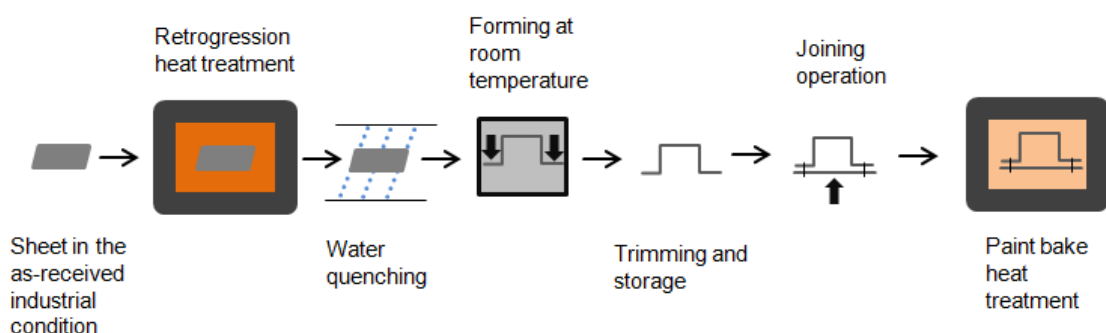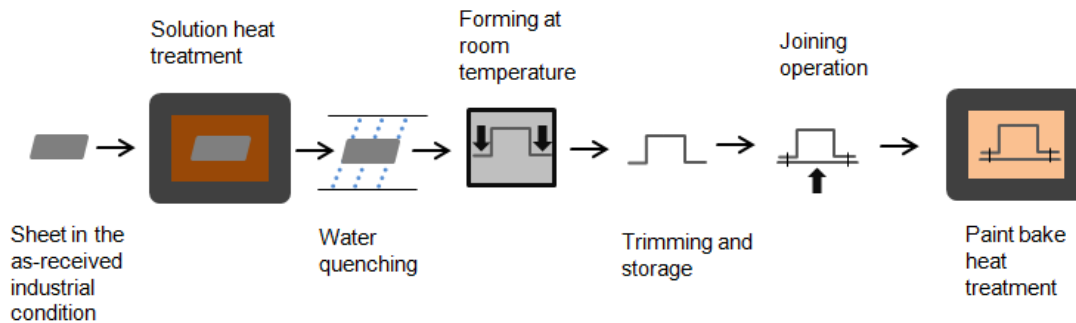

Figure 2-9: *Schematic depiction of the retrogression forming (RF) process steps*

2.5.2 W-temper forming (WTF)

During W-temper forming (WTF), the sheets are heated to solution heat treatment temperature and this temperature is held for some minutes. Thereafter the sheets are water quenched to reach the so-called W-temper state before eventually being formed.

Hardening precipitates are dissolved completely in the W-temper state, so that the formability improvement at room temperature is better compared to retrogression forming and more complex geometries can be formed. After forming, the parts are trimmed and stored until being joined and paint baked. The process steps run through for the W-temper process are shown in Figure 2-10.
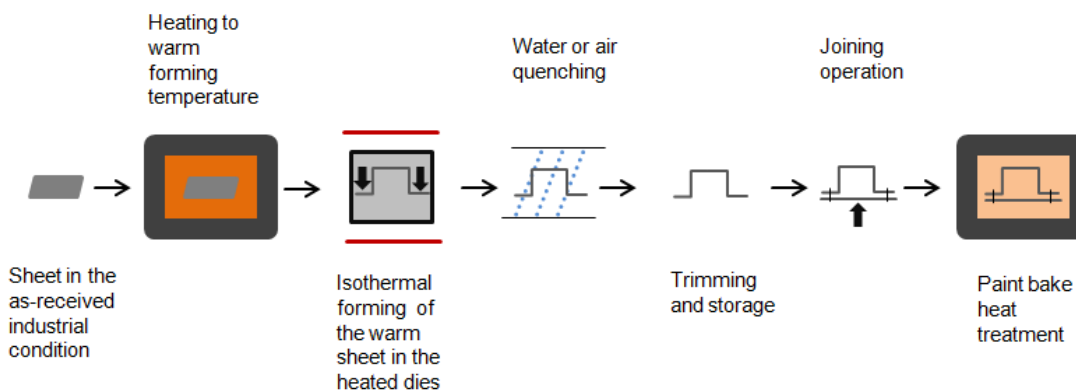
Figure 2-10: Schematic depiction of the W-temper forming (WTF) process steps

From a technological point of view both, W-temper forming and retrogression forming have the advantage of using conventional tools and lubricants from the cold forming process [4].

2.5.3 Warm forming (WF)

During warm forming (WF), both the sheet and the dies are heated. Forming is carried out at an elevated temperature that is about half as high as the melting temperature of the material ($\sim$ 0.5 T_m). It is important that the warm forming temperature stays constant throughout the entire forming procedure (isothermal forming). This requires heatable tools with a precise temperature regulation system. After forming, the parts are water quenched or cooled with forced air before being trimmed, stored and paint baked [4]. Figure 2-11 illustrates the warm forming process chain.
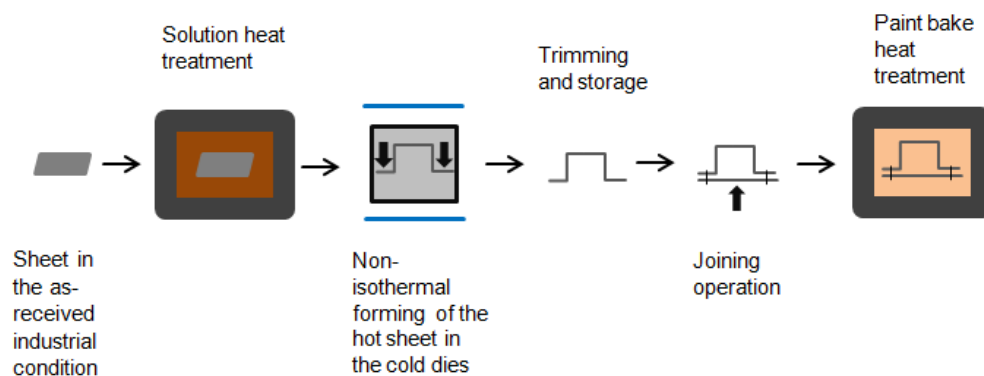
Figure 2-11: Schematic depiction of the warm forming (WF) process steps

Since the hardening precipitates (η' phase) only dissolve partially at the warm forming temperature, formability improvement is limited compared to the hot forming strategy explained next.

2.5.4 Hot forming (HF)

The hot forming process (HF) consists of heating up the sheets to solution heat treatment temperature in a furnace and quenching them in the cold dies. Hot forming is a non-isothermal process that requires quick forming and quenching in order to obtain a sufficiently high formability improvement and a good hardening response during artificial ageing. Just as before, the formed parts are trimmed, stored, joined and finally paint baked [4]. The hot forming process chain is depicted schematically in Figure 2-12. As can be seen, hot forming makes it possible to unite two process steps in one, while for warm forming the quenching has to occur outside the tool in water or forced air.

Figure 2-12: Schematic depiction of the hot forming (HF) process steps

For both warm and hot forming, increasing the temperature during the forming operation does not only dissolve the hardening precipitates (η' phase), but further also enhances the dynamic recovery effect. Dynamic recovery leads to an annihilation of accumulated dislocations inducing an additional decrease in strength. Therefore, the increase in formability during elevated temperature forming builds upon two effects while for W-temper and retrogression forming it is only one. A major disadvantage of hot and warm forming over W-temper and retrogression forming is that the former cannot be carried out using conventional lubricants and tools. Up to now, lubricants available do not fully meet the requirements of elevated temperature forming process chains and also tool design is much more challenging [4].

For all process routes described in Sections 2.5.1 to 2.5.4, the storage time after forming is limited so as to achieve a mechanical joint of good quality. In order to extend this time interval and achieve more stable material properties during storage, process modifications as described in Section 2.5.5 can be taken into account.

2.5.5 Process modifications with respect to an additional stabilisation heat treatment

As discussed in Section 2.4.5, low temperature pre-ageing heat treatments might be suitable to result in a stable condition with good formability and improved paint bake response for the AW-7021 alloy. Therefore, it seems to be worth exploring how the process chains from above could potentially be supplemented with such a stabilisation heat treatment. The following suggestions are not "state of the art", rather they are sought to be investigated within this work.

Post stabilisation forming (PSF)

In a first version, the additional stabilisation heat treatment is suggested to be performed directly after water quenching and before forming at room temperature. This process modification is shown in Figure 2-13 and is referred to as post stabilisation forming (PSF) in the following.
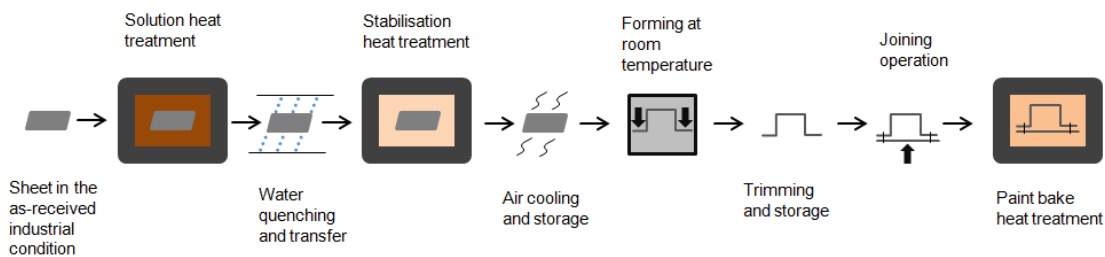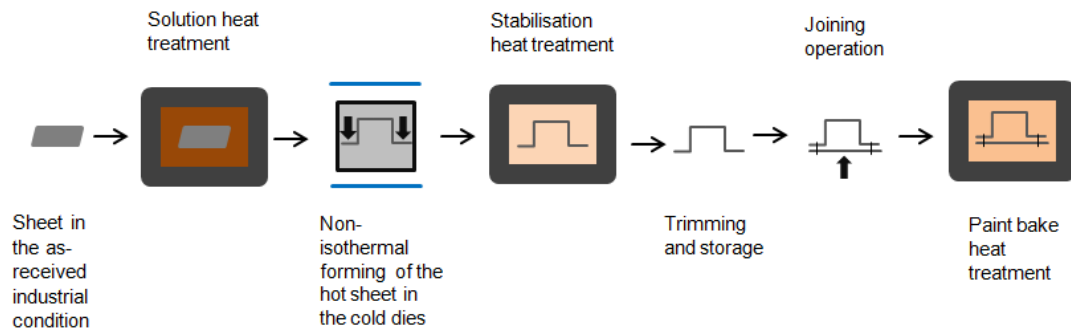

Figure 2-13: *Schematic depiction of the post stabilisation forming (PSF) process steps*

The main advantage of this alternative is thought to be a decoupling of the process chain. In that sense, sheets could be solution heat treated and stabilised at any time without being dependant on an immediate, subsequent forming operation. Stabilised sheets could be prepared even if forming tools and presses are working to full capacity. Eventually, such a process decoupling could be a lever to save resources since the preparation of formable sheets could be grouped to segregated batches then and furnaces could be turned off if enough stock has been produced. The same applies to forming tools and presses. For the case the stabilised state can be kept until the joining operation, it might raise the quality of rivet connections since the procedure could be adjusted to definite hardness values then.

A major drawback of post stabilisation forming might be comparatively high hardness and strength values during forming. Thus, it is questionable whether the formability improvement compared to the as-delivered industrial state is sufficient to produce advanced geometries.

Hot forming with subsequent stabilisation (HF-S)

A second process modification with regard to an additional stabilisation heat treatment is stabilising directly after forming. In this case, non-isothermal hot forming has been chosen as it promises highest formability improvements of all process chains. The modified version is referred to as hot forming with subsequent stabilisation (HF-S) in the following and is depicted in Figure 2-14.

Figure 2-14: Schematic depiction of the hot forming with subsequent stabilisation (HF-S) process steps

The main thought behind this process modification is achieving stable hardness values for the joining operation. Further, the low temperature pre-ageing heat treatment after forming could potentially also increase paint bake response and thus improve the energy absorption behaviour of structural parts.

For both PSF and HF-S, the additional stabilisation heat treatment needs to be weighed in terms of resource efficiency.

2.6 Technological process assessment

This work aims at investigating process chains suitable for producing sheet metal parts form EN AW-7xxx aluminium alloys. Within this section, several technological process criteria as well as possible methods to assess these criteria are explained.

2.6.1 Formability

Formability is the ability of a material to deform plastically without failure or fracture. For sheet metal forming processes, stress-strain states often vary significantly in time and location during the forming of parts. Flow and fracture characteristics heavily depend on the varying stress-strain states. Therefore, formability as a material property is a complex topic and it takes considerable efforts to make reliable statements on how different materials being formed with different strategies will behave [14].

In a first approach, tensile testing is often used to judge formability. It is a very cost-efficient and time-saving way of making statements regarding the flow and fracture behaviour under uniaxial conditions. Although practical forming operations are often biaxial, tensile testing will be used within this work due to its simplicity. A more precise evaluation of formability can occur through additional technological investigation methods like bulge testing and the determination of forming limit diagrams (FLD).

During tensile testing, a material sample of definite geometry is clamped at two ends and pulled apart at a given velocity until it breaks. Force F and elongation ΔL are recorded and divided through the initial cross-section A_0 and initial length L_0 of the sample to determine stress σ and strain ε respectively. Figure 2-5 shows a typical engineering stress-strain curve for an aluminium alloy subjected to tensile testing.

Every stress-strain curve can be divided into three basic stages: elastic deformation (I), uniform plastic deformation (II) and plastic deformation through necking (III). During the elastic deformation stage (I), stress rises linearly with increasing strain. The material sample returns to its initial shape if only loaded elastically. After having reached the yield point, plastic deformation starts and the change in shape gets non-reversible. As long as this plastic deformation occurs in the same way for every area of the sample, one may talk about uniform plastic deformation (II). Uniform plastic deformation ends when reaching the material's ultimate tensile strength. Thereafter, plastic deformation starts to vary throughout the samples geometry and necking (III) begins. For ductile materials, necking will continuously transfer to new sections over a long time so that high strain values can be reached before the sample ultimately tears. For less ductile materials, necking occurs rather localised and fracture is most likely to occur at low strain values already.
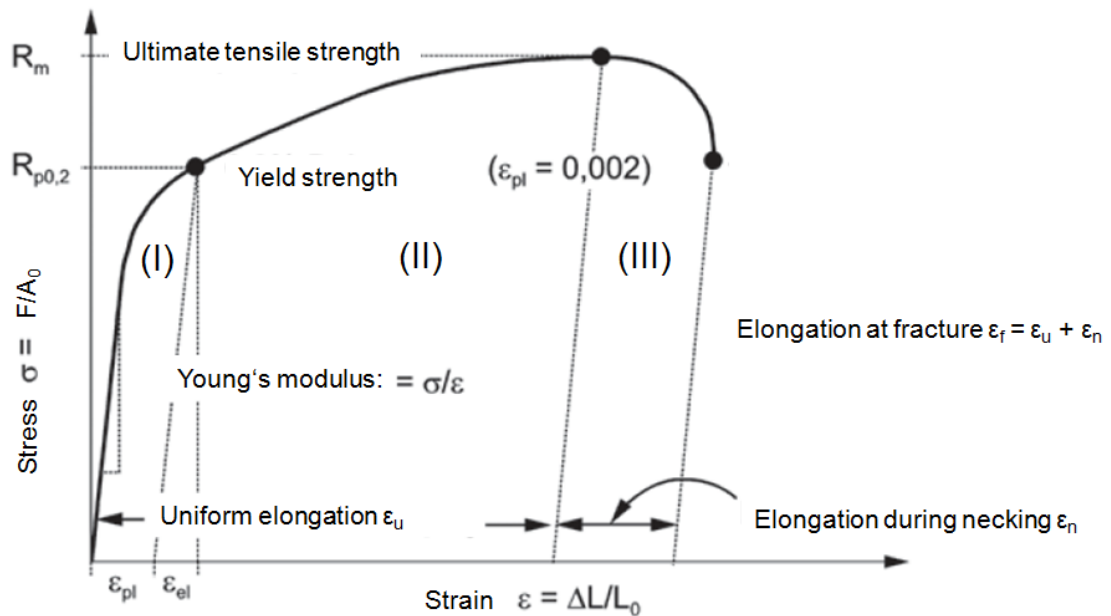
Figure 2-15: *Typical engineering stress-strain curve for an aluminium alloy with corresponding material characteristics* [2]

Important material characteristics that can be read from the stress-strain curve are yield strength $R_{p0.2}$, ultimate tensile strength R_m, uniform elongation ε_u as well as elongation at fracture ε_f.

Yield strength and ultimate tensile strength

When loading a material with stress values equal to or higher than the yield strength $R_{p0.2}$, it begins to deform plastically. Ultimate tensile strength R_m is the maximum stress that a material can be loaded to before it begins to deform non-uniformly. Against the background of formability, low yield strength values are desired. High yield strength to ultimate tensile strength ratios indicate that the material undergoes little strain hardening when being deformed.

Uniform elongation

Uniform elongation ε_u is the maximum elongation that a material can reach before necking starts. High uniform elongation values are desirable for any forming operation because they delay the occurrence of plastic instability. If strain hardening is high, uniform elongation values usually drop considerably [2].

Elongation at fracture

Elongation at fracture ε_f is the maximum elongation a material can reach before tearing. Elongation at fracture is the most important characteristic to assess the ductility behaviour of any material. In order to improve formability, high ductility values must be strived for. Since elongation at fracture varies with respect to the initial length of tensile samples, one should only compare elongation at fracture values that have been measured using the same sample geometry [2].

Strain rate sensitivity

Strain rate sensitivity m_{SR} is an important parameter for characterising formability, especially at elevated temperatures. Mathematically, it can be described according to Equation 2-1:

$$m_{SR} = \left[\frac{\partial \ln \sigma}{\partial \ln \dot{\varepsilon}} \right]_{\varepsilon = \text{constant}}$$
(Equation 2-1)

Strain rate sensitivity describes the phenomenon that the stress-strain curve of one and the same material might look different if loaded with different velocities. If m_{SR} shows a positive value, stress levels are lower for the case the material is loaded slowly. Contrarily, if m_{SR} shows a negative value, stress levels are higher for the case the material is loaded slowly. The strain rate sensitivity of a material is an important parameter for choosing die speeds during the development of a forming operation.

2.6.2 Post-forming material properties

Assessing the post-forming material properties of heat treatable aluminium sheet metal parts should take place because of two considerations: On the one hand side, the hardness evolution (natural ageing behaviour) after forming is of interest since joining most commonly occurs through mechanical methods (e.g. self-pierce riveting) for aluminium parts. On the other hand side, the increase in yield strength after paint baking (paint bake response) is an important characteristic with respect to structural stability and crushworthiness. Hardness testing, differential scanning calorimetry, cross-sections of rivet connections as well as tensile testing have been used within this work to assess post-forming material properties.
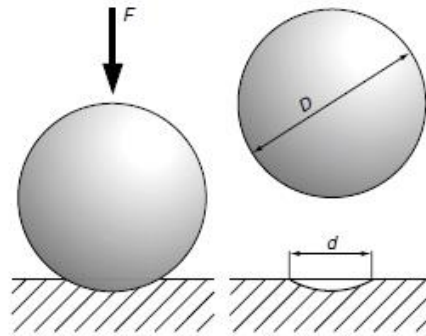
Hardness testing

The natural ageing behaviour of age-hardenable aluminium alloys is usually assessed through hardness testing. Hardness can be defined as the resistance of a material against changes in shape during the indentation of another (harder) material. There are different methods for measuring the hardness of a material. Since resistance against indentation obviously depends upon the geometry as well as hardness of the indenting object and the load type used, it is crucial to always give additional information about the method used when talking about hardness values [8].

The method used within this work is the static hardness testing method according to Brinell (cf. Figure 2-16). DIN EN ISO 6506 specifies the Brinell method: A carbide sphere of diameter D is pushed into the material sample with a definite force F. The diameter of the resulting indentation d is measured and the hardness value is calculated according to Equation 2-2:

$$HBW = \frac{0.102 * 2F}{\pi * D * (D - \sqrt{D^2 - d^2})} \qquad \text{(Equation 2-2)}$$

The hardness values determined are usually followed by the abbreviation HBW, the sphere diameter D and the indentation force F multiplied by 0.102. For instance, 100 HBW 2.5/62.5 means that the Brinell hardness value of 100 has been measured with a sphere diameter of 2.5 and an indentation force of 613 N (62.5/0.102) [8].


Figure 2-16: *Visualisation of the hardness testing method according to Brinell* [8]

Differential scanning calorimetry (DSC)

Described in DIN EN ISO 11357-1, differential scanning calorimetry (DSC) is a useful technique in order to track the precipitation state during natural and artificial ageing. It builds upon the fact that materials with different microstructural composition require different amounts of heat to increase in temperature. There are two types of DSC devices: heat flow based devices and power compensated devices. Within this work, a heat flow based DSC device has been used.

In heat flow based devices, a test sample and a reference sample are subjected to a definite temperature profile. Upon heating, the difference in heat flow $\dot{Q}$ into the test sample and into the reference sample is recorded as a function of temperature T. Figure 2-17 exemplarily shows a heat flow-temperature curve of an AW-7021 sample.

As soon as the test sample undergoes a phase transformation (change in precipitation state), more or less heat will be required to keep it on the same temperature level as the reference sample. In that sense, the dissolution of precipitates in the test sample corresponds to endothermic (positive) events in the recorded heat flow-temperature curve. Since the dissolution of precipitates can be regarded as the dissolution of a thermodynamically stable state, more heat will be required to further increase the temperature of the test sample. Vice versa, the formation of precipitates corresponds to exothermic (negative) events in the recorded heat flow-temperature curve. In this case, less heat must flow into the test sample because the sample has obviously been in a thermodynamically unstable state before.
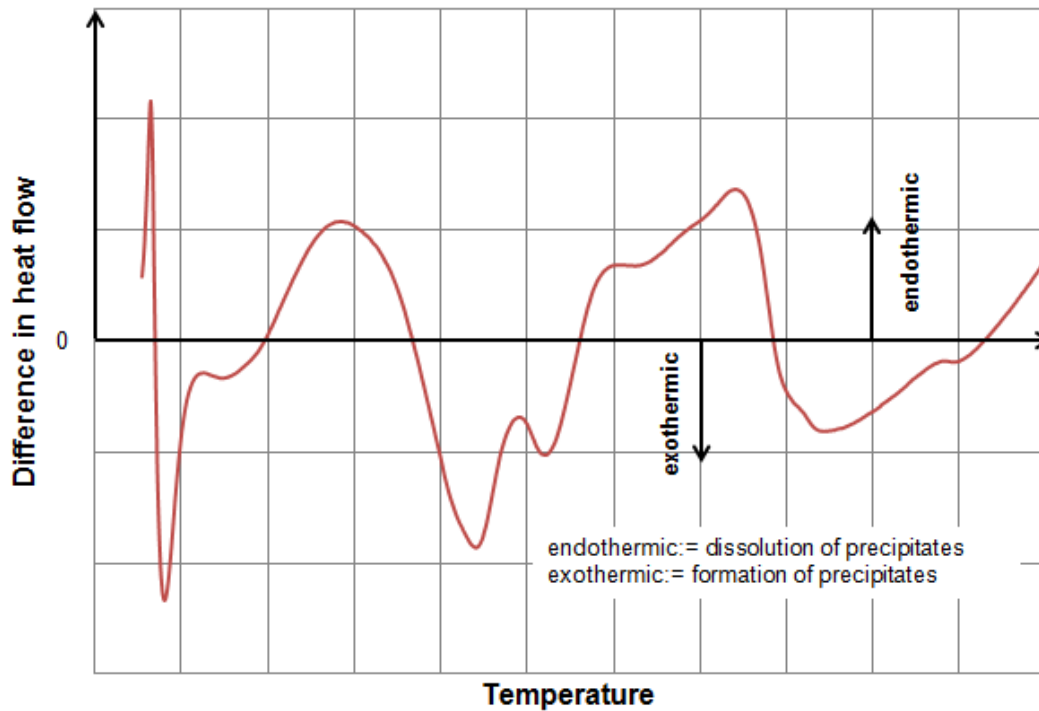
**Figure 2-17:** *Exemplary DSC measurement of an AW-7021 sample*

By means of assessing the height of endothermic or exothermic peaks and the temperatures at which they occur, one can get an overview on the precipitation states present within a material. The results from DSC testing can eventually be linked to differences in mechanical properties as the sheets pass through the process chains.

Joinability

Thermal methods such as spot welding are often not a suitable option to join aluminium sheets. Therefore, it is mechanical joining methods that prevail for aluminium in industrial use. The technique of self-pierce riveting is of particular importance as it shows a high capability for automation [15].

Especially for crash-relevant structures, joints of high quality are essential. For rivet joints, common tests to assess joint quality under dynamic loads are cross or shear tension experiments. These tests require considerable efforts in terms of time and money though. A quick and inexpensive method for visually assessing the quality of a riveting procedure is preparing cross sections.

Figure 2-18 shows a cross section of a joint that has been produced through self-pierce riveting. Freedom of cracks is a basic prerequisite in order to achieve good joint strength. Beyond that, it is important that the joint performs well in terms of meeting several geometric quality criteria. Particularly crucial measures have been included in the illustration below and are explained in the following [15]:
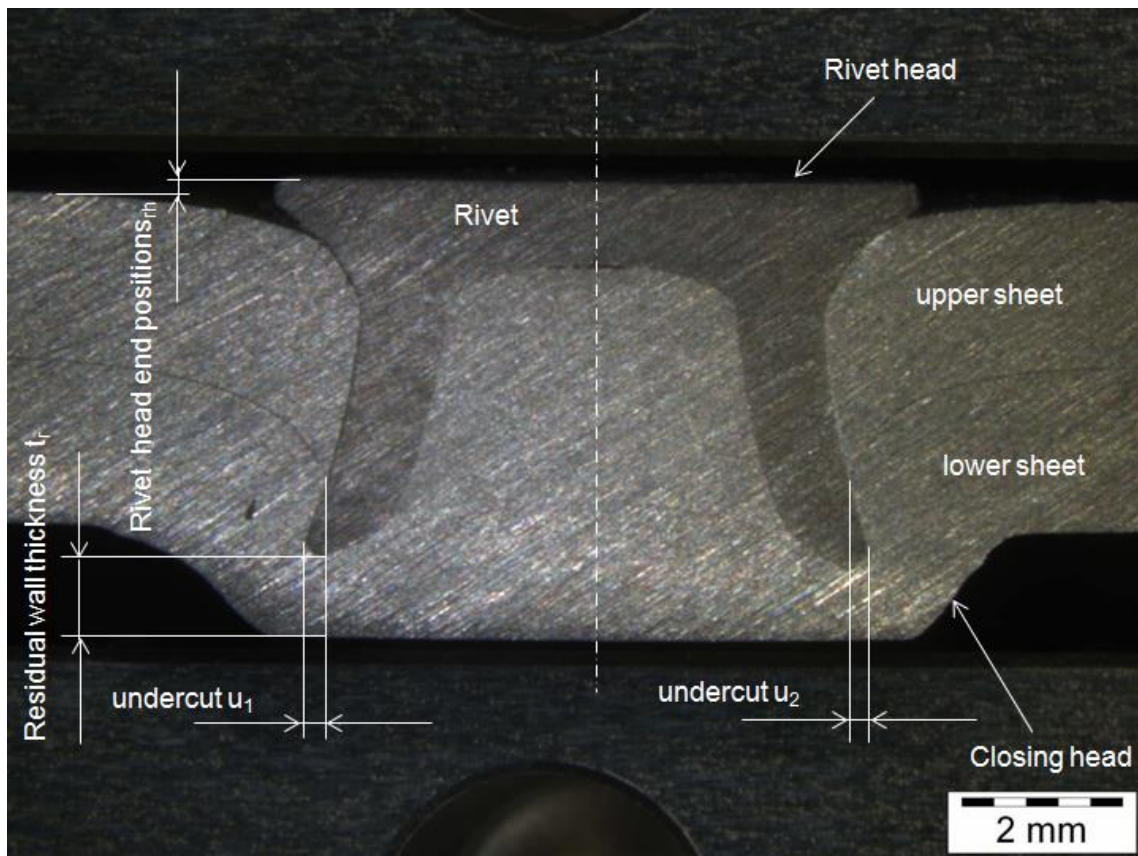
Figure 2-18: Geometric criteria for assessing the quality of a rivet joint

- **Undercut** $u_{1,2}$**:** This geometric quality criteria is determined through measuring the distance between the most outward point of the rivet and the point where upper and lower sheet meet along the outer rivet edge. A uniformly pronounced undercut is important so that the joint can withstand high stress when loaded.
- **Residual wall thickness** t_r**:** The residual wall thickness is the smallest measure between the rivet tip and the outer edge of the lower sheet. It should not be too small in order to prevent a formation of subtle cracks that could endanger joint tightness. Otherwise, joint strength could decrease significantly over time due to corrosion.
- **Rivet head end position** s_{rh}**:** Just as for the residual wall thickness, a proper rivet head end position is important for assuring the tightness of the rivet connection. In the ideal case, the rivet head should be at the same height as the edge of the upper sheet or slightly below it. For the cross section in Figure 2-18, the rivet head transcends the upper sheet and a gap appears between rivet head and upper sheet at the left side. The formation of such geometries should be avoided.

The cross section from Figure 2-18 and those presented in Section 5.2.3 have been prepared by LKR researcher Georg Kirov. I would like to thank him for the provision of the data set at this point.

Tensile testing

The fundamentals of tensile testing have been presented in Section 2.6.1 as a means of assessing formability. Of course, tensile testing can also be used to assess post-forming material properties, especially paint bake response.

In order to achieve high mean crush force levels and thus improve energy absorption of automotive structural parts (cf. Section 2.6.3), high yield strength values after artificial ageing are strived for. At the same time, good ductility is desired so as to increase folding capability of crash elements. This is a contradiction however, since in most cases elongation at fracture will inevitably decrease if yield strength is increased. The goal during the determination of suitable artificial heat treatments must thus be reasoned in finding a good trade-off between strength and ductility.

2.6.3 Energy absorption behaviour

In a crash situation, automotive structural parts need to have the ability to collapse in a controlled manner so as to absorb adequate amounts of energy and eventually limit loads on passengers. For aluminium alloys, energy absorption behaviour is governed by localised plastic deformation. The experimental assessment of a structure's energy absorption behaviour occurs through crush testing. Crush testing can be carried out in two different ways: quasi-static testing and dynamic testing [16].

Under quasi-static conditions, the structure is crushed at a constant speed. Conducting quasi-static tests gives a first impression on how the structure might collapse when loaded dynamically. Especially the mean crush force levels (see definition below) determined through quasi-static crush testing suggest which energy amounts might be absorbed during dynamic testing. This helps to configure the dynamic test setup with respect to mass and initial velocity of impactors used. In a real crash situation, the structure is subjected to a decrease in crushing speed. As most metals such as aluminium alloys happen to be strain rate sensitive, dynamic crush testing is essential to make reliable statements about the energy absorption behaviour under close-to-reality conditions [16].

Quasi-static crush testing is a rather simple method providing a first insight into a structure's capability for energy absorption so it will be used within this work. Dynamic testing requires considerably more experimental effort. It will be studied within a follow-up project to this thesis.

Irrespective of which method is used quasi-static or dynamic testing, several characteristics can be obtained from the force-length diagrams recorded during crush testing. These parameters are most commonly used to assess a structure with respect to its crushworthiness. Figure 2-19 exemplarily shows a crushed structure that has been loaded with a force F and compressed for a length of l. Important crushworthiness parameters are explained with respect to the associated diagram.
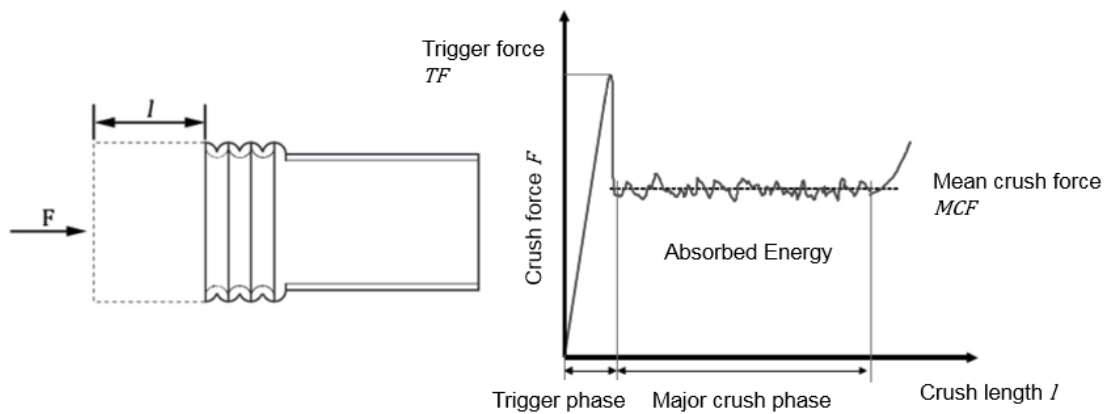
Figure 2-19: *Exemplary representation of a crushed structure and the associated force-length diagram* [16]

- **Trigger force** *(TF)***:** The trigger force is the maximum force reached during crush testing. It always appears at the beginning of crushing. In order to limit the physiological load on passengers, the trigger force should not be too high.
- **Mean crush force** *(MCF)***:** The mean crush force is the averaged force determined from the major crush phase.
- **Crush force efficiency** *(CFE)***:** Crush force efficiency is defined as the ratio between mean crush force and trigger force (cf. Equation 2-3).

$$CFE = \frac{MCF}{TF} * 100 \, [\%]$$
(Equation 2-3)

High crush force efficiency ratios indicate that the structure is capable of absorbing adequate amounts of energy without evoking excessively high trigger forces. Such a behaviour is desired in order to reduce the occupants' injury risk during a crash.

- **Energy absorption** *(EA)* **and specific energy absorption** *(SEA)***:** The amount of absorbed energy corresponds to the area below the force-length curve. With an incremental length element *dl'*, the crush force *F* and the total crush length *l*, it is calculated according to Equation 2-4.

$$EA = \int_{l'=0}^{l} F(l')dl'$$
(Equation 2-4)

In order to make the amount of absorbed energy comparable for different geometries or test setups, it is usually divided through the structure's initial mass *m* to obtain specific energy absorption *SEA* (cf. Equation 2-5).

$$SEA = \frac{EA}{m}$$
(Equation 2-5)

High specific energy absorption values are an important indicator for lightweight engineering also.

2.7 Resource efficiency

From an industrial viewpoint, resources are the basis for the production of goods. According to VDI-ZRE 2011, resources can be divided into economic resources (personnel, equipment and machinery, financial means, knowledge) and natural resources (renewable and non-renewable raw material, energy). Efficiency is defined as achieving a desired result without wasting resources.

Within this work, the focus is on a more efficient use of natural resources. The two main levers for increasing resource efficiency in an industrial setting might be seen in product optimisation and process optimisation respectively. Product optimisation aims at designing goods that provide a potential for material and energy savings in use. A lighter B-pillar within a car on the road is a typical example for product optimisation. Process optimisation is about saving energy and material during the manufacturing of goods. Lower press loads and reduced cycle times can for instance be seen as a means of reducing energy consumption during forming and thus increasing resource efficiency [17].
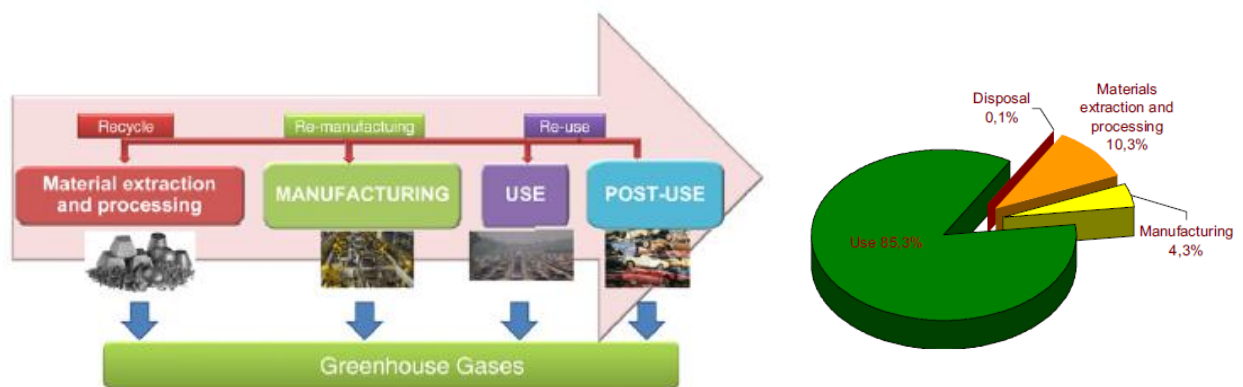
Figure 2-20: *Percentage distribution of greenhouse gas emissions during the life-cycle of a car* [6]

Ingarao et al. [6] have reported that about 85 % of the greenhouse gas emissions during the life-cycle of a car occur when it is driven on the road (cf. Figure 2-20). Against this background, lightweight engineering can be seen as a key contributor to increasing resource efficiency in the automotive industry. Still, the emissions deriving from the other stages of the vehicle's life cycle should not be neglected and thus methods in order to conscientiously decrease them must be developed. A powerful tool to allow for optimisation during manufacturing is the creation of energy- and material flow based system descriptions (cf. Section 4.11).

3 Research design

This chapter shall give an overview of the research design for the master thesis. First, the research purpose is presented and several delimitations are made with respect to alloys and process routes to be investigated. Second, the precise task is specified by research questions and the approach to assess these questions is described.

3.1 Research purpose

The purpose of this thesis is to examine process chains for the production of automotive structural parts from EN AW-7xxx aluminium sheets. Both, the materials science perspective and a view from the resource efficiency side shall be used to assess selected process routes for possible industrial application. The focus of this research will be on the process step of sheet metal forming. Beyond that, the subsequent joining operation, the natural ageing as well as the artificial ageing behaviour during paint baking will be investigated. The research target is complemented by a study on how different process chains differ with respect to their energy absorption behaviour of test crush elements.

In order to make the topic researchable within the scope of a master thesis, it will be narrowed down to an examination of the modified EN AW-7021-V2 alloy and the EN AW-7075 alloy. While Al-Zn-Mg-Cu alloys like EN AW-7075 promise better post-forming strength and are less susceptible to stress-corrosion cracking, Al-Zn-Mg alloys like EN AW-7021 have the advantage of being less quench sensitive and can be joined through welding more easily. By means of comparing the alloys EN AW-7021-V2 and EN AW-7075, two important groups of heat treatable AW-7xxx alloys are covered [4, 13].

The two main process routes that have been chosen for this research are the W-temper forming and hot forming process chains (cf. Section 2.5). These two process routes are of particular interest because of their similarity to already existing industrial solutions. Except its additional pre-forming heat treatment, W-temper forming closely resembles the cold forming process for medium-strength aluminium alloys. Hot forming process chains are already in place for steel [4].

Recent research has shown that low-temperature pre-ageing heat treatments might result in a stable condition with good formability and joinability through self-pierce riveting for the EN AW-7021 alloy [13]. Therefore, this thesis shall also investigate how W-temper forming and hot forming can be supplemented by process modifications with regard to an additional stabilisation heat treatment for the EN AW-7021 alloy (cf. Section 2.5.5). Having the sheets or the formed parts in a stable condition might be a promising way to enhance resource efficiency and facilitate logistics.

3.2 Research approach

The precise research task is defined by the questions below. These research questions (RQ) are followed by the used research approach, respectively. RQ 1 to 3 are addressed by a quantitative, experimental approach.

(RQ 1) How do the alloys EN AW-7021 and EN AW-7075 perform in terms of **formability** *when being processed with the strategies of hot forming (HF), W-temper forming (WTF) and post stabilisation forming (PSF)? (Note: HF and HF-S do only differ after forming.)*

Formability of the different process chains is primarily assessed through tensile testing. Samples to be tested are in the same state as during the actual forming operation. Results are analysed using the material properties commonly displayed by stress-strain curves. Beyond that, strain rate sensitivity during elevated temperature forming is characterised. Visual assessment of formed parts is used to judge the process chains with respect to dimensional accuracy, cracks and spring back behaviour. For the hot forming process chain, thermocouples are mounted on test sheets to record the temperature intervals run through during hot forming. Quenching rates from cold die-quenching are compared to water quenching rates and critical cooling rates from literature respectively.

(RQ 2) How do **material properties** *of the alloys EN AW-7021 and EN AW-7075* **change along the process chains** *of HF, HF-S, WTF and PSF?*

The change of material properties along the process chains is assessed using hardness measurements, differential scanning calorimetry (DSC) and tensile testing. All samples are taken from the side-wall section of formed parts (cf. Section 4.3). Natural ageing behaviour is observed during a 21 day time span, starting directly after forming. A comparison of hardness values with DSC phase transformation peaks is used to ascertain integrity of conclusions drawn. Tensile testing is done at different strain rates. Tensile samples have either been naturally aged for 21 days or have undergone tempering. A central output of tensile testing is how the process chains differ with respect to their paint bake response. Strain-rate dependency of the materials at the end of the processes is another property that tensile testing seeks to investigate. Apart from tracking the change of material properties along the different process chains, joinability of the hot forming and W-temper forming strategies is assessed through the preparation of rivet cross sections.

(RQ 3) How do test crush elements from EN AW-7021 and EN AW-7075 that have been produced with the process routes of HF, HF-S, WTF and PSF differ with respect to their **energy absorption behavior***?*

Energy absorption behaviour of formed and joined test parts is determined through quasi static crush testing. Force-length diagrams are recorded for the parts processed with different process routes. Out of these diagrams, parameters like crush force efficiency (CFE) and specific energy absorption (SEA) are calculated. A visual assessment of the parts' folding and cracking behaviour is also used.

RQ 4 is addressed by a qualitative approach.

*(RQ 4) How suitable is the process chain that promises highest resource efficiency during end use to also **save resources** during **production**? (Note: Resource efficiency during end use can be related to high specific energy absorption.)*

The systems thinking principle (Black-Box approach) is used to develop a material and energy flow based process description of a selected process route. By means of qualitatively discussing relevant system in- and outputs, a first overview on the potential of resource efficiency during production is given. In order to ensure consistency of conclusions drawn, the evaluation will build upon observations made by RQ 1 to 3.

4 Materials and methods

Within this chapter, the materials and methods used to assess the research questions presented in Chapter 3 are explained.

4.1 Investigated aluminium alloys

The sheets used within this work are the EN AW 7021-V2 sheet in T4 condition and the EN-AW 7075 sheet in T6 condition with a thickness of 2 mm each. The chemical composition in percent by weight (wt. %) of these two sheets is shown in Table 4-1.

Table 4-1: Chemical composition of sheets used in wt. % [13]

	Al	Si	Fe	Cu	Mn	Mg	Zn	Ti	Cr	Rest
AW 7021-V2 T4	rest	max 0.25	max 0.4	max 0.16	max 0.1	1.6 – 2.1	6.0 – 6.8	max 0.1	max 0.05	max 0.5
AW 7075 T6	rest	0.19	0.11	1.50	0.04	2.64	6.06	0.04	0.18	max 0.5

Although the Zn content of the investigated EN-AW 7021-V2 alloy slightly exceeds the composition limit of a standard EN-AW 7021 alloy, it is referred to as EN-AW 7021 within this work [13].

4.2 Investigated process chains

The process chains investigated by this thesis are hot forming (HF), W-temper forming (WTF), hot forming with subsequent stabilisation (HF-S) and post stabilisation forming (PSF). In the following, the temperature-time process sequence as it has been used within this work is presented.

4.2.1 Hot forming (HF)

Figure 4-1 shows the temperature-time curve for the hot forming process chain. Hot forming was carried out for both, the AW-7021 and the AW-7075 alloy. First, the furnace was heated to solution heat treatment temperature which lies at 515°C for AW-7021 and 480°C for AW-7075. As soon as the furnace had reached the necessary temperature, the blanks were inserted. The blank temperature was monitored using thermocouples. When the blanks had reached their solution heat treatment temperature, they were kept in the furnace for another 5 min (AW-7021) or 15 min (AW-7075). Thereafter the non-isothermal hot forming was conducted. The formed parts were joined through self-pierce riveting within a time span of up to 1 hour after forming and stored for 21 days until eventually being paint baked (1SPB: 185°C, 25 min) or peak aged (PA: 120°C, 24 h). Cooling after the 1SPB and PA heat treatments occurred using cooling air of a fan.
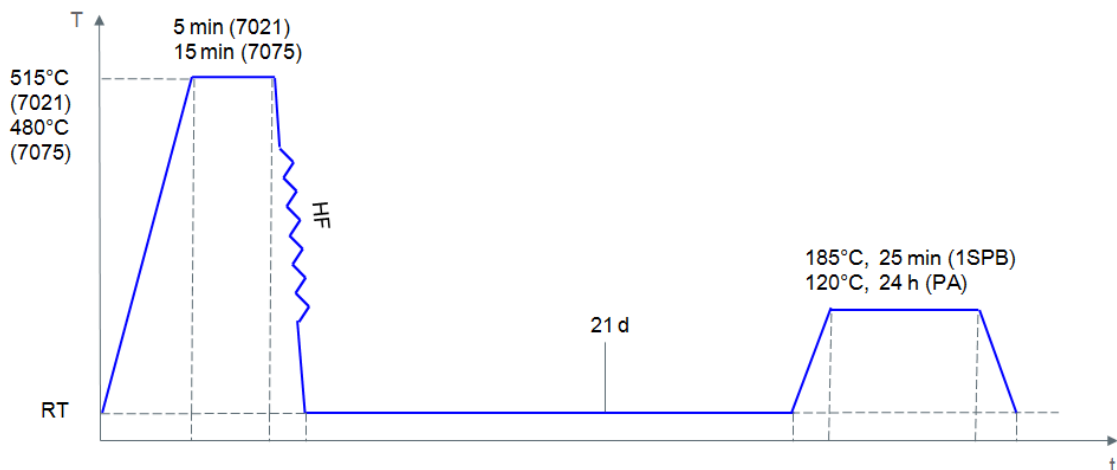
Figure 4-1: *Temperature-time process sequence for hot forming (AW-7021, AW-7075)*

4.2.2 Hot forming with subsequent stabilisation (HF-S)

The process sequence for hot forming with subsequent stabilisation is depicted in Figure 4-2. This process chain was only run through for the AW-7021 alloy. Stabilising at 80°C for 1h was chosen to study the influence of an additional low temperature pre-ageing heat treatment on process chain level. Due to an internal project decision, the stabilisation heat treatment was lowered by 10°C compared to what Österreicher et al. [13] have found (cf. Section 2.4.5). This is because it was assumed that proper self-pierce riveting should be possible more accurately after stabilising with lower temperatures due to potentially lower hardness values. The hardness evolution after stabilising with 80°C for 1h was recorded retrospectively and can be found in Section 5.2.1. The stabilisation heat treatment was carried out directly after forming and die quenching. The joining operation was performed 7 days after stabilising. Storage time

with 21 days after cooling from 80°C/ 1h and artificial ageing heat treatment conditions were the same as before.
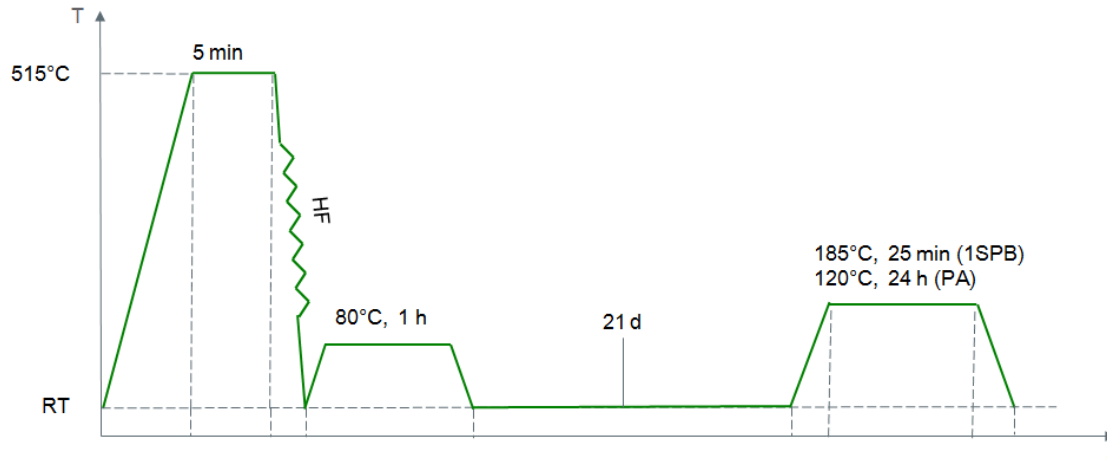
Figure 4-2: *Temperature-time process sequence for hot forming with subsequent stabilisation (AW-7021)*

4.2.3 W-temper forming (WTF)

W-temper forming as shown in Figure 4-3 was investigated for both alloys. Quenching in a water bath was used to maintain the sheets in the supersaturated solid solution. The sheets were dried and formed in the W-state within less than 1 hour after quenching. Joining, storage and artificial ageing occurred under the same temperature-time conditions as for the hot forming process chain.
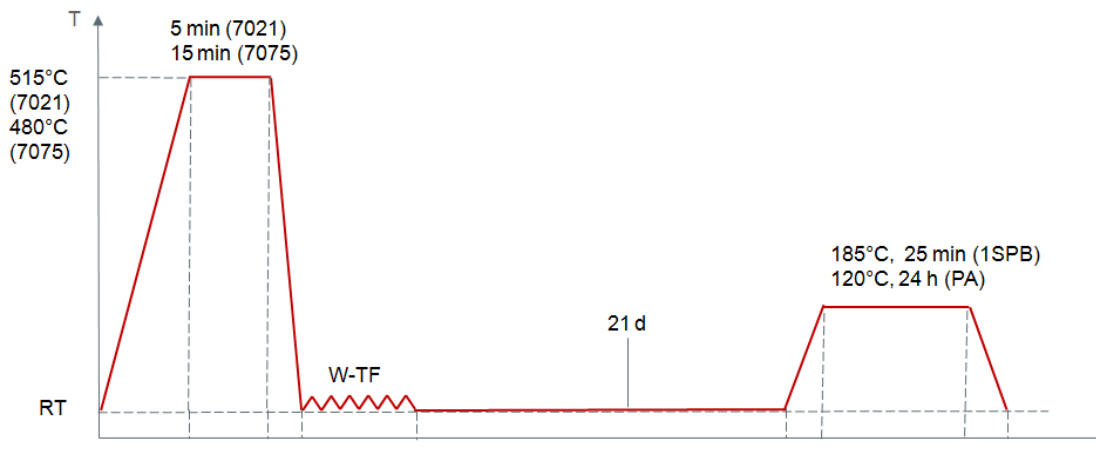
Figure 4-3: *Temperature-time process sequence for W-temper forming (AW-7021, AW-7075)*

4.2.4 Post stabilisation forming (PSF)

Figure 4-4 illustrates the temperature-time process sequence for post stabilisation forming of the AW-7021 alloy. Solutionising, quenching in the water bath, stabilising at 80°C/1h and conducting a 1SPB or PA heat treatment were performed just as already

explained for the other process chains. Since the sheets were in a stable state prior to forming, this step was not as time-critical as for the WTF process chain. In that sense, forming was postponed and carried out 7 days after solutionising. Joining was conducted right after post stabilisation forming. The remaining storage interval until artificial ageing was 14 days then.
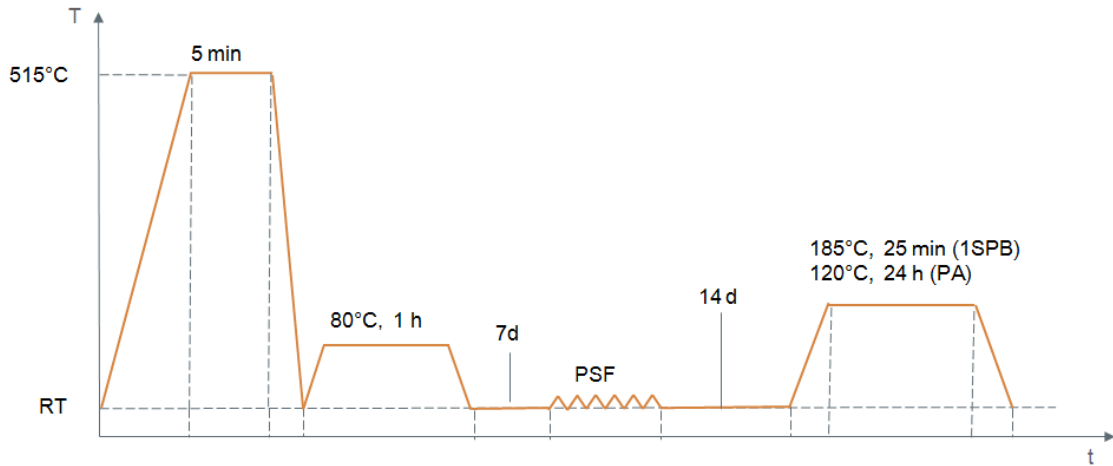
Figure 4-4: *Temperature-time process sequence for Post stabilisation forming (AW-7021)*

4.3 Sheet metal forming of top-hat profiles

Sheet metal forming of top-hat profiles was used to qualitatively evaluate forming characteristics of the different process chains and eventually produce crush test parts. Forming was carried out in a 1.6 MN hydraulic press with square blanks of 300 mm x 300 mm in size. The geometry of the test profiles is depicted in Figure 4-5. It includes the cover plate which was joined to the profiles after forming in order to conduct the quasi-static crush tests. The nomenclature of bottom area, side-wall section and flange area as shown below will be used to refer to the part geometry in the following.
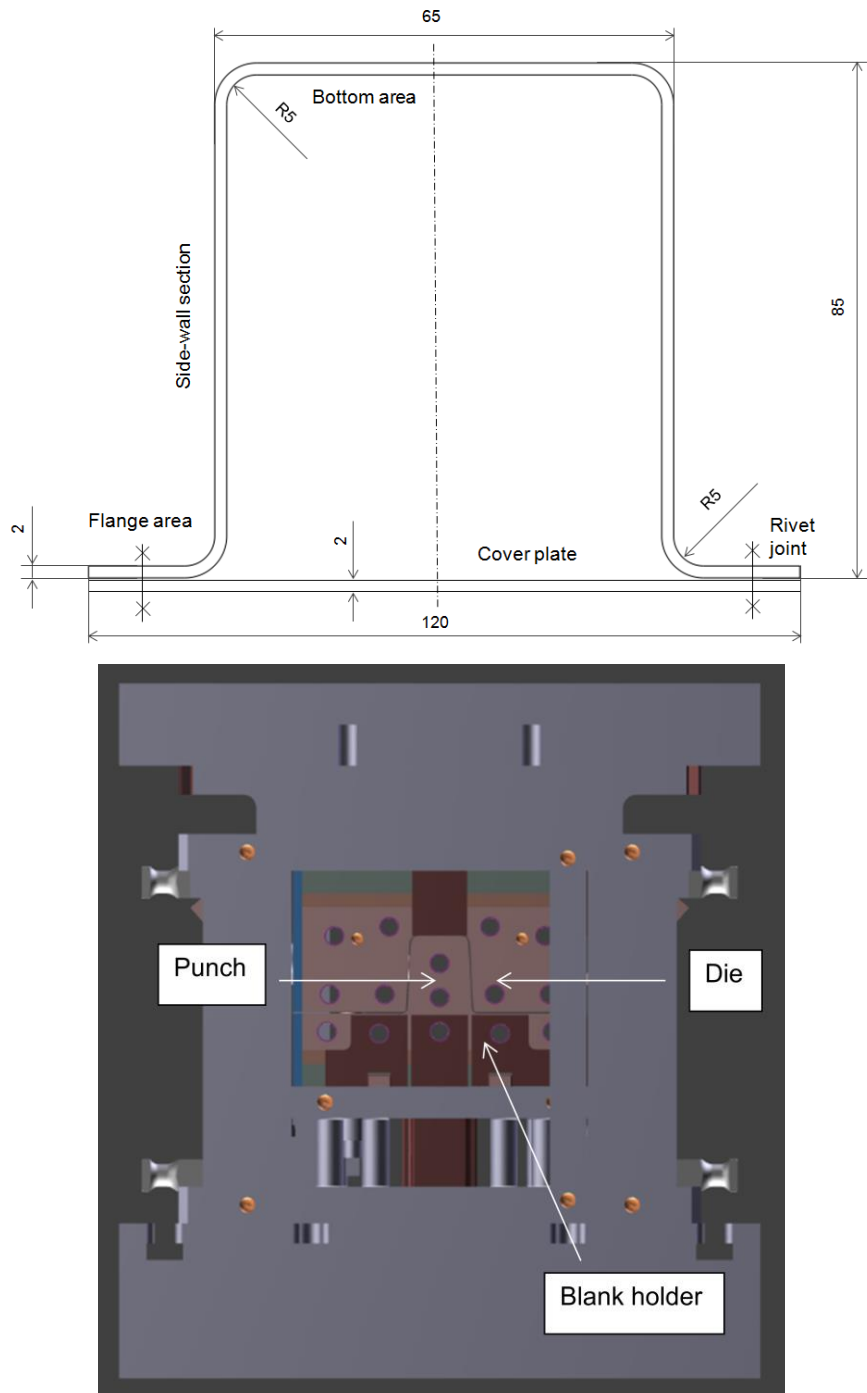
Figure 4-5: Cross section of formed top-hat profiles and corresponding test tool

The corresponding tool can be seen as well in Figure 4-5. The upper part contains the die with a cavity to fit the punch at the lower part. The blank holder is situated at the lower part of the tool. During forming, the die would move downwards to draw the blank over the fixed punch. Die, punch and blank holder all contain cooling channels that have been flushed with cold water during hot forming.

Before forming, the tool was lubricated using a white high-temperature paste. The blanks were inserted manually into the tool with their rolling direction lying parallel to the longitudinal tool axis. They were positioned along the punch with the help of two centring marks on the blanks. Thereafter the die moved into the punch for 85 mm with a speed of 50 mm/sec. No blank holding force was applied in order to reduce spring back after forming.

For hot forming, it would take approximately 20 to 25 seconds from taking the blanks out of the furnace until the start of die quenching. During transfer, the sheet lost approximately 70°C for the AW-7021 alloy and 55°C for the AW-7075 alloy as could be shown by thermocouple measurements (cf. Section 5.1.2).

For the W-temper process, forming was carried out immediately after water quenching and after 1 day of natural ageing. Post stabilisation forming was done 7 days after applying the stabilisation heat treatment to the blanks. Table 4-2 summarises the experimental setup used for sheet metal forming.

Table 4-2: Experimental setup for sheet metal forming

Parameter	Value
Test device	Neff DZP 160, Top-hat profile tool
Blank holding force	0 kN
Die speed	50 mm/sec
Drawing depth	85 mm
Lubricant	Molyduval Moralub FSZ – White high-temperature paste
Sheet thickness	2 mm
Blank outline	300 mm x 300 mm, 0° rolling direction along the longitudinal tool axis

4.4 Quenching rate determination

The sheets were heated to their solution heat treatment conditions and subsequently either quenched in a water bath (water quenching) or in the cold dies during hot forming (cold die quenching). Temperature was recorded using type K thermocouples and an EBI 40 temperature logger. For water quenching, the thermocouples were fixed to the blank surface. For cold die-quenching, two small holes have been drilled into the blanks in rolling direction. The position of the holes were chosen to be just in the centre of bottom and flange area respectively. Three measurements were carried out for each alloy to ensure reproducibility. Figure 4-6 illustrates the measurement setup.
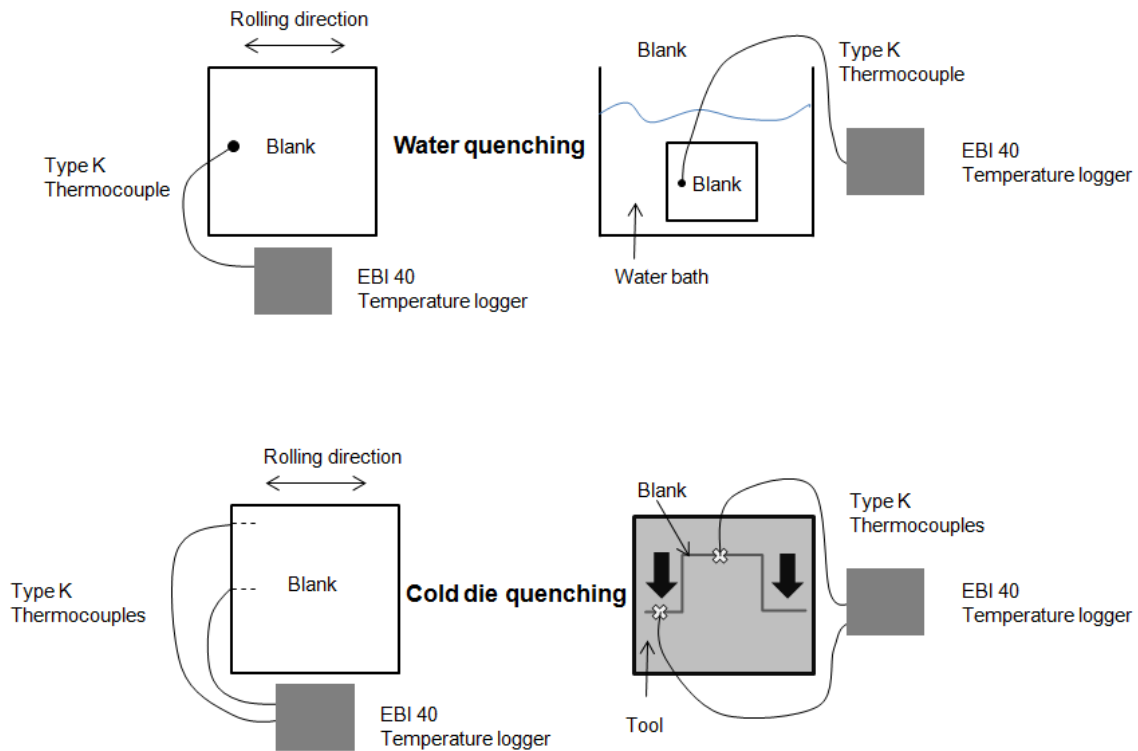
Figure 4-6: Schematic depiction of the test setup used for determining quenching rates

4.5 Tensile testing of forming states

Tensile testing was used to quantitatively evaluate forming characteristics of the different process chains. Tensile testing was conducted using a "Bähr DIL 805A/D" dilatometer. The test setup including the geometry of tensile samples used is shown in Figure 4-7. The sample is surrounded by an induction coil which heats the sample to test temperature. Temperature is recorded by two thermocouples. The displacement measuring system can be seen in the right half of the test device. It consists of a quartz sensor measuring elongation change and an inductive transducer for generating a digital signal. The change in force is measured by a load cell.

Tensile samples have been taken from the undeformed sheets in the as-delivered condition or stabilised state respectively. The longitudinal sample axis was parallel to 0° rolling direction. Tests have been carried at two strain rates (0.01 sec^{-1}, 1 sec^{-1}) and 3 measurements have been conducted per forming state to ensure reproducibility.
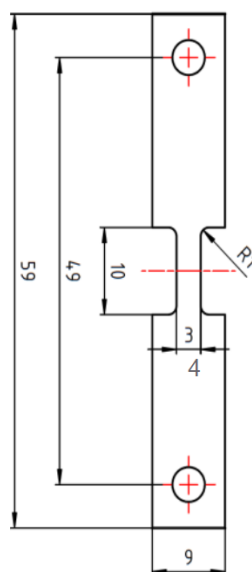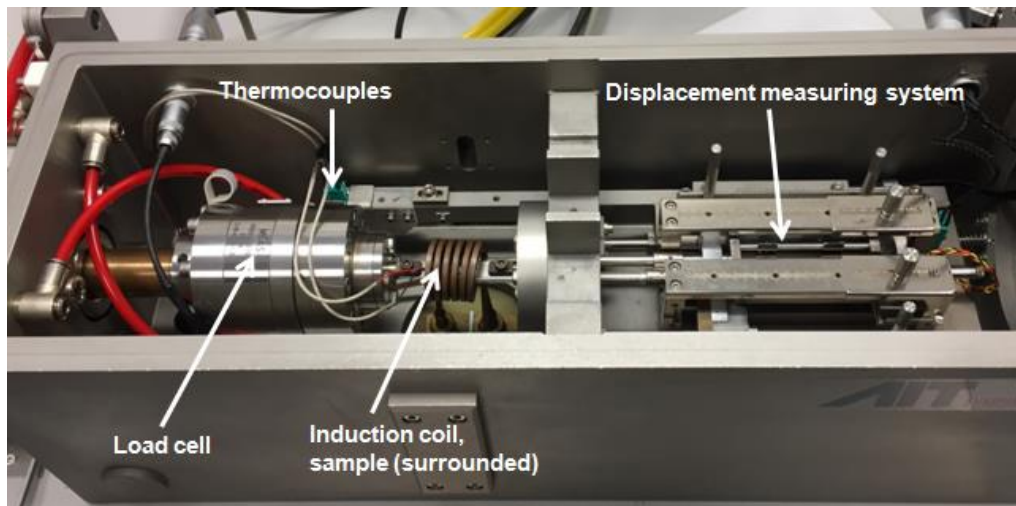
Figure 4-7: "Bähr DIL 805A/D" dilatometer and corresponding tensile sample geometry

As shown in Section 5.1.2, the temperature intervals run through during hot forming are between 440-140 °C for the AW-7021 alloy and between 420°C-120°C for the AW-7075 alloy. Four temperatures from these intervals have been chosen for each alloy to assess forming characteristics during hot forming. The samples were heated to these test temperature within 6 seconds, held at this temperature for another 4 seconds and subsequently tested.

For W-temper forming, the samples were heated to solution heat treatment temperature (AW-7021: 515°C, AW-7075: 480°C) with a heating rate of 10 °K/sec, held at this temperature for 5 min (AW-7021) and 15 min (AW-7075) respectively and eventually quenched with 200 K/sec. The test time was chosen to be immediately after quenching or after a natural ageing period of 1 day respectively. For both, hot forming and W-temper forming the heat treatments were carried out directly within the dilatometer.

For post stabilisation forming, the solution and stabilisation heat treatment was performed outside of the dilatometer prior to machining the samples. The samples were tested at room temperature in the stabilised state.

For reference purpose, additional tests at room temperature of samples in the as-delivered T4 (AW-7021) and T6 (AW-7075) condition were carried out. Table 4-3 summarises the parameters used for tensile testing of forming states.

Table 4-3: Test parameters for tensile testing of forming states

| Parameter	Value
Test device	Bähr DIL 805A/D
Sample geometry	8 mm (reduced section length) x 3 mm (reduced section width); longitudinal sample axis parallel to 0° rolling direction
Strain rates	0.01 sec^{-1}, 1 sec^{-1}
Test temperatures HF 7021	140°C, 240°C, 340°C, 440°C
Test temperatures HF 7075	120°C, 220°C, 320°C, 420°C
Test state WTF 7021, WTF 7075	W state (W), W & 1 day natural ageing state (W&1d na)
Test state PSF 7021	Stabilised state (S)
Test state reference measurements	T4 (AW-7021), T6 (AW-7075)

4.6 Hardness testing

Natural ageing and artificial ageing behaviour of the different process chains was studied using hardness testing according to Brinell. The assessment was done for the side-wall section of formed top-hat profiles. Test times were 1h, 2h, 3h, 4h, 1d, 7d, 14d and 21d after forming for the natural ageing behaviour. For reference purpose, additional measurements of undeformed samples in the W and S state were carried out. The artificial ageing behaviour was studied after 1 step paint baking (1SPB) and after peak ageing (PA) respectively. The test parameters used are summarised in Table 4-4.

Table 4-4: Test parameters for hardness testing

Parameter	Value
Test device	Instron Wolpert DIA-Testor
Method	Brinell hardness (HBW 2.5/62.5)
Assessment region	Side-wall section
Natural ageing test times	1h, 2h, 3h, 4h, 1d, 7d, 14d and 21d after forming
Artificial ageing test states	1SPB, PA

Figure 4-8 illustrates the experimental setup used for hardness testing. The hardness values were determined automatically by the test device. A test force of 62.5 kp and a sphere diameter of 2.5 mm were used to create the indentation. A total of three indentations per test time or state were performed respectively.
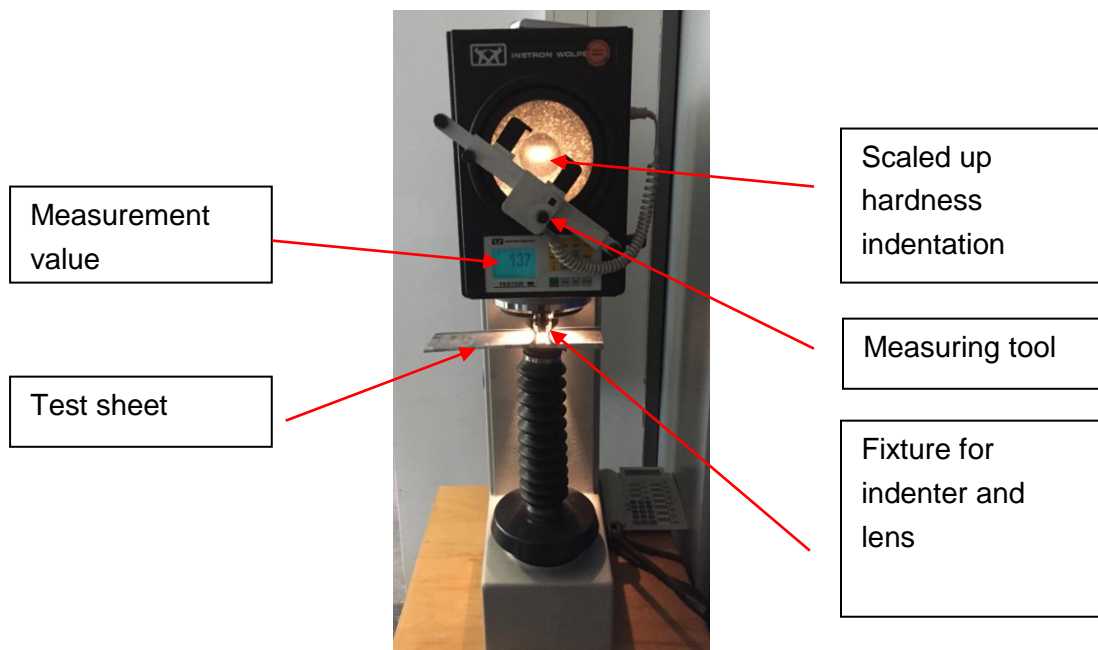
Figure 4-8: Experimental setup used for hardness testing

4.7 Differential scanning calorimetry (DSC)

Differential scanning calorimetry experiments were performed using the heat-flow based DSC Netzsch 204 F1 test device. Table 4-5 gives an overview on the test parameters used.

Table 4-5: Test parameters for differential scanning calorimetry measurements

Parameter	Value
Test device	DSC Netzsch 204 F1
Method	Heat flow based measurement
Heating rate	10 K/sec
Heating interval	25 °C - 600 °C
Sample geometry	ø 2 mm x 2 mm
Assessment region	Side-wall section
Natural ageing test times	1h and 21d after forming
Artificial ageing test state	1SPB

The samples were taken from the side-wall section of formed parts. Test times were 1h and 21d after forming in order to judge the natural ageing behaviour. The artificial ageing behaviour was assessed after 1 step paint baking (1SPB). For reference purpose, additional measurements of samples taken from undeformed sheets in the W state were carried out. All samples had a cylindrical geometry with dimensions of ø 2 mm x 2 mm. Each of them was placed into a pan and then heated separately from room temperature to a final temperature of 600°C using a heating rate of 10 K/sec. An empty reference pan was heated along with the test samples and the exchanged heat flow between the two pans was measured. Two temperature vs. heat flow curves per test time or state were recorded to ensure reproducibility of conclusions drawn. Figure 4-9 illustrates the experimental setup.
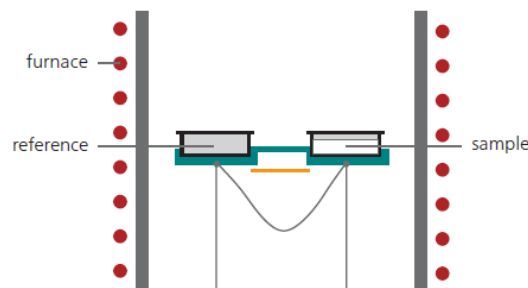
Figure 4-9: Schematic depiction of the DSC test setup used [18]

In order to avoid mistakes when assessing the precipitation sequence, a baseline correction has been conducted for the recorded curves. In the course of a baseline

correction, a measurement of pure aluminium is subtracted from the sample measurement. The obtained curves are then more likely to be free from device-specific errors [9]. As it happens quite frequently that the curves still show some kind of curvature after subtracting the pure aluminium measurement, they further need to be zero-level corrected. Zero-level correction is conducted by subtracting a polynomial from the already manipulated curve. In that way, the intensity of precipitation reactions can be interpreted correctly. The dissolution of precipitates can then easily be identified in the form of positive, endothermic peaks and the formation of precipitates in the form of negative, exothermic peaks respectively. Figure 4-10 exemplarily shows the data handling procedure for the 7021 W sample. The subtracted polynomial was a third degree polynomial, just as for all the other evaluated measurements. For comparison reasons, the recorded heat flows ($\dot{Q}_{sample}$, $\dot{Q}_{baseline}$) have been divided through sample mass m and heating rate β to obtain excess specific heat capacity c_p (cf. Equation 4-1). This guarantees that the results can be compared amongst each other and with other publications respectively.

$$c_p = \frac{\dot{Q}_{sample} - \dot{Q}_{baseline}}{m * \beta} \qquad \text{(Equation 4-1)}$$

For more detailed considerations on how to perform a baseline correction, it is referred to Osten et al. [19] at this point.
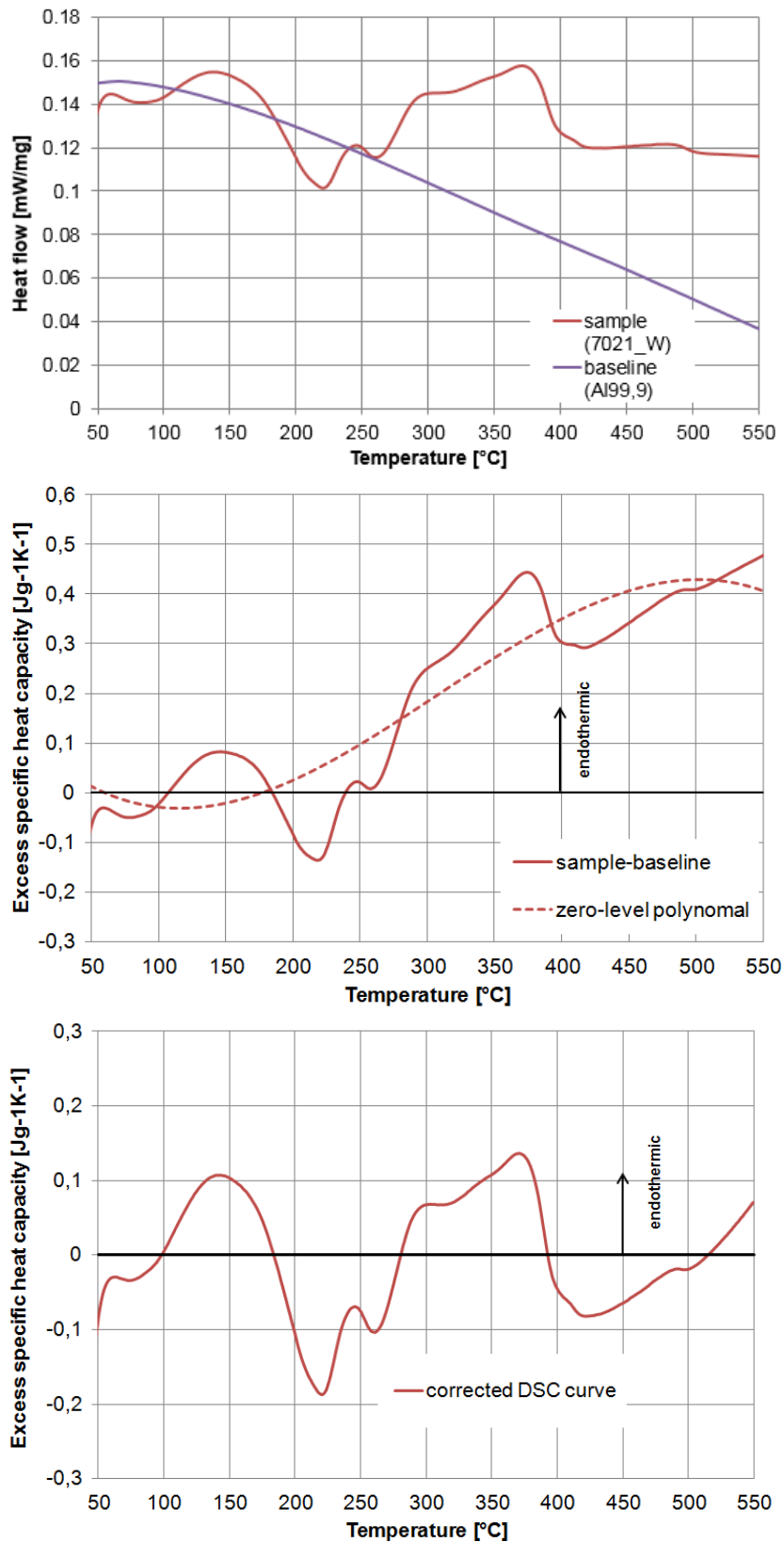
Figure 4-10: *Data handling procedure to obtain a baseline and zero-level corrected DSC curve using the 7021 W curve as an example*

4.8 Tensile testing of samples from the side-wall section of formed parts

Tensile samples were machined from the side-wall section of formed top-hat profiles (parallel to 0° rolling direction) in order to evaluate post-forming strength and ductility. Figure 4-11 depicts the location and the orientation within the formed parts that tensile samples have been taken from.
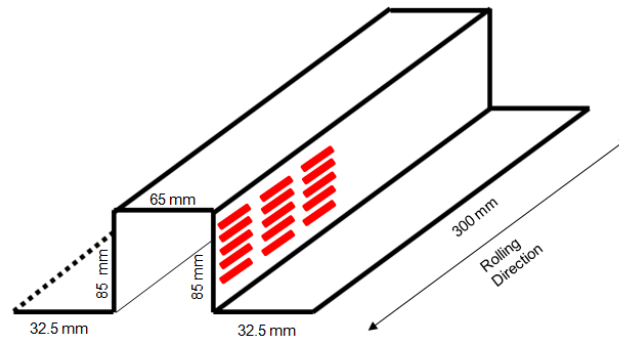
Figure 4-11: *Location and orientation of tensile samples within the formed parts*

Samples were tested after 21 days of natural ageing. Some of the samples were further heat treated using 1 step paint baking (185°C, 25 min) or peak ageing (120°C, 24 h) cycles respectively. Test strain rates were chosen to be 0.01 sec^{-1} and 1 sec^{-1}. The tests have been carried out at room temperature using a "Bähr DIL 805A/D" dilatometer. A description of this test device as well as the specification of the corresponding sample geometry are given in Section 4.3. For reference purpose, additional tests of samples taken from undeformed sheets were conducted. The reference samples were in the as-delivered T4 (AW-7021) or T6 (AW-7075) condition respectively. The change of mechanical properties as the sheets pass through the process chains was eventually assessed averaging the data of 3 measurements per process step. Test parameters are summarised in Table 4-6.

Table 4-6: *Test parameters for tensile testing of samples from the side-wall section of formed parts*

Parameter	Value
Test device	Bähr DIL 805A/D
Sample geometry	8 mm (reduced section length) x 3 mm (reduced section width); longitudinal sample axis parallel to 0° rolling direction; cf. Section 4.4
Strain rates	0.01 sec^{-1}, 1 sec^{-1}
Natural ageing test state	21d after forming
Artificial ageing test states	1SPB, PA
Test state reference measurements	T4 (AW-7021), T6 (AW-7075)

4.9 Preparation of rivet cross sections

Tests have been conducted combining Böhlhoff C-SKR type rivets of hardness class H4 with the FM die geometry as illustrated in Figure 4-12. Test stripes taken from the flange area of formed parts have been joined with EN AW-6016-T4 FH sheets of 2 mm thickness. The former were used as the lower sheet while the latter as the upper. EN AW-6016-T4 FH blanks would eventually also be used as cover plates to increase buckling resistance of test crush parts.
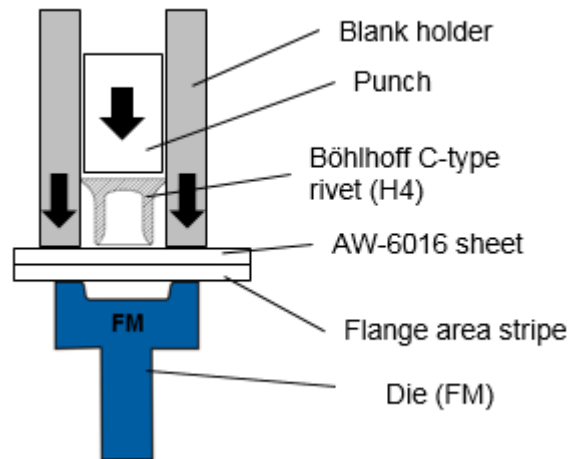
Figure 4-12: Test setup used for self-pierce riveting

Self-pierce riveting has been carried out within a time span of up to 1 hour after forming. Rivet insertion occurred in a stroke-controlled way. Criteria used for assessing joint quality were visual ones. Cross sections of the rivet joints have been prepared and the process chains were judged according to geometric parameters like undercut (u_1, u_2), residual wall thickness t_r and rivet head end position s_{rh}. For a detailed description on these geometric parameters, see Section 2.6.1.

4.10 Quasi-static crush testing

Quasi-static crush testing was performed on the servo-hydraulic ITC 255 device with a maximum punch force of 1000 kN. The formed and joined top-hat profiles were placed between two plane-parallel steel plates and compressed for 120 mm with a constant speed of 10 mm/sec. All samples had an initial part length of 295 mm and were tested in the 1SPB state. Punch force and punch displacement were recorded in order to quantitatively evaluate crushworthiness of the different process chains. Three measurements were carried out per process chain respectively. Figure 4-13 illustrates the test setup. The cross-section of the compressed samples is displayed in Section 4.3.

Figure 4-13: Test setup used for quasi-static crush testing

A summary of the test parameters is shown in Table 4-7.

Table 4-7: Test parameters for quasi-static crush testing

Parameter	Value
Test device	ITC 255 press with a maximum punch force of 1000 kN
Initial part length	295 mm
Crush length	120 mm
Test speed	10 mm/sec
Test state	1SPB

4.11 Energy and material flow based system description

In engineering, it is common to describe systems and processes through mathematical calculations and/or experimental investigations. This analytical way of tackling problems aims at identifying all possible connections of single system or process elements as closely as possible. Such an approach might be misleading though, when trying to analyse larger, more complex processes or even process chains with respect to their resource efficiency balance. In order to allow for an adequate reduction of complexity, the so-called Black-Box approach (systems thinking) can be used. The Black-Box approach deliberately neglects the detailed, inner relationships of a process, it rather focuses on creating an overall description of process reactions through in- and outputs [17].

Figure 4-14 illustrates how the systems thinking principle can be applied to forming process chains. Every process step can be regarded as a Black-Box. Within such a Black-Box, inputs are transformed into outputs through the help of process support factors. Influencing factors control and disturb the transformation process, so that outputs may vary even if process input and support are the same. The different process steps are linked to form a continuous process chain since outputs of preceding process steps may serve as an inputs for subsequent ones [17].
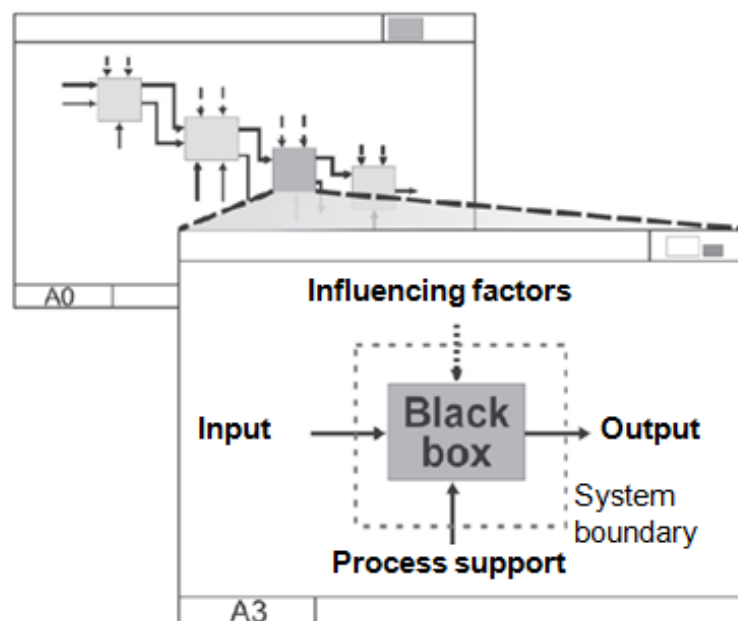
Figure 4-14: *Black-Box principle for the description of forming process chains* [17]

In order to a allow for a system description from a resource efficiency viewpoint, process in- and outputs represent energy and material flows within this work. These material and energy flows leave the system boundary in a transformed way in the form of products or emissions respectively. Tangible, intangible and human process support enable the transformation. They are not consumed during the transformation though,

but are rather available for a repeated execution of the respective process step. Influencing factors such as command and disturbance variables steer the transformation process and need to be tracked carefully so as to achieve the desired outputs [17]. Figure 4-15 shows the classification of input, output, process support and influencing factors used to describe forming process chains from a resource-efficiency perspective.
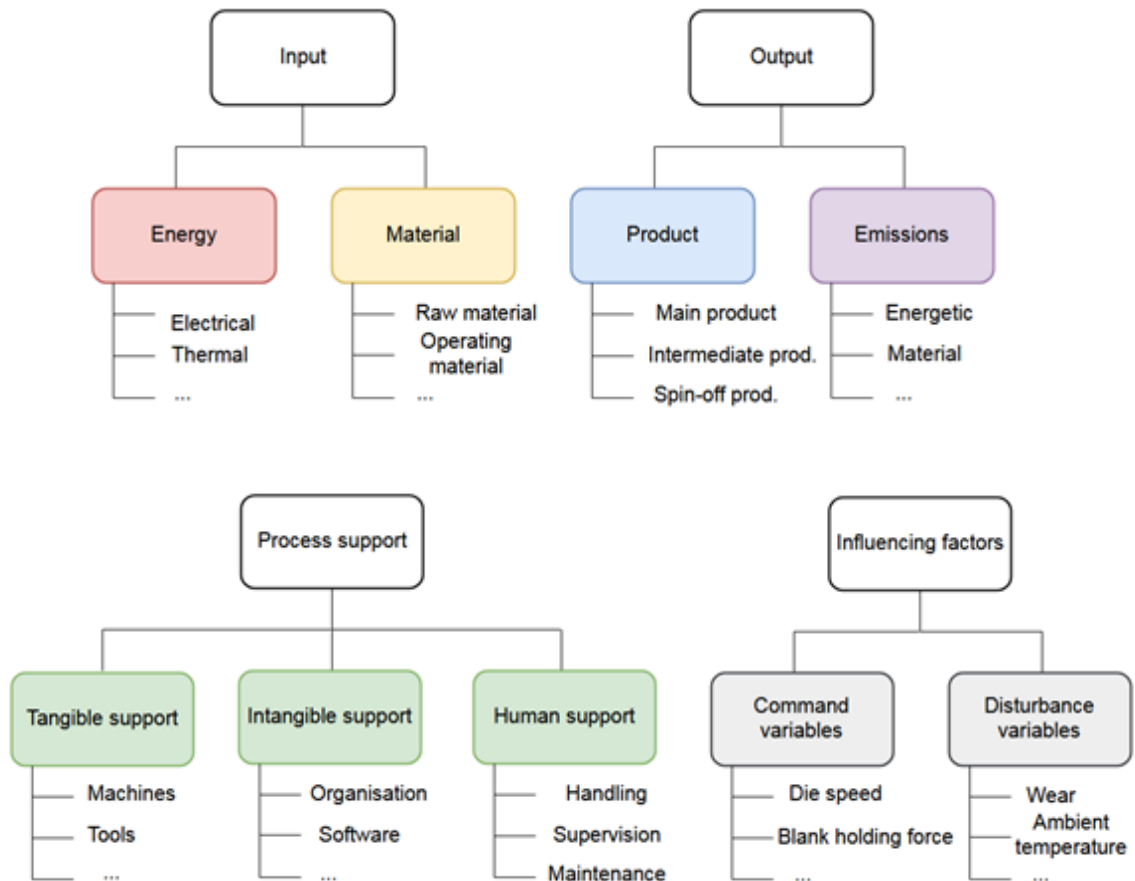
Figure 4-15: *Classification of input, output, process support and influencing factors*

5 Results and discussion

The results gained from the investigations presented in Chapter 4 are described below. A discussion with regard to relevant theoretical concepts or previous measurements has been included in the respective explanations.

5.1 Formability

The comparison of formability for the process chains dealt with in this thesis mainly occurred through uniaxial tensile testing. In addition, dimensional accuracy and fracture behaviour was studied through visual assessment of formed prototype parts. For the hot forming process chains, the quenching rates during die-quenching have been recorded and compared to conventional water quenching.

5.1.1 Visual assessment of formed top-hat profiles

The results from the visual assessment of formed top-hat profiles are presented in Table 5-1. A description of the corresponding experimental setup can be found in Section 4.3.

For the hot forming process chain, parts with a linear side-wall section and no spring back in the flange area could be formed with both, the AW-7021 and the AW-7075 alloy. W-temper forming yielded parts with spring back in the flange area. For W-temper forming of the AW-7075 alloy, dimensional accuracy was worse than for the AW-7021 alloy. The side-wall section was curved here and a more pronounced spring back in the flange area was observed. Interestingly enough, it is possible to form parts without fracture out of AW-7021 sheets after 1 day of natural ageing. The AW-7075 alloy in contrast tears at the transition of side-wall section and flange area after 1 day of natural ageing. For post stabilisation forming, it was not possible to obtain parts with particularly good dimensional accuracy either. The parts formed with PSF 7021 closely resemble the WTF 7075 ones.

The results of this investigation show that forming states and the associated material properties can influence dimensional accuracy significantly. At a given Young's modulus, spring back will increase with higher yield strength. This is because permanent deformation only starts at very high stress levels then. The result is that a greater proportion of the total deformation occurs elastically. As shown in Section 5.1.3, yield strength is reduced considerably during hot forming. The yield strength of the AW-7021 alloy in the W state with a value of about 110 MPa is still in a range that is suitable for producing parts with fairly good dimensional accuracy. The remaining process chains apparently have a too large elastic deformation component so that curved-side wall sections and extensive spring back in the flange area arise.

The effect of strain hardening is amongst others believed to be decisive whether a part tears or not. For post stabilisation forming (315 MPa), yield strength values are about 30 MPa higher compared to the W&1d na forming state of the AW-7075 alloy (285 MPa). For the ultimate tensile strength values however, no significant difference could be observed between these two process chains. Both process chains showed on average an ultimate tensile strength of 460 MPa. The higher yield strength to ultimate tensile strength ratio of the post forming process chain might be a reason why it was capable of producing crack-free parts, while the AW-7075 sheet would tear after 1 day of natural ageing when formed with the W-temper forming process.

Table 5-1: *Visual assessment of formed top-hat profiles*

	AW-7021	AW-7075
Hot forming (HF)		
W-temper forming (WTF) W		
W-temper forming (WTF) W & 1d na		
Post stabilisation forming (PSF)		
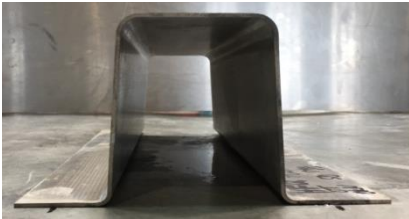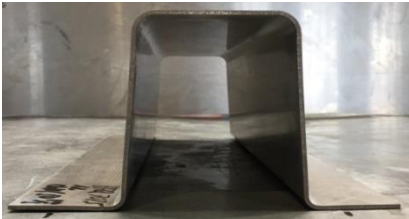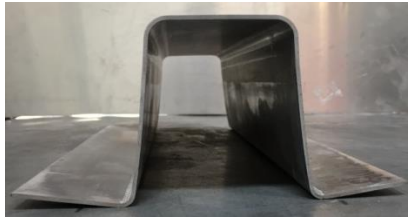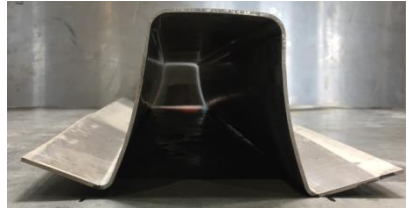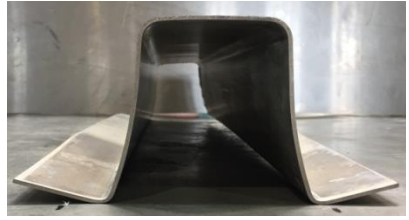
5.1.2 Quenching rate determination

Figures 5-1 and 5-2 show the cooling curves recorded for water and cold die quenching. For both alloys, the averaged curves from quenching at the flange and bottom area during non-isothermal hot forming as well as the averaged curves from water quenching are presented. A description of the corresponding experimental setup can be found in Section 4.4.

As can be seen from the diagrams, for cold die quenching it takes about 20 to 25 seconds from taking the blanks out of the furnace until the start of die quenching. The sheets lose approximately 70°C (AW-7021) and 55°C (AW-7075) during this time span. Hot forming itself takes about 3 seconds, while the critical temperature range between 400°C and 290°C is run through within roughly 0.9 seconds. This interval is generally regarded as the one most prone to producing early and undesired precipitation [2]. For AW-7021 an average quenching rate of 122 K/s and for AW-7075 of 128 K/s is achieved within the critical temperature range respectively. Quenching rates at the bottom area with 127 K/s (AW-7021) and 140 K/s (AW-7075) are priniciply higher than at the flange area with 117 K/s (AW-7021) and 116 K/s (AW-7075). This is due the longer contact of the bottom area with the tool that starts already during positioning.

For water quenching, handling times are significantly shorter and quenching starts already 5 to 7 seconds after taking the sheets out of the furnace. Temperature loss during transfer is therefore limited to 20°C (AW-7021) and 10°C (AW-7075). The critical temperature range between 400°C and 290°C is run through within 0.25 to 0.3 seconds. This eventually yields much higher quenching rates compared to cold die quenching with 448 K/s for AW-7021 and 365 K/s for AW-7075 respectively.

Beck et al. [11] have reported that the critical cooling rates are at 10 K/s for AW-7021 and 100 K/s for AW-7075. As shown above, these values are surpassed for both alloys and quenching methods so that the supersaturated solid solution is kept throughout the entire quenching event and a negative influence on paint bake response and ductility can be excluded.

A further adjustment of quenching rates to avoid unnecessary warping or residual stress has not been conducted at this point. This issue must however be addressed during the design of production lines (water quenching with spray nozzles) and during tool design respectively.
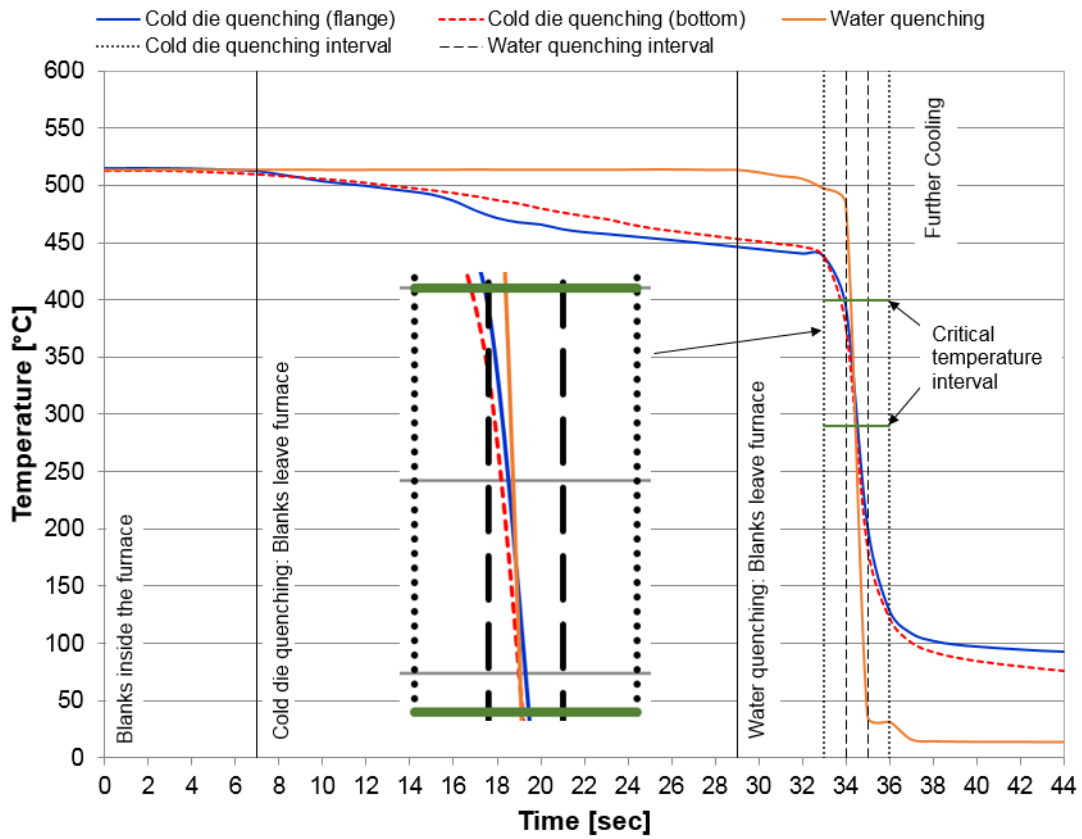
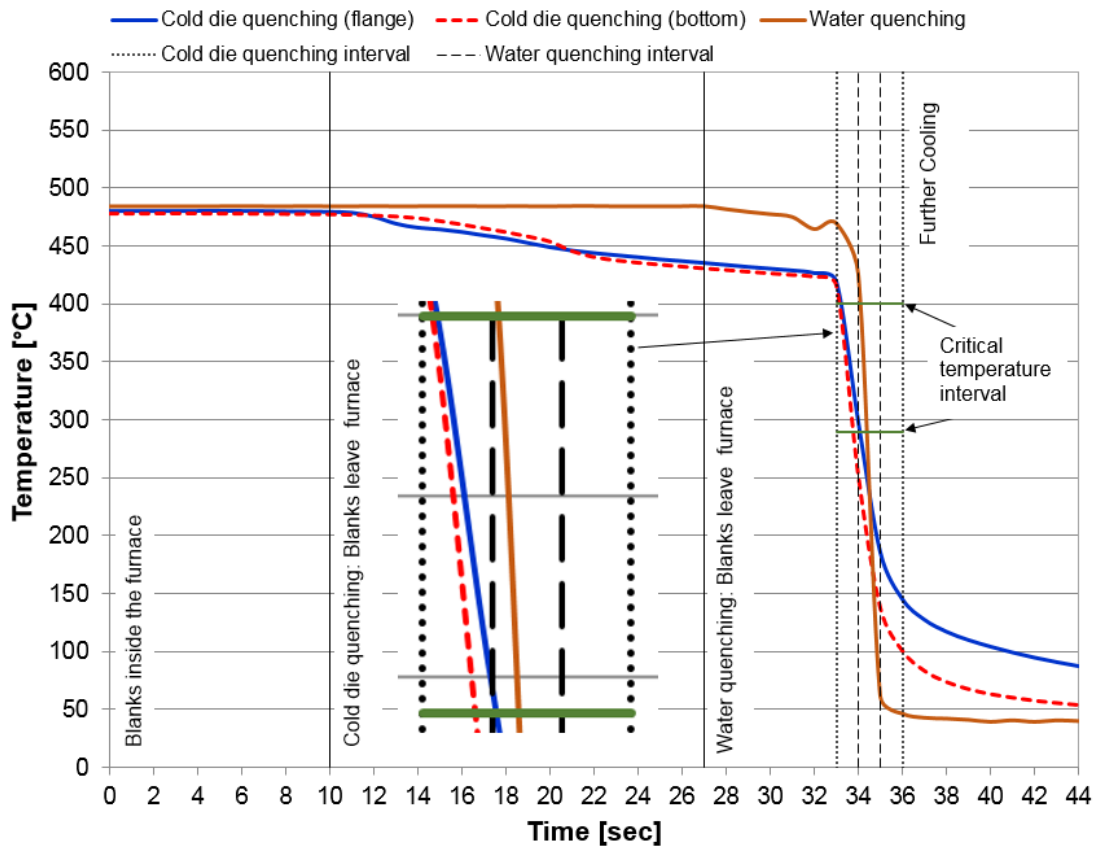**Figure 5-1:** *Water quenching and cold die quenching curves for AW-7021*

Figure 5-2: *Water quenching and cold die quenching curves for AW-7075*

5.1.3 Tensile testing of forming states

Tensile testing aimed at evaluating parameters like yield strength, ultimate tensile strength and elongation at fracture for the AW-7021 and the AW-7075 alloys in the respective forming states. Beyond that, strain rate sensitivity for the different forming states was examined through varying test speed by a factor of 100.

Figures 5-3 to 5-7 show the engineering stress-strain curves from tensile testing of the different forming states. For all process chains, reference measurements of the as-delivered condition have been included in the respective diagrams. The nomenclature used in the legend in order to refer to the curves has the following structure: Alloy_ProcessChain_FormingState_StrainRate (e.g.: 7021_HF_140_1sec^{-1}). A description of the corresponding experimental setup can be found in Section 4.5.

Stress-strain curves

Comparing the curves measured at elevated temperatures to those measured at room temperature (T4, T6, W, W&1d na, S), it becomes obvious that ultimate tensile strength is lower at the 0.01 sec^{-1} strain rate for the curves at elevated temperature. For the measurements at room temperature, it is the 1 sec^{-1} strain rate that yields lower ultimate tensile strength values. This phenomenon can be assessed quantitatively by determining the strain rate sensitivity of the different forming states and is discussed in one of the subsections below.

In Section 2.6.1, a classification of stress-strain curves into three stages has been introduced: elastic deformation stage, uniform deformation stage and necking stage. When looking at Figures 5-3 to 5-7, it is noticeable that the appearance of these stages is different for the HF curves compared to the WTF and PSF curves. For the WTF and PSF curves, the strains where uniform deformation ends and necking starts are generally much higher than for the HF curves. However, the latter exhibit a prolonged necking stage so that fracture eventually occurs at considerably higher total strain values. An explanation for the differently-sized stages might be seen in diffusion-controlled mechanisms. Especially at elevated temperatures, necking continuously transfers to new sections so that the local deformation slows down and the stress decreases slowly over a broad strain range. At room temperature contrarily, microvoids and atoms cannot diffuse that easily. As a consequence, more dislocations accumulate and strain hardening occurs up to a stress level where microvoids have grown large enough to initiate localised necking. Stress drops rapidly then and fracture occurs at comparatively low strain values [20].
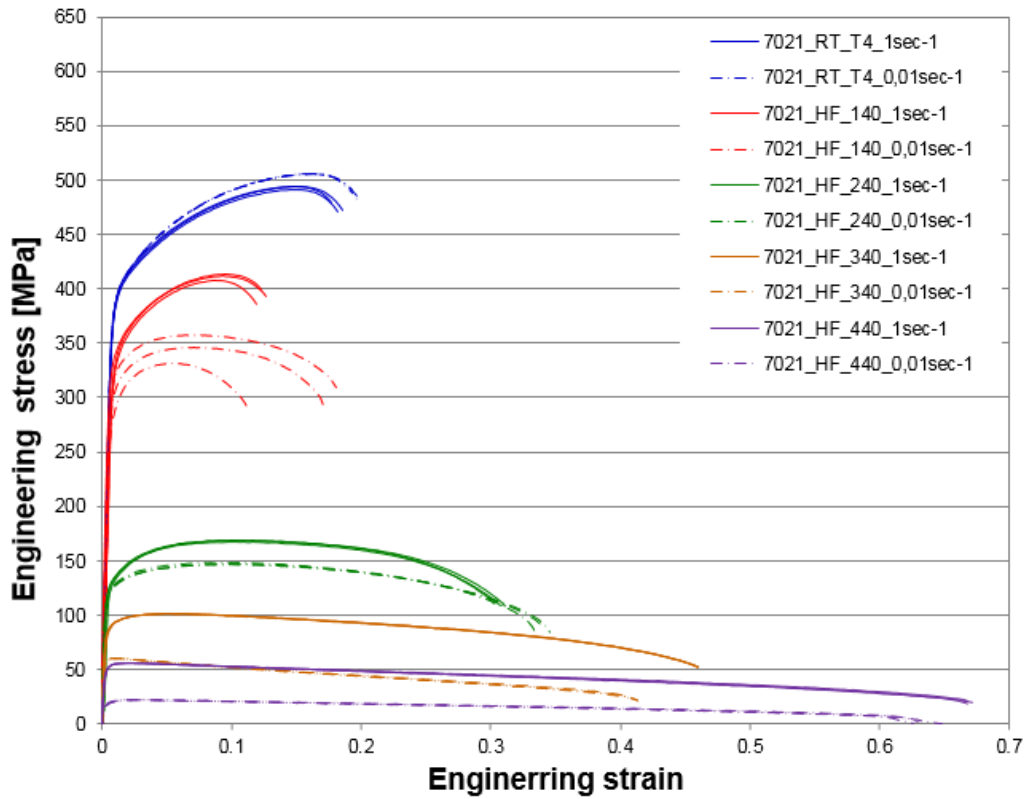
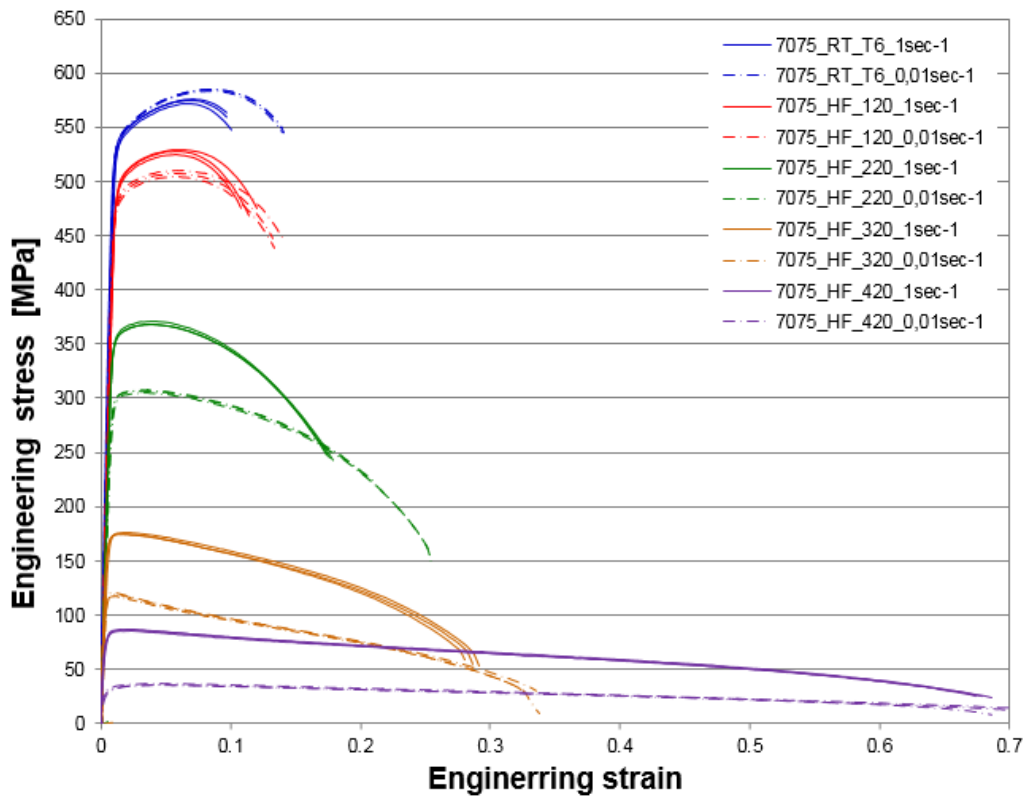**Figure 5-3:** *Engineering stress-strain curves for HF 7021*

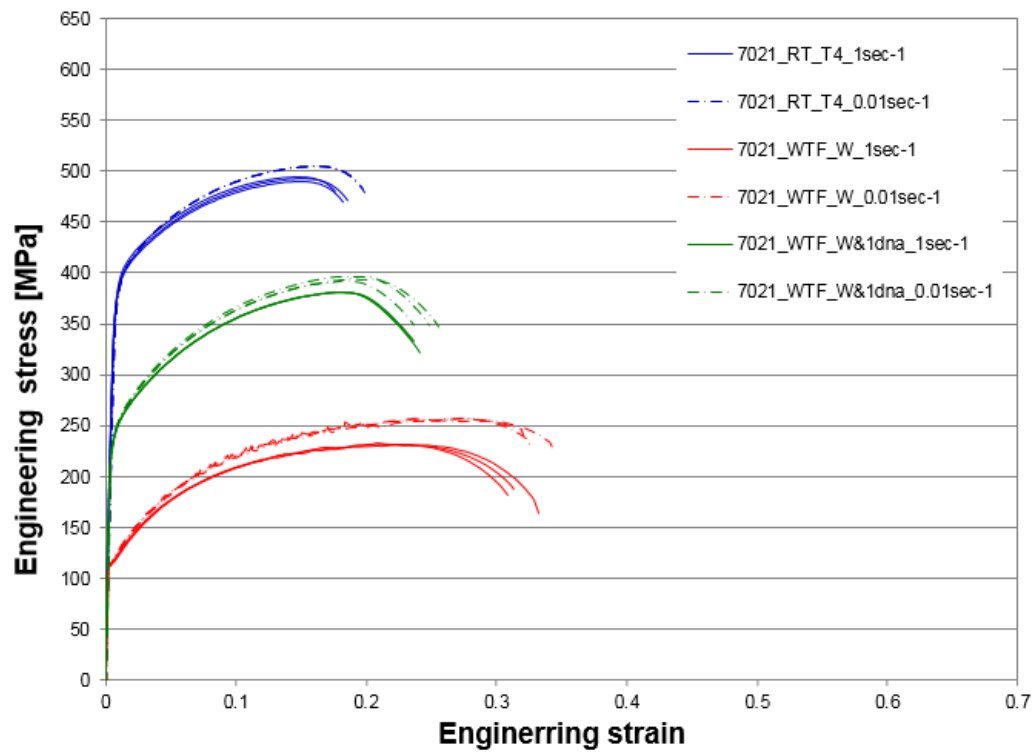Figure 5-4: Engineering stress-strain curves for HF 7075

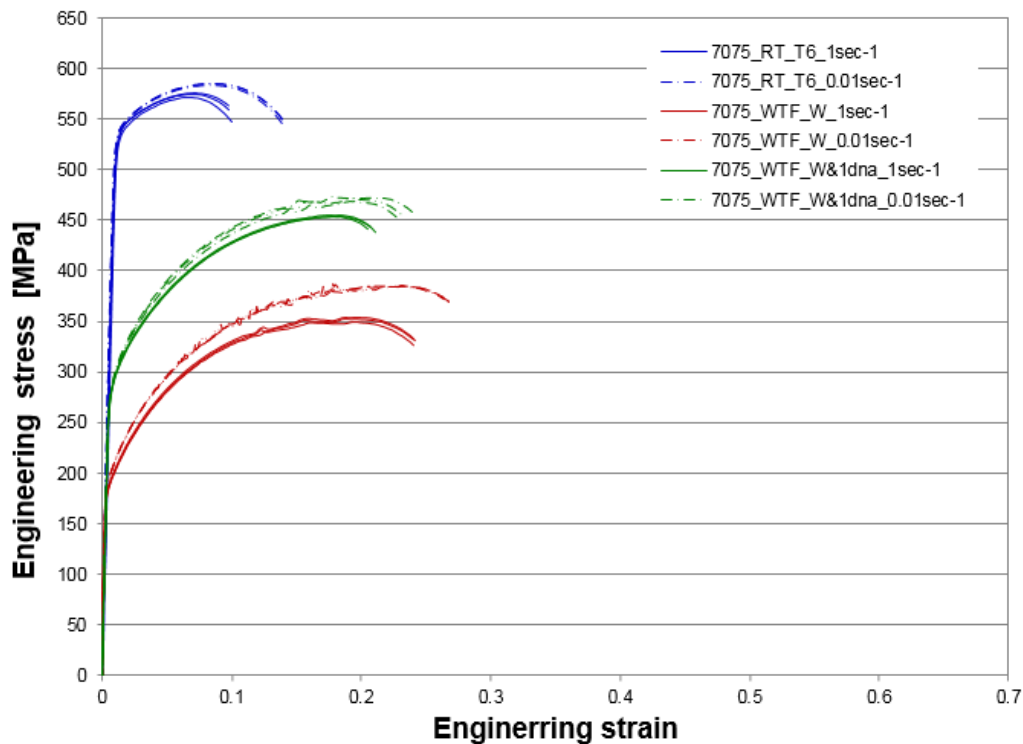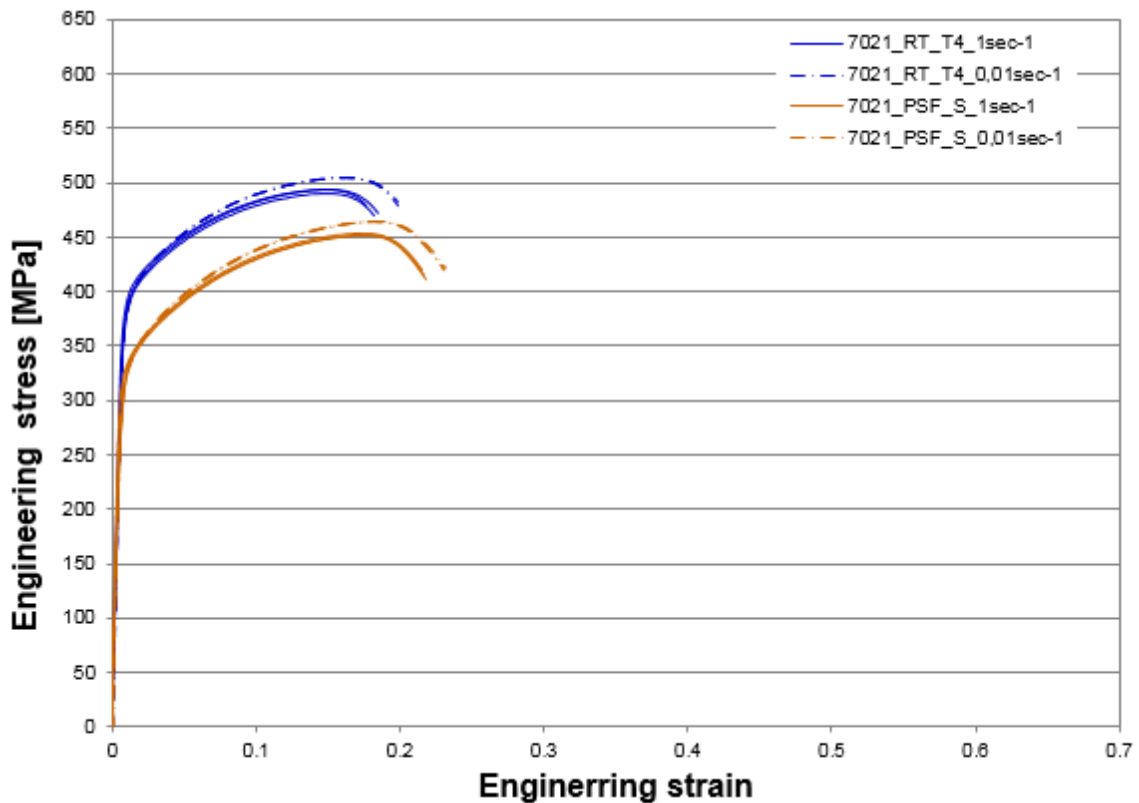**Figure 5-5:** *Engineering stress-strain curves for WTF 7021*

**Figure 5-6:** *Engineering stress-strain curves for WTF 7075*

Figure 5-7: *Engineering stress-strain curves for PSF 7021*

Yield strength and Ultimate tensile strength

As can be seen from Figure 5-8, for the hot forming states yield strength and ultimate tensile strength both decrease with increasing temperature and decreasing strain rate. Especially for temperatures above 300°C, stress-strain curves show low stress levels and the difference between yield strength and ultimate tensile strength gets small. The effect of strain hardening is thus limited particularly at higher deformation temperatures and dynamic softening mechanisms prevail during and after the uniform deformation stage.

For the W-temper forming states, yield strength and ultimate tensile strength increase after 1 day of natural ageing by approximately 130 MPa for the AW-7021 alloy and by 90 MPa for the AW-7075 alloy. A significant difference in yield strength between the 1 sec^{-1} and the 0.01 sec^{-1} strain rate could not be observed for any of the alloys or forming states investigated. The ultimate tensile strength however is higher at the 0.01 sec^{-1} strain rate for both alloys and forming states.

For the post stabilisation forming state, yield strength values are about 60 MPa below the as-delivered T4 condition and ultimate tensile strength is approximately 50 MPa lower. Yield strength is slightly lower at 0.01 sec^{-1} than at 1 sec^{-1} for both, the as-delivered T4 and the stabilised condition. What concerns ultimate tensile strength, the 0.01 sec^{-1} strain rate yields higher stress values though. This suggests that during strain hardening, a transition from positive to negative strain rate sensitivity must occur.
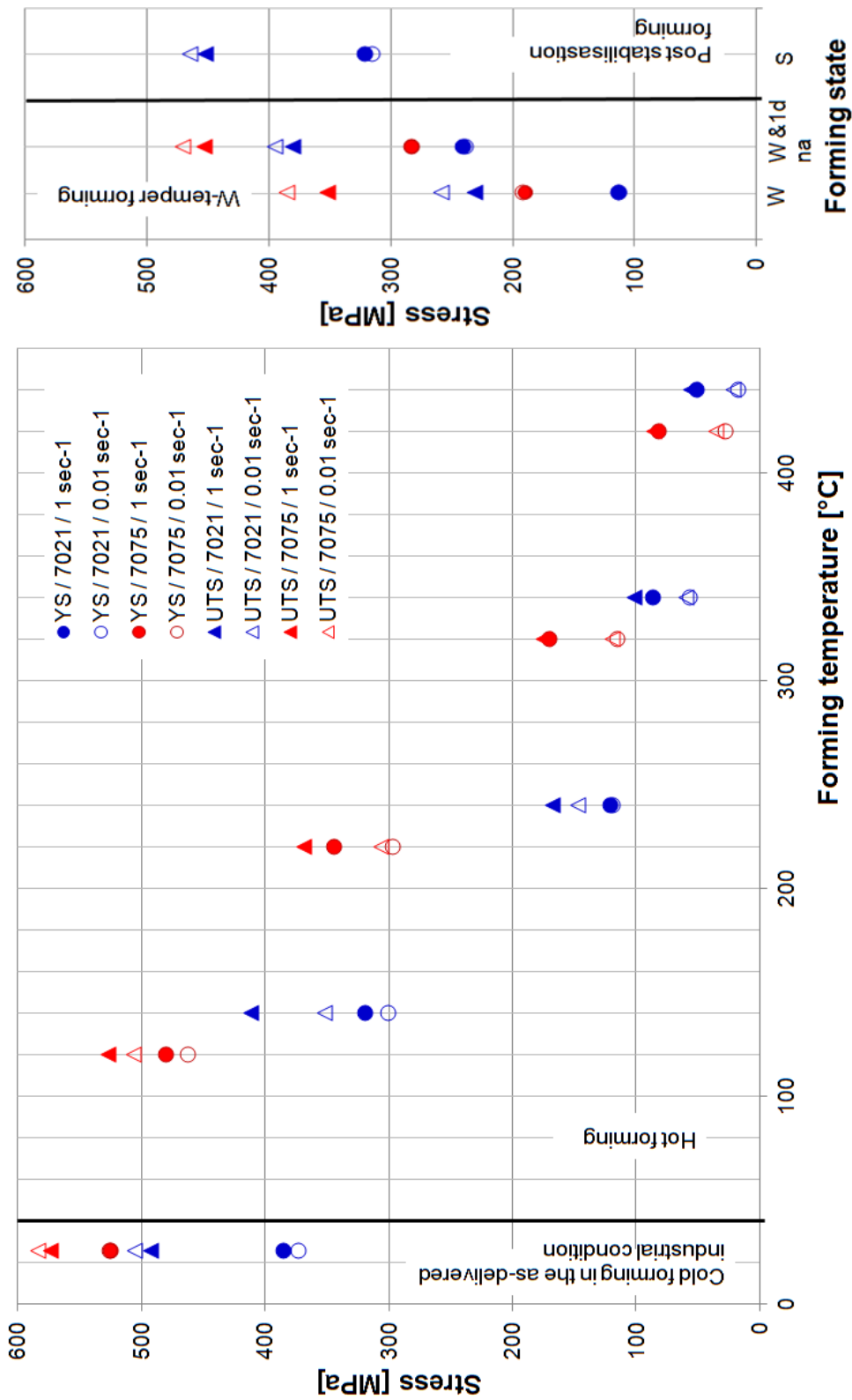
Figure 5-8: *Yield strength (YS) and Ultimate tensile strength (UTS) of the AW-7021 and AW-7075 alloys at different forming temperatures/ forming states and strain rates*
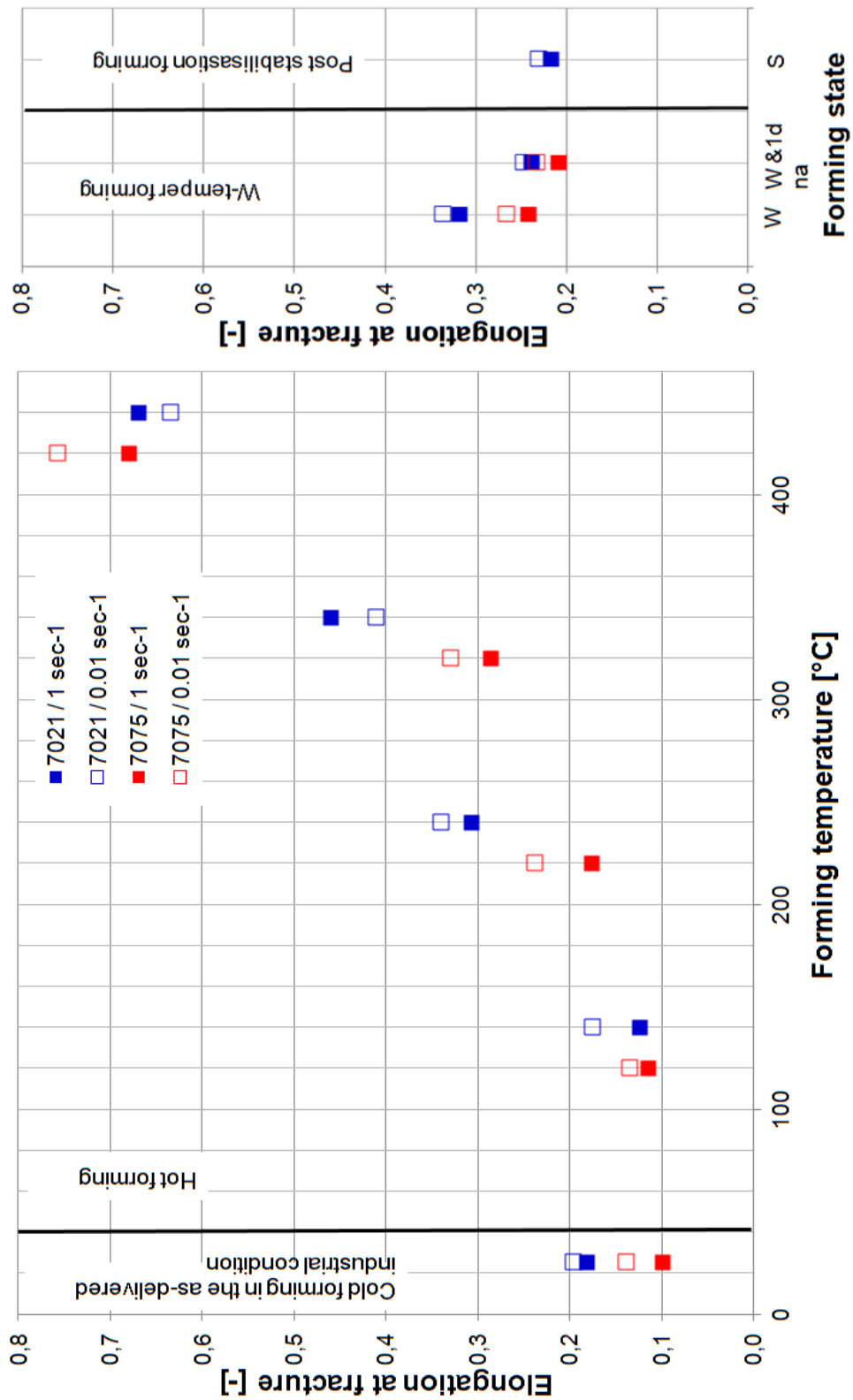
Elongation at fracture

Elongation at fracture can be regarded as a measure of ductility. It must be handled with care though, since different sample geometries with varying initial lengths might yield different values (cf. Section 2.6.1). The effects of strain rate and forming state on elongation at fracture are shown in Figure 5-9.

For the hot forming states, elongation at fracture increases with rising temperature. It was found to be higher than 60 % from 400°C onwards for both alloys and strain rates. What particularly stands out for the AW-7075 alloy is the fact that it yields higher elongation at fracture values at temperatures above 400°C than the AW-7021 alloy. Since the solution heat treatment temperature of the AW-7075 alloy (480°C) is lower than the one of the AW-7021 alloy (515°C), it can be assumed that for AW-7075 more hardening precipitates have already dissolved into the aluminium matrix.

For the W forming state, elongation at fracture is similar to hot forming at 220°C and 240°C respectively. The AW-7021 alloy shows values that are about 10 % higher than those of the AW-7075 alloy. After 1 day of natural ageing, only minor differences exist between the two alloys.

The S forming state performs slightly better in terms of elongation at fracture than room temperature forming in the as-delivered T4 industrial state. The values are a little bit above the 20 % line for the S forming state.

For almost all forming states, elongation at fracture was found to increase with decreasing strain rates. However, for hot forming of the AW-7021 alloy at 340°C and 440°C, the deformation capability is greater for the 1 sec^{-1} strain rate. Zhou et al. [20] claim that the effects of strain rate on elongation at fracture are governed by two opposite phenomena. On the one hand side, increasing the strain rate might result in more tangled dislocations eventually blocking each other so that the plastic deformation capability is decreased. On the other hand side, especially when strain rates are low, microvoids and microcracks have more time to grow and coalescence. Early material failure would then be more likely at lower strain rates. For hot forming of the AW-7021 alloy, the first phenomenon seems to prevail at lower temperatures. At temperatures above 300°C however, the latter starts to outweigh the former.

Figure 5-9: Elongation at fracture of the AW-7021 and AW-7075 alloys at different forming temperatures/ forming states and strain rates
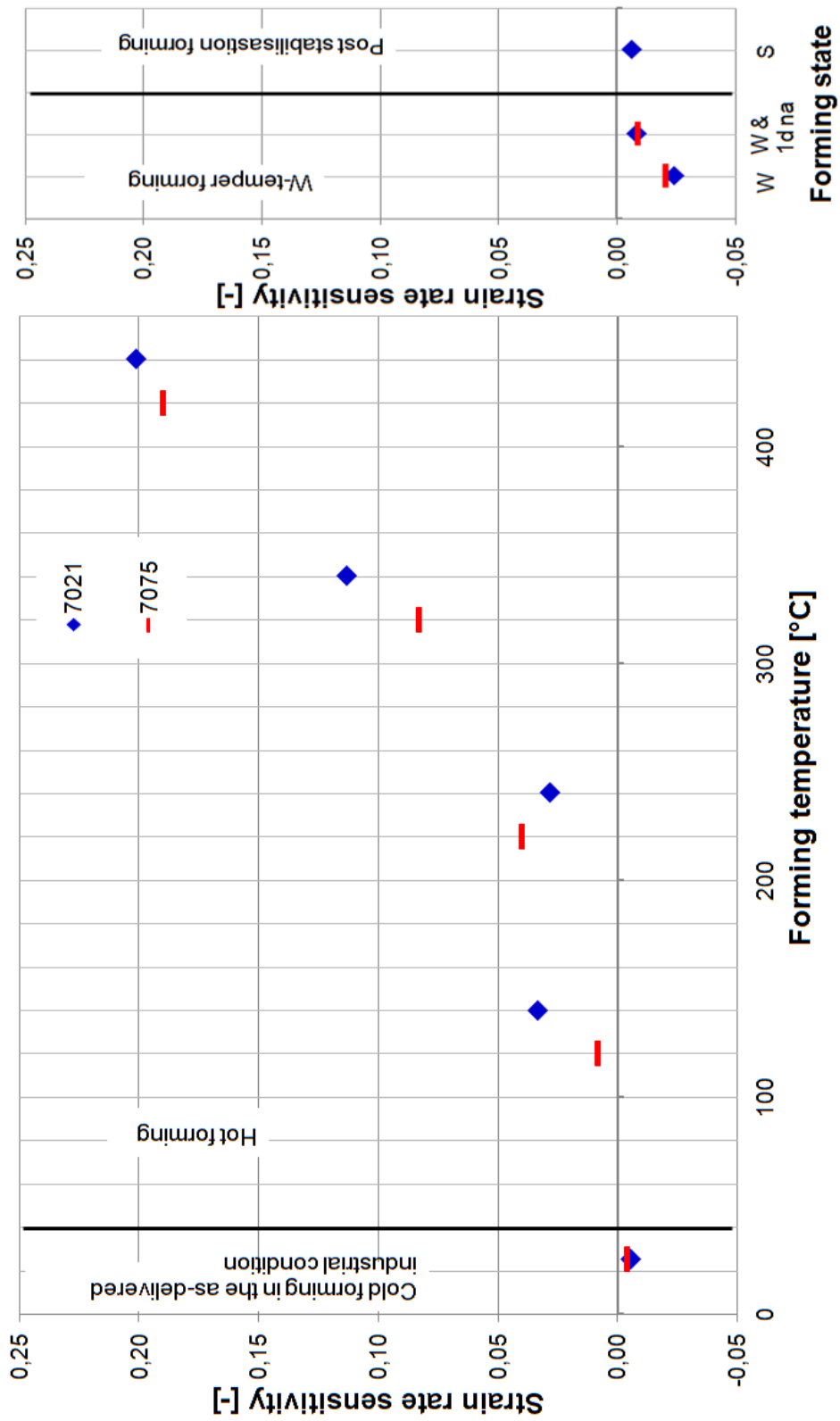
Strain rate sensitivity

Strain rate sensitivity m_{SR} has been determined at uniform elongation according to Equation 2-1 in Section 2.6.1.

In Figure 5-10, strain rate sensitivity is plotted against the different forming states. As can be seen from the diagram, all hot forming states have positive m_{SR} values. Strain rate sensitivity increases with rising temperature and particularly high values are obtained at temperatures above 300°C.

W-temper forming states are less strain rate sensitive and show negative m_{SR} values. In the S state, strain rate sensitivity is comparable to cold forming in the as-delivered industrial condition.

The variation of strain rate sensitivity for the different forming states builds upon two mechanisms. Thermally-activated processes are believed to cause the clearly positive strain rate sensitivity for the hot forming states. Dynamic recovery and the dissolution of hardening precipitates take place more comprehensively during longer time spans. Since low strain rates increase deformation periods, they allow more time for dynamic recovery and the dissolution of hardening precipitates to happen. As a consequence stress is reduced for the 0.01 sec^{-1} curves compared to the 1 sec^{-1} curves [21].

The W-temper forming and post stabilisation forming states are less strain rate sensitive since diffusion-controlled mechanisms are not that pronounced compared to hot forming. The slightly negative strain rate sensitivity values can be explained through the growth of solute atom clusters. Clustering of solute atoms close to dislocations tends to obstruct further dislocation movement and therefore an increase in stress can occur [22, 23]. At high strain rates, the clusters are still small since they simply do not have enough time to grow big enough. The dislocations can therefore pass more easily. When decreasing the strain rate, the solute atoms have more time to accumulate so that an increase in stress is the result. Since more solute atoms are available in the W state than in the W&1d na, S, T4 or T6 states, the solute atom clusters are larger and the strain rate sensitivity value is slightly more negative for the W state.

Figure 5-10: *Strain rate sensitivity of the AW-7021 and AW-7075 alloys at different forming temperatures/ forming states*

5.2 Post-forming material properties

Natural ageing behaviour was evaluated during a time span of 21 days after forming. In addition, paint bake response as well as peak ageing behaviour were studied. Assessment methods used were hardness testing, differential scanning calorimetry and tensile testing. Joinability was evaluated through the preparation of rivet cross sections.

5.2.1 Hardness testing

For every natural or artificial ageing state, an averaged value from 3 measurements is shown in the following. The single measurement values can be found in Appendix 3. A description of the corresponding experimental setup is given in Section 4.6.

Natural ageing behaviour
Figure 5-11 shows the hardness evolution due to natural ageing over the course of 21 days for the different process chains. Additional measurements of undeformed sheets in the W and S state have been included in the diagram for reference purpose.
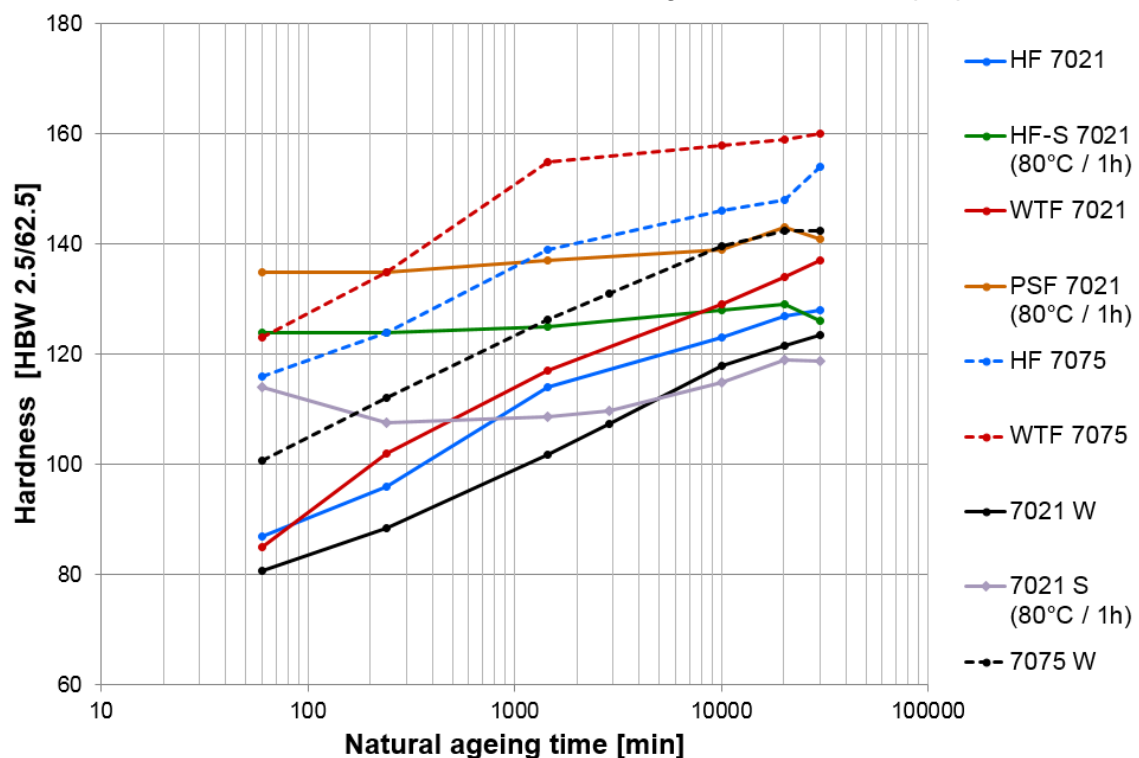
Figure 5-11: Natural ageing behaviour of the different process chains

As expected, forming considerably increases the hardness of the sheets. The HF and WTF curves hence represent a parallel shift of the undeformed W curves. Also the HF-S and PSF curves have moved to higher hardness levels compared to the undeformed S curve. Obviously, the hardness of samples formed at room temperature (WTF 7021, WTF 7075 and PSF 7021) is higher than the hardness of samples produced through hot forming (HF 7021, HF 7075 and HF-S 7021). This holds true during the entire 21 day period and corresponds to the observations made in Section

5.1.3, where the strain hardening effect was found to be clearly reduced for the HF process chains compared to the WTF and PSF process chains.

A clear increase in hardness could be observed for the non-stabilised samples (HF 7021, HF 7075, WTF 7021, WTF 7075) throughout the entire observation period. Joining through self-pierce riveting is therefore time-sensitive. In order to achieve a joint of good quality, it is advisable to conduct the joining operation as soon as possible after forming. Introducing quality standards might still be difficult though due to the arbitrariness of natural ageing.

Contrarily, the HF-S 7021 and PSF 7021 samples did not vary significantly in hardness during the 21 day time span. Joining through self-pierce riveting is consequently not that time-sensitive for these two process chains. Therefore, determining a well-functioning riveting procedure at the respective hardness levels of HF-S 7021 and PSF 7021 would facilitate the introduction of quality standards for the joining operation. This applies particularly for the HF-S 7021 process chain since it yields lower hardness values than HF 7021 at the end of the observation period.

Artificial ageing behaviour

The artificial ageing behaviour of the different process chains is depicted in Figure 5-12. For comparison reasons, the hardness values of the as-delivered initial condition as well as after 21 days of natural ageing are included in the chart. Only minor differences could be observed between the samples from the same alloy after conducting a 1 step paint baking (1SPB) heat treatment. The hardness after 1SPB was on average at 154 HBW for the 7021 alloy and at about 164 HBW for the 7075 alloy. After executing a peak ageing (PA) heat treatment though, more significant variations could be observed with respect to how the sheet had been processed before. For instance, HF 7021 samples showed hardness values of approximately 167 HBW while for PSF 7021 values of about 176 HBW were detected. In the same way, WTF 7075 with a value of 185 HBW was significantly harder than HF 7075 (179 HBW) after peak ageing. This tendency should be kept in mind with respect to the circumstance that parts could be subjected to a 3SPB heat treatment in an industrial setting. Such an artificial ageing procedure consists of 3 successive heat treatments so that the total furnace exposure time increases compared to the 1SPB variant. Kumar et al. [21] have shown that variations in how an alloy is processed can lead to differences in hardness after 3 SPB.
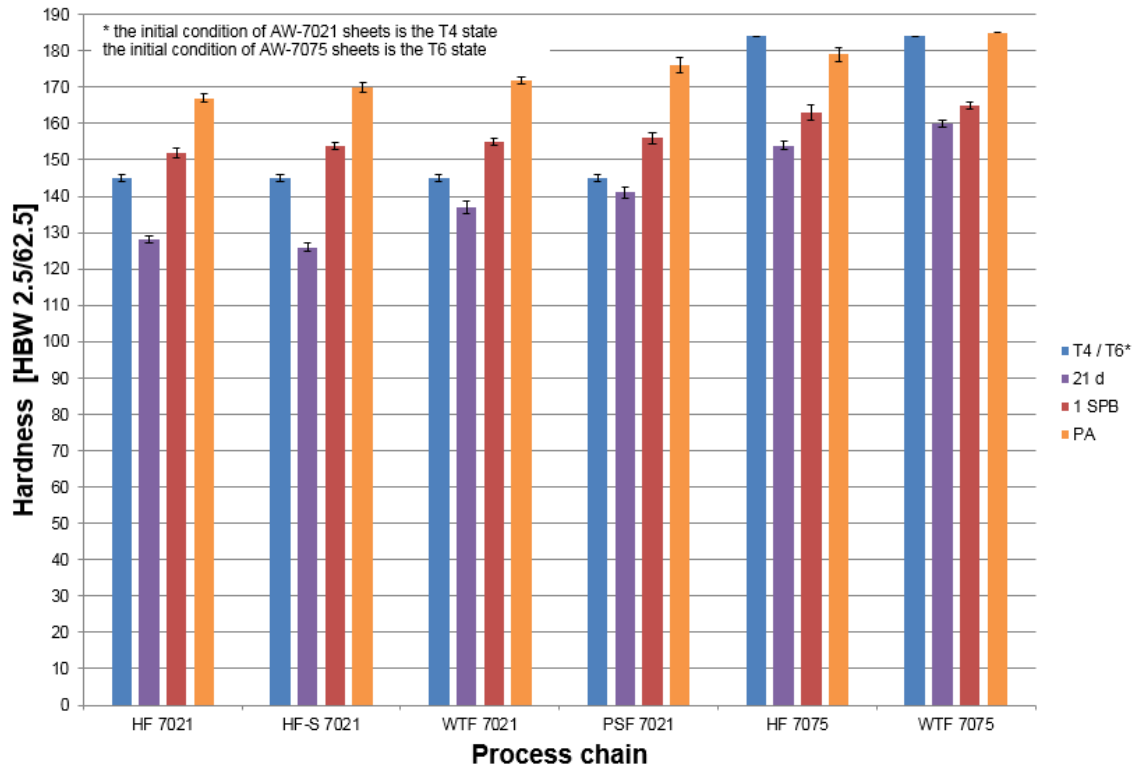
Figure 5-12: Artificial ageing behaviour of the different process chains

5.2.2 Differential scanning calorimetry

The differential scanning calorimetry (DSC) experiments aimed at revealing differences in the precipitate microstructure of the sheets as they pass through the different process chains. The results were interpreted in accordance with the findings of [13, 24, 25], where the authors propose a precipitation sequence for Al-Zn-Mg alloys that looks the following:

α-supersaturated solid solution → GP zones → η' phase → η phase
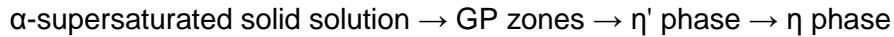
All of the curves shown in the following are representative curves out of two measurements. A description of the corresponding experimental setup can be found in Section 4.7.

DSC curves recorded 1 hour after forming
Figure 5-13 and Figure 5-14 show the DSC curves for AW-7021 and AW-7075 directly after forming or stabilising respectively. All of the samples have been taken from formed parts except for the 7021 W and 7075 W samples. The W samples have been taken from the undeformed sheet and have only been heat treated. They are included for comparison reasons in the diagrams. For 7021 HF-S, the measurements have been carried 1 hour after the stabilisation heat treatment and for 7021 PSF, they were performed 1 h after forming in the stabilised condition. The remaining process chains 7021 HF, 7075 HF, 7021 WTF and 7075 WTF were all tested 1 h after hot forming or forming in the solution heat treated and water quenched condition. For all curves, minima in the negative excess specific heat capacity value range correspond to the formation of precipitates (exothermic reaction, cf. Section 2.6.2). Maxima in the positive value range correspond to their dissolution (endothermic reaction, cf. Section 2.6.2).

A number of 6 peaks appears for the AW-7021 alloy (cf. Figure 5-13). When heating the W sample, an exothermic peak (1) appears at 71°C indicating the formation of GP zones. The sample was thus in the α-supersaturated solid solution state prior to the test. The GP zones dissolute during the endothermic peak (2) at 138°C. On further heating, the η' and η phases start to form as indicated by the exothermic peaks (3) and (5). The dissolution of all η' and η phases takes places during the broad endothermic event (4,6) between approximately 290 and 370 °C.

The formation of GP zones does not occur for the samples taken from formed parts (7021 HF, 7021 WTF, 7021 HF-S, 7021 PSF). The corresponding minimum (1) is missing for these curves. The formation of GP zones has thus already taken place before the measurement. Peak (3) is much more pronounced and peak (5) is less pronounced for 7021 HF and 7021 WTF compared to the other samples. This could be related to a concurrent, overlapping formation of η' and η phases for 7021 HF and 7021 WTF. The predominant phase is most likely the η' phase, nucleating sources for the η phase might be rare.

The AW-7075 alloy shows peaks that are very similar to the AW-7021 alloy (cf. Figure 5-14). For all 7075 samples, peak (5) appears at lower temperatures and is more pronounced than for the 7021 samples. This is in line with artificial ageing results from Section 5.2.1, since η' is the key hardening phase for Al-Zn-Mg alloys. Peak (1) is more pronounced for the 7075 W sample which is linked to the alloy's higher content of alloying elements. Also, for the 7075 W sample an additional peak (7) could be observed. This peak is most likely linked to the formation of an additional T ($Mg_3Zn_3Al_2$) phase [13]. For the formed samples, the additional peak (7) does not occur. They show more η' phase and η phase precipitation instead as indicated by the larger peaks (3) and (5).

DSC curves recorded 21 days after forming
In Figure 5-15 and Figure 5-16, the DSC signals recorded 21 days after forming or stabilising for AW-7021 and AW-7075 are shown respectively. Again, the undeformed W samples are included in the diagrams for comparison reasons. As expected, no significant difference between the 1h and 21d signals could be observed for the 7021 HF-S and 7021 PSF process chains. This indicates that the precipitate microstructure is stable over the storage period of 21 days. For HF 7021, HF 7075, WTF 7021 and WTF 7075 though, the natural ageing effect can clearly be observed. Especially peak (2) has changed considerably for the non-stabilised process chains. It turned out to be about 0.036 $Jg^{-1}K^{-1}$ (HF 7021), 0.029 $Jg^{-1}K^{-1}$ (WTF 7021), 0.059 $Jg^{-1}K^{-1}$ (HF 7075) and 0.044 $Jg^{-1}K^{-1}$ (WTF 7075) higher after 21 days respectively. One can thus conclude that the amount of GP zones has risen for the non-stabilised process chains, which is line with their increase in hardness observed in Section 5.2.1. Since peak (2) also occurs at lower temperatures for process chains HF 7021, WTF 7021, HF 7075 and WTF 7075, the GP-zone distribution is most likely finer after 21 days as well.

DSC curves recorded after 1 SPB
As discerned from the DSC curves after 1SPB in Figure 5-17 and Figure 5-18, peaks (2) and (3) are less pronounced and appear at lower temperatures compared to DSC signals from 1h and 21d natural ageing. Further, all curves feature an own endothermic peak (4), which is linked to the dissolution of the η' phase. The predominant precipitate within the 1SPB samples prior to heating is thus the hardening phase η'. This holds true for all process chains and explains the increase in hardness and yield strength after conducting a 1SPB heat treatment.
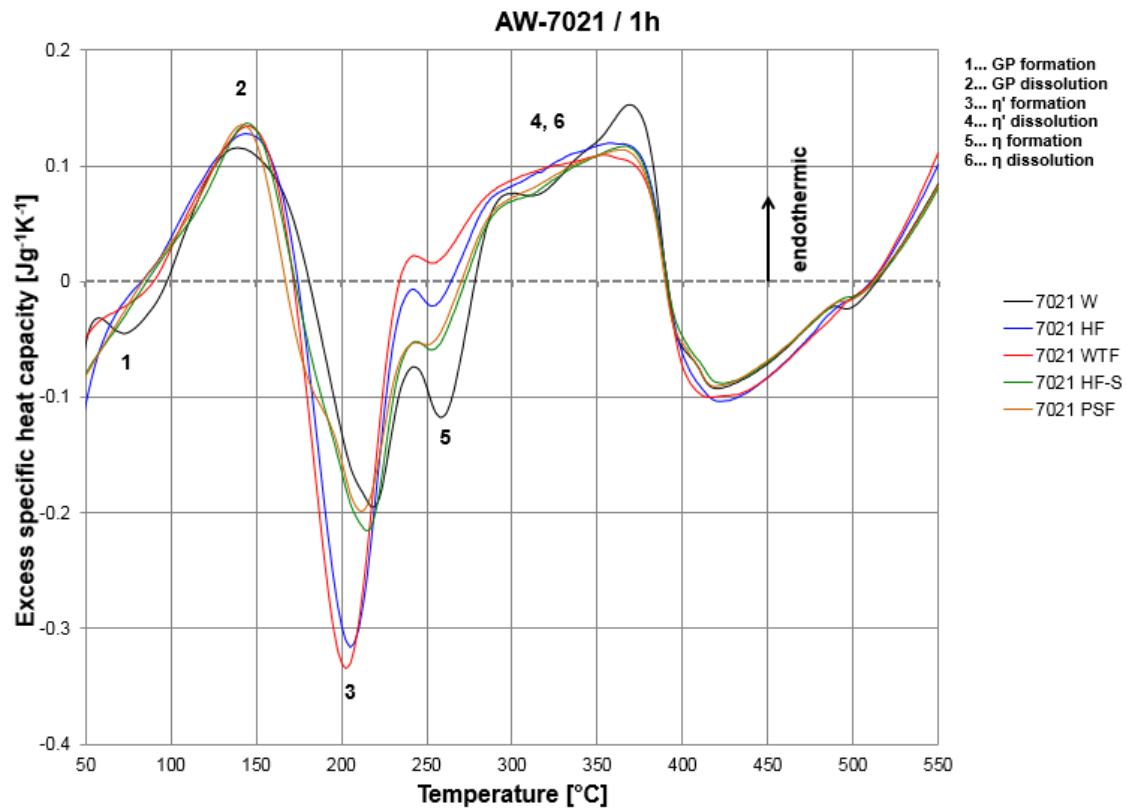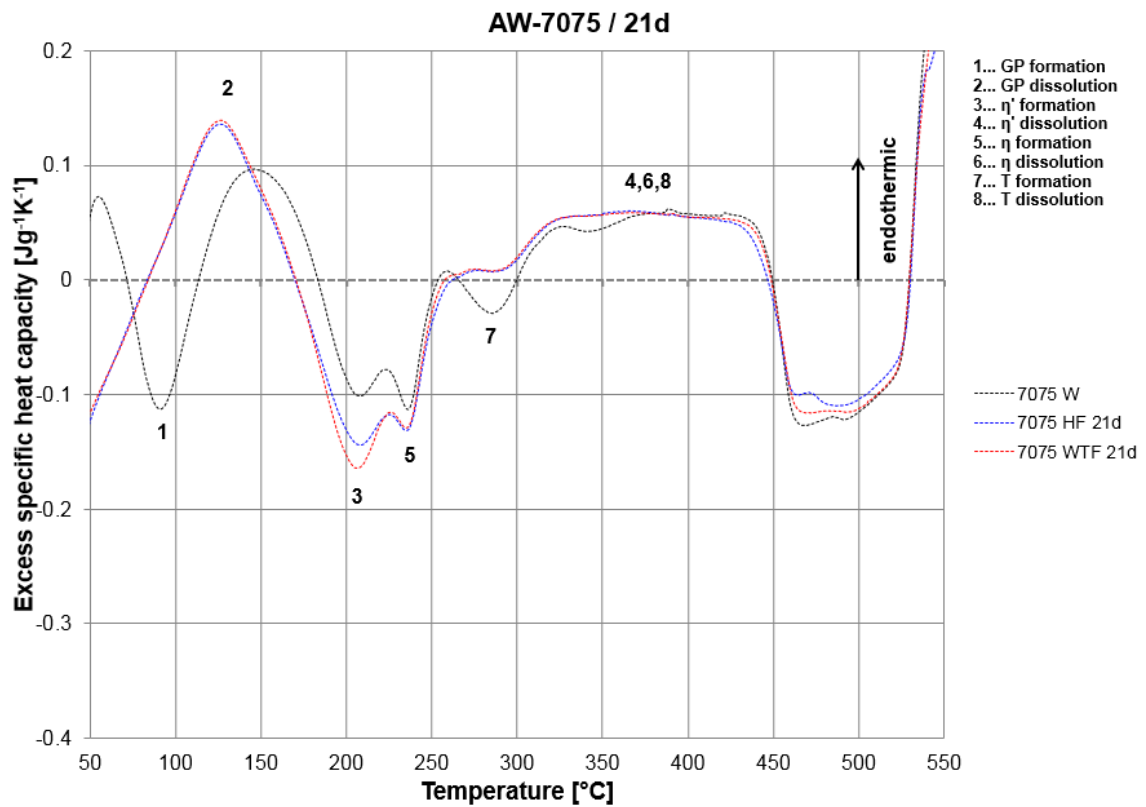
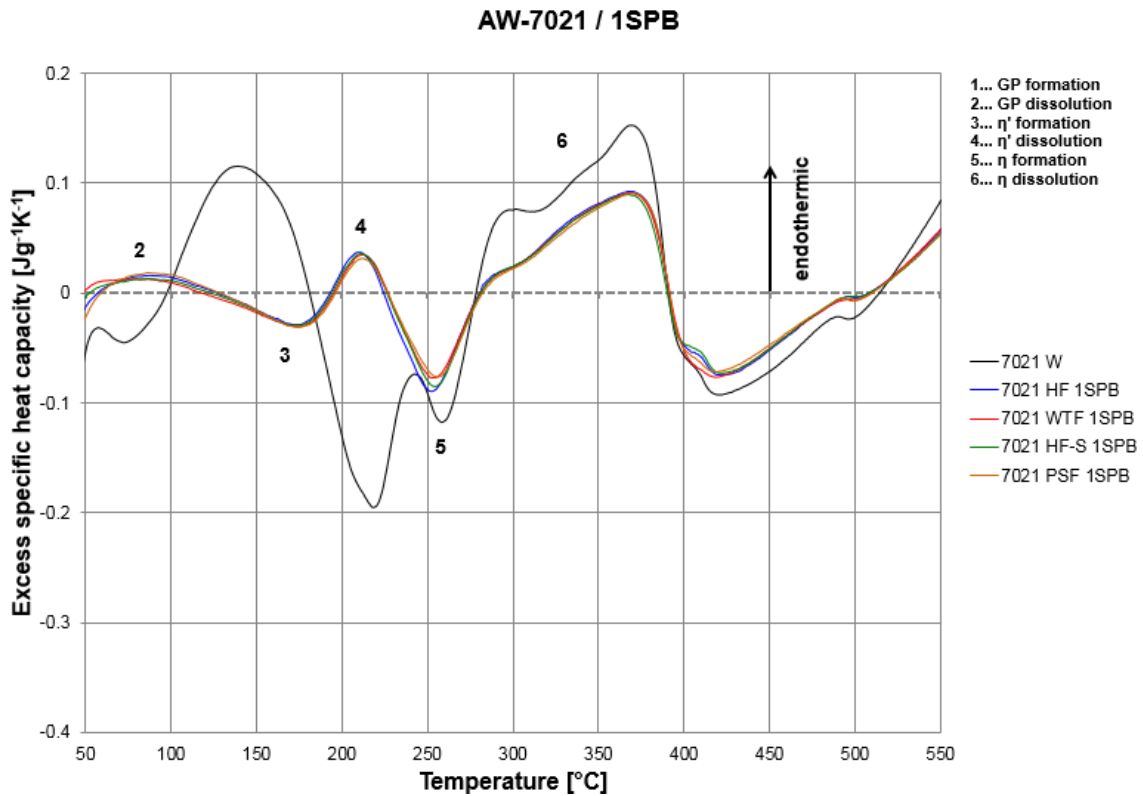**Figure 5-13:** *DSC curves of formed AW-7021 samples measured 1 hour after forming*
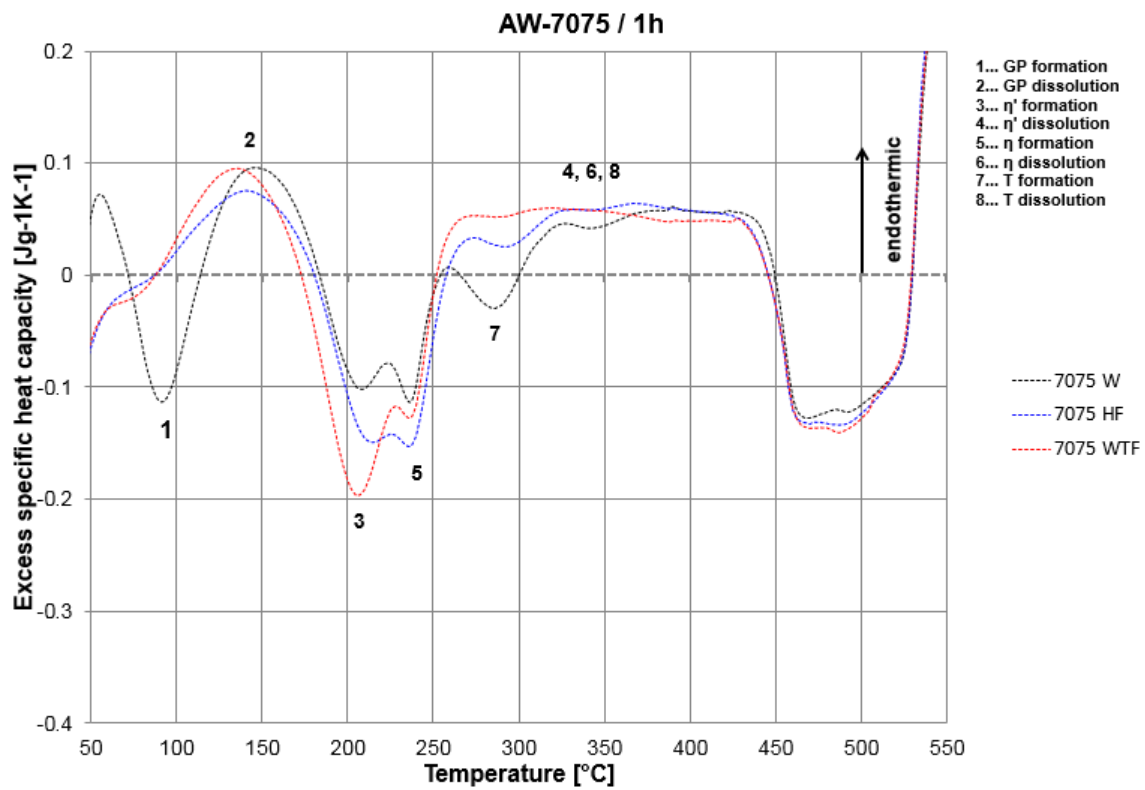
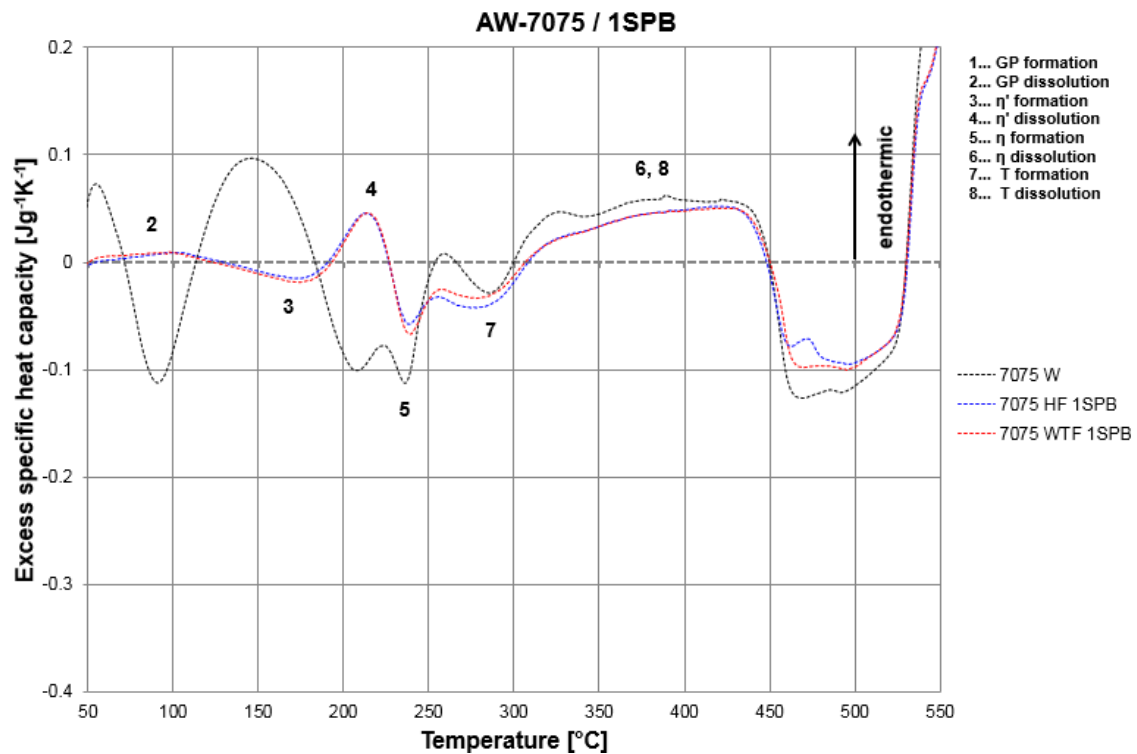**Figure 5-14:** *DSC curves of formed AW-7075 samples measured 1 hour after forming*
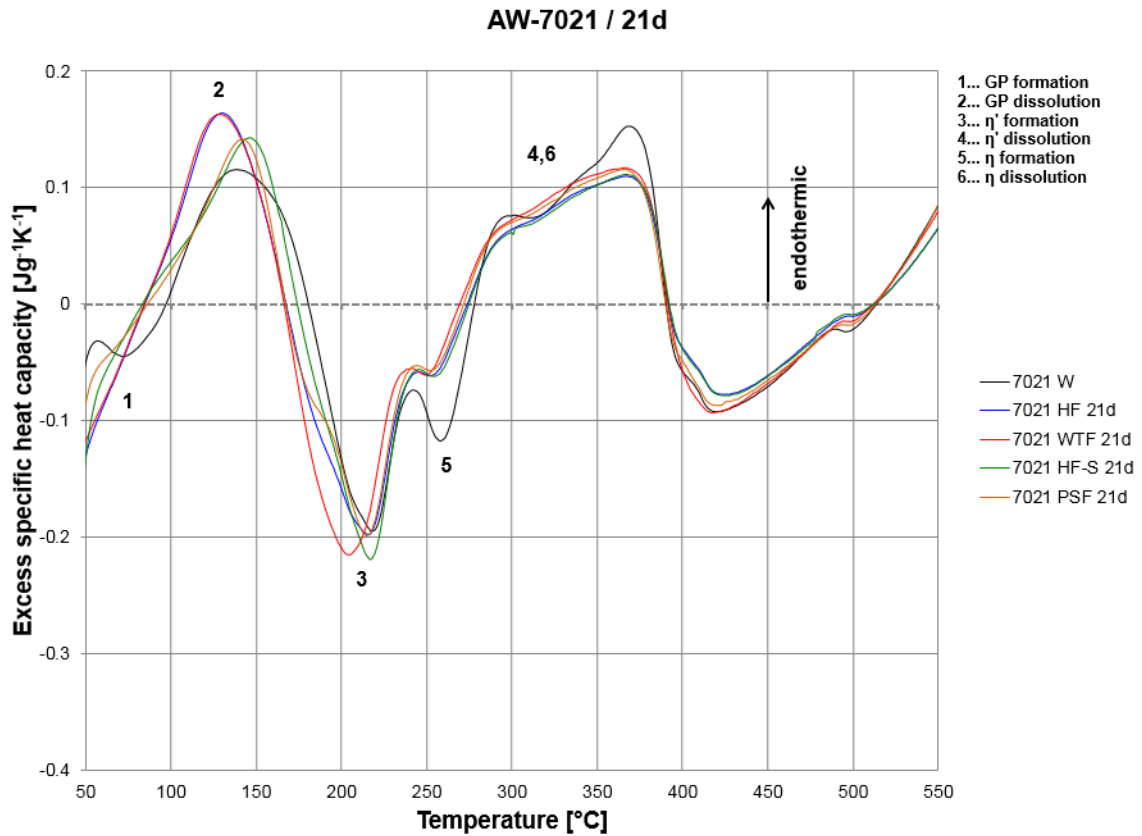
Figure 5-15: *DSC curves of formed AW-7021 samples measured 21 days after forming*

Figure 5-16: *DSC curves of formed AW-7075 samples measured 21 days after forming*

Figure 5-17: *DSC curves of formed AW-7075 samples measured after 21 days storage and subsequent 1SPB*

Figure 5-18: *DSC curves of formed AW-7075 samples measured after 21 days storage and subsequent 1SPB*

Evolution of precipitate microstructure along the process chains

The results from the DSC investigations above provide insight about the natural ageing and artificial ageing behaviour of the different process chains on microstructure level. Especially with respect to the appearance and pronouncement of peaks (1) and (2), conclusions about the phases predominant in the respective test state can be made. Table 5-2 summarises the findings.

Table 5-2: *Precipitate microstructure of the AW-7021 and AW-7075 sheets in different heat-treated or formed and naturally as well as artificially aged conditions*

	1 h	21 d	1SPB
7021 W	α-supersaturated solid solution	-	-
7021 HF	GP zone	GP zone (fine distribution)	η' phase
7021 WTF	GP zone	GP zone (fine distribution)	η' phase
7021 HF-S	GP zone	GP zone	η' phase
7021 PSF	GP zone	GP zone	η' phase
7075 W	α-supersaturated solid solution	-	-
7075 HF	GP zone	GP zone (fine distribution)	η' phase
7075 WTF	GP zone	GP zone (fine distribution)	η' phase

5.2.3 Joinability

As explained in Section 4.9, the rivet-die combination H4-FM was chosen for the production of test crush parts. Cross sections have been prepared for the hot forming process chains (HF 7021, HF 7075) and W-temper forming process chains (WTF 7021, WTF 7075) respectively. None of the joints riveted with the H4-FM combination exhibited cracks, dangerously low residual wall thickness values or cavities between upper and lower sheet. Still, the process chains themselves differed to some extent with respect to their joint quality as can be seen from the measurements shown in Figures 5-19 to 5-22.

Particularly the influence of hardness becomes obvious from the cross sections below. While the HF 7021 and WTF 7021 flange area test stripes had a hardness of approximately 85 HBW at the time of joining, HF 7075 and WTF 7075 showed hardness values of 116 HBW and 123 HBW respectively (cf. Section 5.2.1). The EN AW-6016-T4 FH sheet had a hardness of about 80 HBW and would therefore always be the softer material.

As discussed in Section 2.6.2 the parameter primarily important for the strength of the joint during the application of mechanical stress is its undercut. Especially for the HF 7021 process chain, a joint with comparatively high and uniform undercut was achieved. WTF 7021 also yielded comparatively high undercut values, but the rivet as a whole just as its undercut showed a slightly asymmetric behaviour. Process routes HF 7075 and WTF 7075 showed reduced undercut values compared to the HF 7021 and WTF 7021 process chains. Especially the WTF 7075 joint showed a comparatively asymmetric cross section so that it is more likely that cracks in the rivet base area and an anisotropic joint failure during quasi-static crush testing might occur [15].

What concerns the rivet head end position, it is noteworthy that for HF 7021 and WTF 7021 the rivet head transcends the upper sheet less compared to the process chains where the flange area stripes are harder (WTF 7075 and HF 7075). The limited penetration capability of the rivet for HF 7075 and WTF 7075 manifests itself also in a gap between upper sheet and rivet head. Such a gap is of course undesired, as it limits the maximum force that the joint can absorb and makes it more susceptible to corrosion. The gap between rivet cavity and upper sheet for the HF 7021 and WTF 7021 joints is also not optimal (see requirements towards a perfectly riveted joint below). Although the rivets show an augmented expansion for these two process chains, their rivet heads still slightly transcend the upper sheet. This might be due to missing material here. Since the residual wall thickness is sufficient for all process chains though, a slightly increased stroke could solve the gap issues.

At this point, it must be stated that none of the cross sections presented does entirely fulfil the criteria for a perfectly riveted joint. This would require that the rivet head end position is in the same plane or slightly below the upper sheet, that the rivet maintains full contact to the sheets in every position and that a uniformly pronounced undercut at both sides is achieved [15]. In order to find such an optimum solution for each process chain, a comprehensive, statistical analysis of the variation of multiple process parameters would be required. Besides varying rivet hardness classes and die geometries, this would for instance also include investigating riveting forces and strokes. In addition, joint quality would have to be assessed using cross and shear tension tests apart from preparing cross sections [15]. Nevertheless, this study is believed to give a basic overview on the applicability of the hot forming and W-temper forming process chains for self-pierce riveting. A central learning is that hot forming is obviously more suitable for subsequent self-pierce riveting due to less strain hardening that is induced into the material.
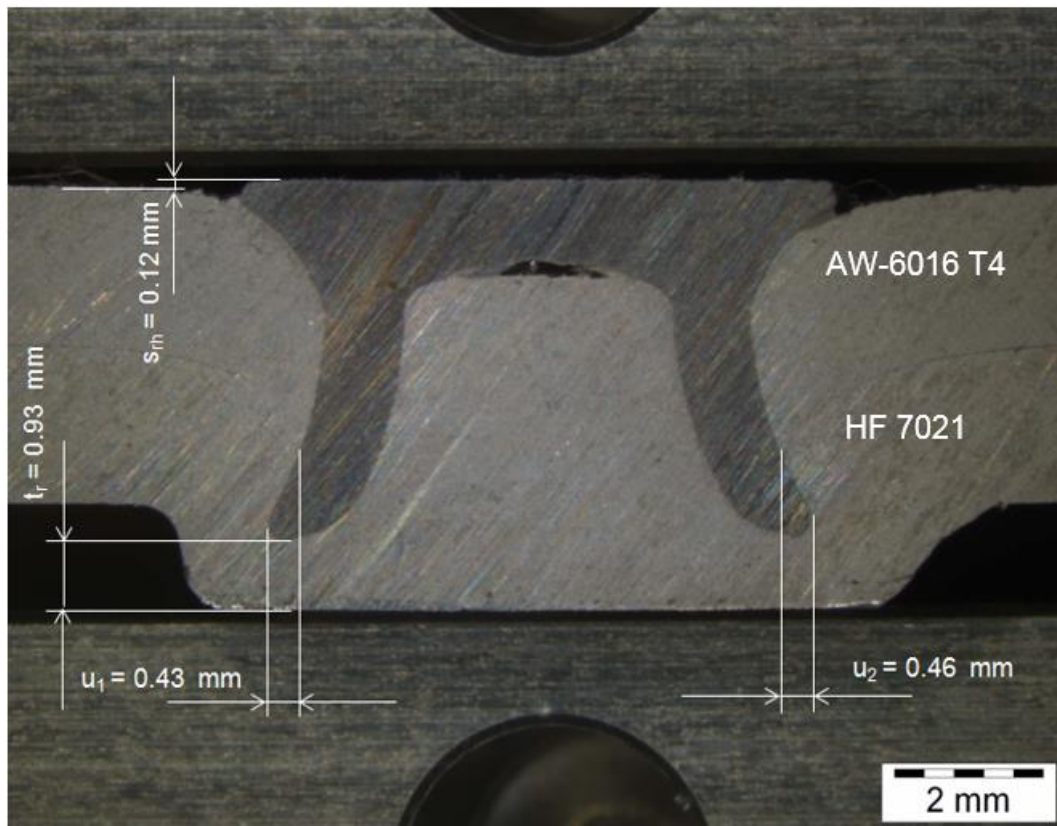
Figure 5-19: Cross section of the HF 7021 & AW-6016 joint (H4/FM)
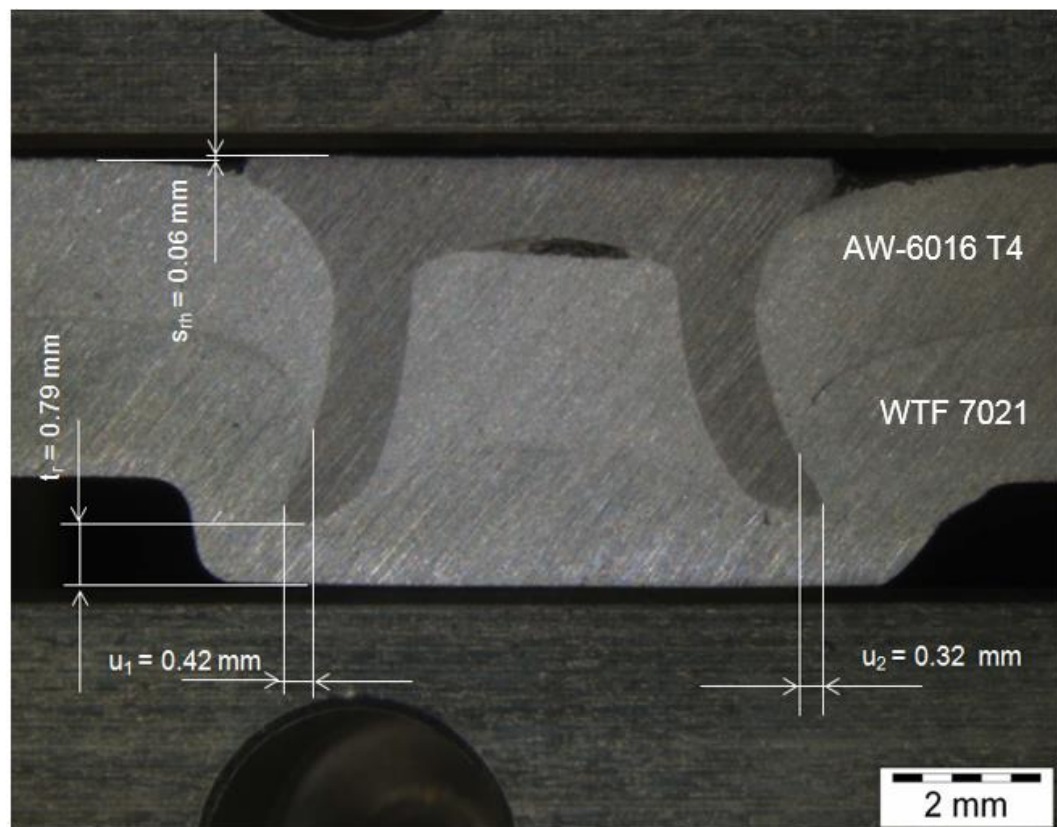
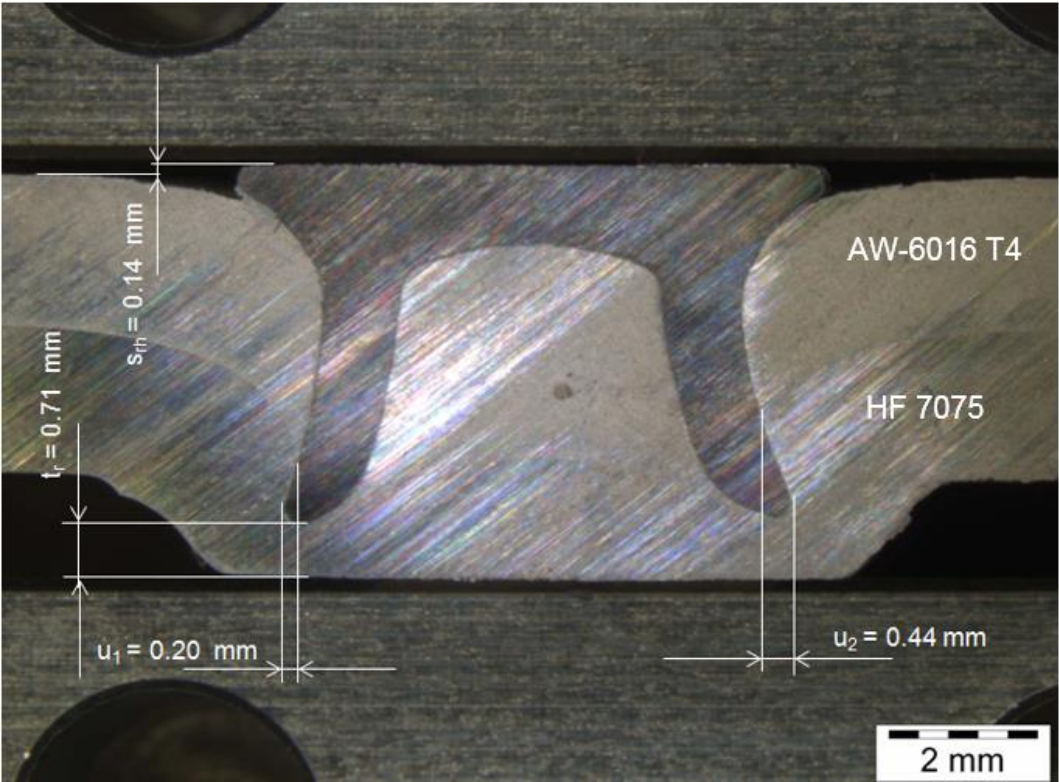*Figure 5-20:* Cross section of the WTF 7021 & AW-6016 joint (H4/FM)

Figure 5-21: *Cross section of the HF 7075 & AW-6016 joint (H4/FM)*
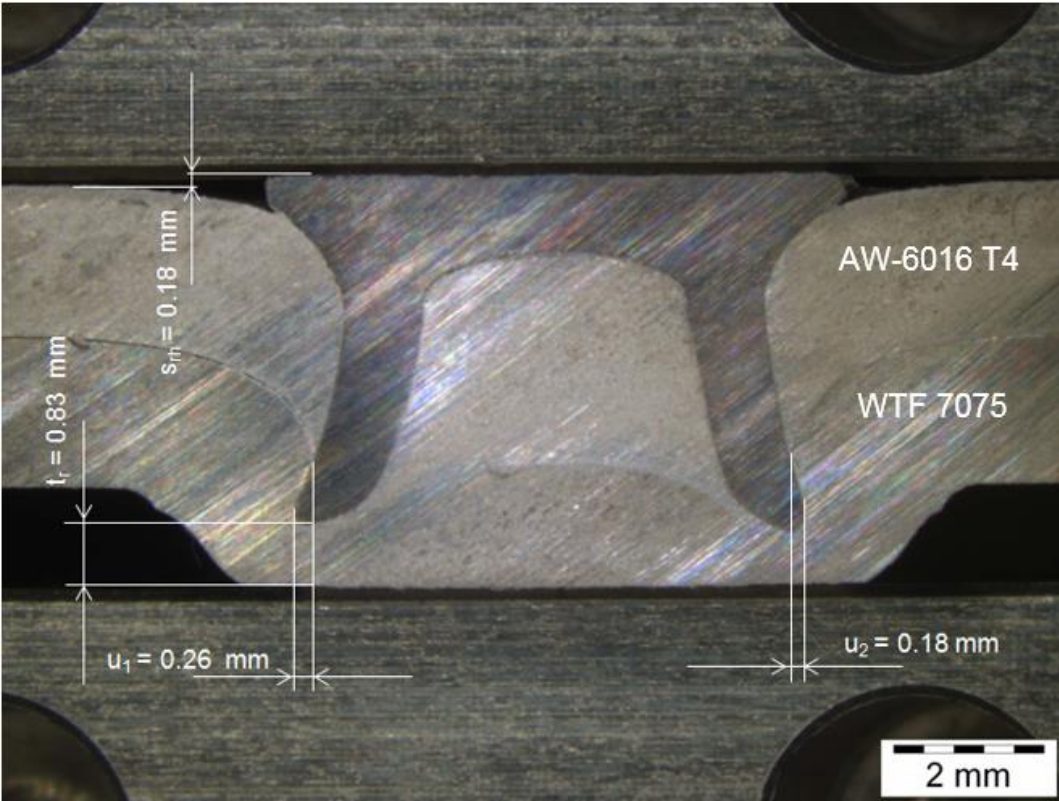

Figure 5-22: *Cross section of the WTF 7075 & AW-6016 joint (H4/FM)*

5.2.4 Tensile testing of samples taken from the side-wall section of formed parts

The process steps run through during the production of top-hat profiles have been described in Section 2.5 and Section 4.2. Forming, storage and artificial ageing alter the strength and ductility of the sheets. Figures 5-23 to 5-25 illustrate these changes for the HF 7021, WTF 7021, HF-S 7021, PSF 7021, HF 7075 and WTF 7075 process chains respectively. The data shown has been extracted from tensile testing curves which are displayed in Appendix 4. Process steps assessed are the as-delivered T4 (AW-7021) or T6 (AW-7075) condition of the undeformed sheets, the formed and 21 days naturally aged state (21d) as well as the formed, 21 days naturally aged and paint baked state (1SPB). Special attention is given to the 1SPB state, since it is the condition that crush-testing of top-hat profiles was performed in. In order to judge the quality of the 1SPB heat treatment, additional samples have been tested in a formed, 21 days naturally aged and peak aged state (PA). A more detailed description of the experimental setup can be found in Section 4.8.

As expected, strength generally increases and elongation at fracture decreases after tempering (1SPB) compared to non-tempered samples (21d). For all process chains, yield strength in the 1 SPB state is lower than the theoretical maximum that could be achieved during peak ageing. What concerns strain rate dependency, yield strength is slightly higher for the 1 sec^{-1} strain rate in most cases. Only HF 7075 and WTF 7075 show a reverse behaviour here. Elongation at fracture is generally increased by 1 to 2 % when testing with 0.01 sec^{-1} compared to 1 sec^{-1}.

Surprisingly, the AW-7021 process chains on average show slightly higher yield strength values after 1SPB than the AW-7075 process chains. After 21 days of natural ageing though, the AW-7021 process chains had considerably lower yield strength values than the AW-7075 process chains. This suggests that the given storage and heat treatment conditions better suit the AW-7021 process chains so as to achieve a satisfying paint bake response.

HF-S 7021 could be identified as the process chain with highest yield strength values in the 1SPB state. This indicates that low temperature pre-ageing heat treatments are suitable to improve paint bake response. Hansen et al. [12] have found that pre-ageing between 70°C - 150 °C increases the proportion of GP(II) zones in AW-7xxx series alloys prior to paint baking. GP (II) zones are thermally more stable than GP(I) zones. The latter most commonly form during natural ageing at temperatures below 60°C and need to dissolve entirely before the η' phase can precipitate during artificial ageing. GP(II) zones however can transform directly into the main strengthening η' phase [2]. This leads to a microstructure where the density of η' precipitates is higher. The ameliorated paint bake response of HF-S 7021 is therefore most likely related to its stabilisation heat treatment after die quenching.

For both alloys, samples taken from hot formed parts (HF 7021, HF 7075) showed slightly higher yield strength values in the 1SPB state than samples taken from parts produced through W-temper forming (WTF 7021, WTF 7075). For the WTF process chains, this might be due to more plastic strain induced during forming. Ostermann [2] has reported that artificial ageing is generally accelerated and ultimately lower strength values are achieved the more AW-7xxx series alloys have been strain hardened prior to tempering.

Interestingly enough, for the AW-7075 alloy the yield strength value of the initial T6 condition could not be recovered after forming, 21 days of natural ageing and subsequent peak ageing. As the as-delivered T6 condition has been generated immediately after quenching, this suggests that for the AW-7075 alloy age hardening response might be reduced by longer preceding natural ageing periods. Also, the effect of strain hardening due to forming might play a role in yield strength reduction of the HF 7075 and WTF 7075 PA states compared to the initial T6 state. PA samples show a by 3 to 4 % higher elongation at fracture compared to T6 samples. This gives further evidence that precipitation of hardening η' phases is not that pronounced after peak ageing as this is the case for the T6 condition of the AW-7075 sheets prior to forming.

Ultimate tensile strength is about 30 to 40 MPa higher for AW-7075 process chains than for AW-7021 process chains in the 1SPB state. Since AW-7021 process chains do however have slightly higher yield strength values than AW-7075 process chains in the 1SPB state, their tensile testing curves appear flatter after having reached the yield point. This eventually expresses itself in higher elongation at fracture values for the AW-7021 process chains. Especially stabilised samples (HF-S 7021 and PSF 7021) show comparatively high elongation at fracture values. This indicates that an additional stabilisation heat treatment does not only favour an improved paint bake response, it does at the same time also help the material retain some of its initial ductility. Both of these effects are extremely desired in car crash situations.
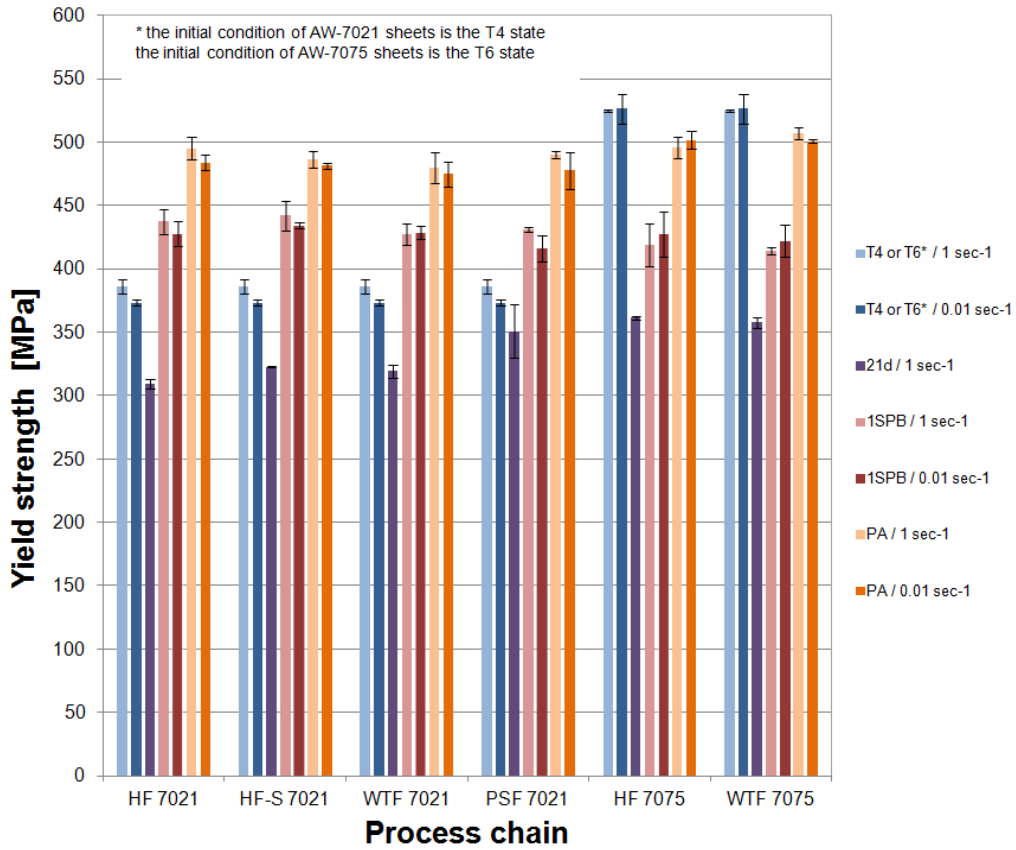
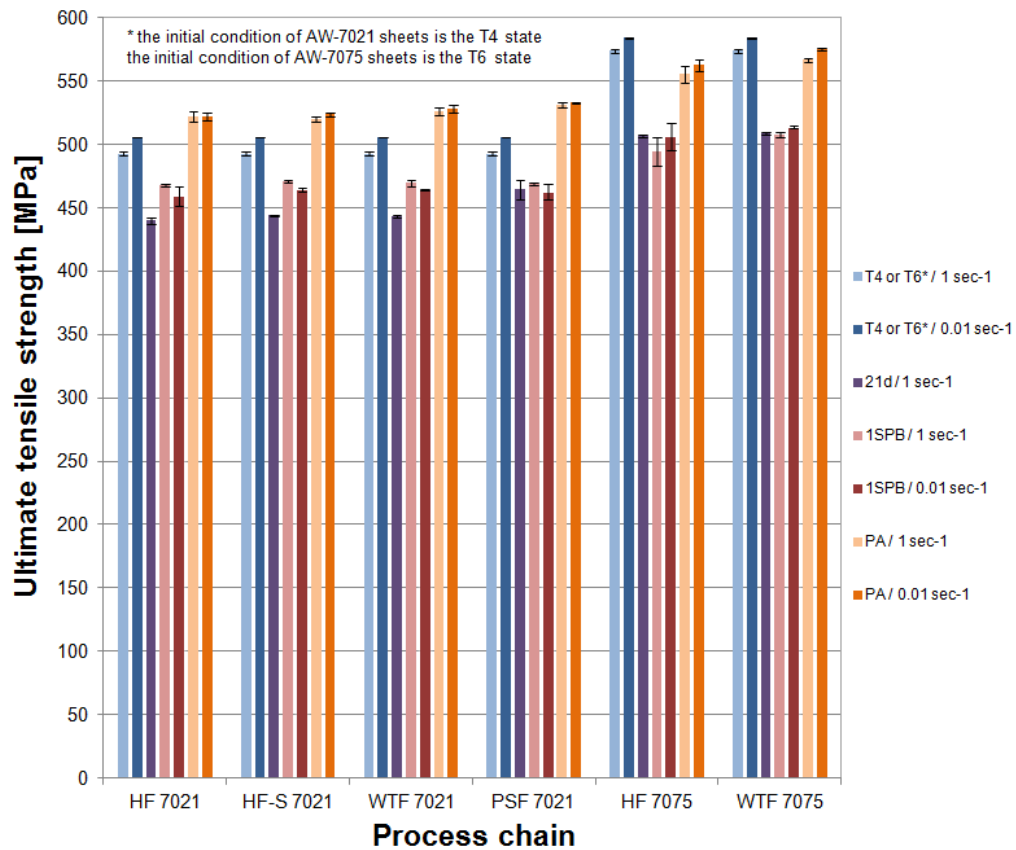**Figure 5-23:** *Effect of process steps on yield strength*

Figure 5-24: *Effect of process steps on ultimate tensile strength*
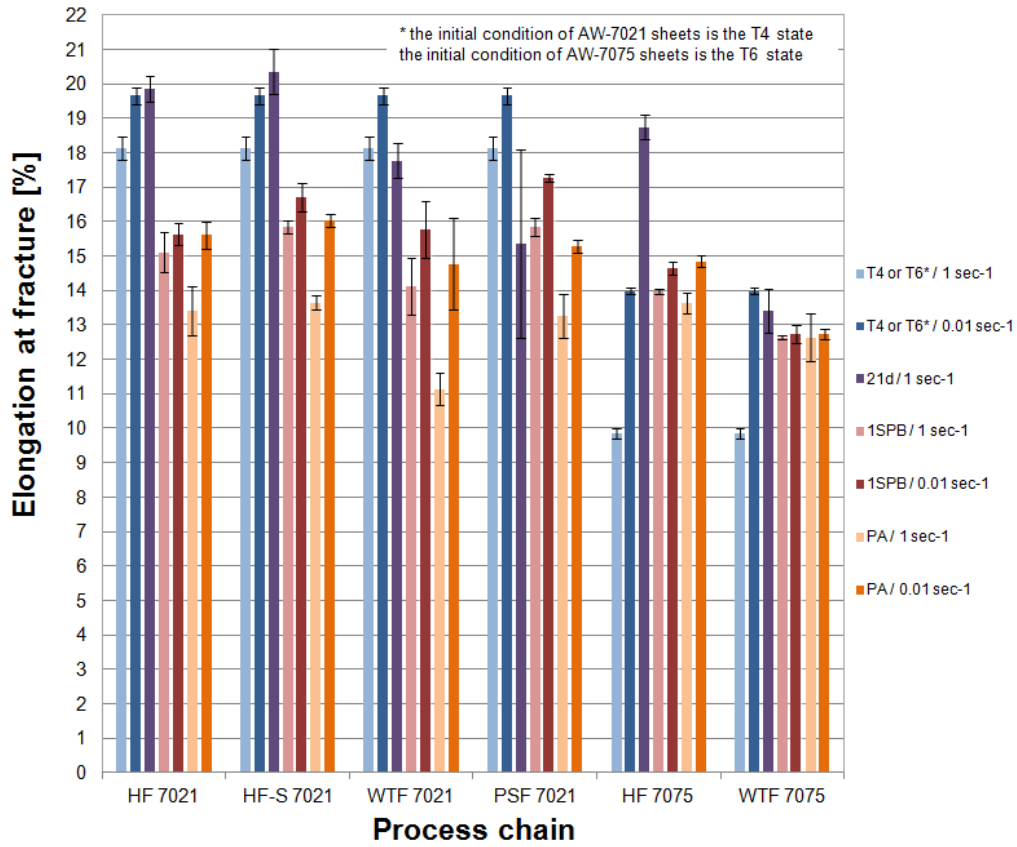
Figure 5-25: *Effect of process steps on elongation at fracture*

5.3 Energy absorption behaviour

Quasi-static crush testing of formed and joined top-hat profiles was used in order to estimate the energy absorption behaviour of the different process chains on component level. Characteristics such as specific energy absorption and crush force efficiency were derived from the force-length curves recorded. Further, a visual assessment of the components' folding and cracking behaviour was conducted.

5.3.1 Visual assessment of compressed samples

Table 5-3 illustrates the deformation and damage behaviour of compressed parts that have been produced by the six different process chains.

A key finding after repetitious crush testing was that plasticity of unstabilised profiles (HF 7021, WTF 7021, HF 7075, WTF 7075) is obviously not high enough to initiate a periodical deformation pattern. Local strain reaches a critical value even before the profile has produced a complete fold. Consequently, rupture takes place either at the tip of the fold or in the flange radius close to where cover plate and top-hat profile have been joined. The rest of crushing continues rather arbitrarily then through bursting at the rivet connections, tearing along the side-wall section or shearing off the cover plate.

Some stabilised profiles (HF-S 7021, PSF 7021) conversely were able to produce two entire folds and did not exhibit major cracks. The additional heat treatment carried out with these parts has most likely raised their capability for tolerating higher local deformation. It seems to be noteworthy, that most of HF-S 7021 parts tend to fold at the end while PSF 7021 parts rather deform in the centre. For the HF-S 7021 parts, the cover plate was involved in creating the folding pattern while for the PSF 7021 parts, it was partly sheared off due to bursting at some rivet connections. A sheared off cover plate negatively affects the part's stability and thus crushworthiness. Folding is then more likely to continue where the cover plate is missing and the amount of energy absorbed by a single fold is reduced.

Besides conducting an additional stabilisation heat treatment, it is especially the integration of appropriate trigger mechanisms into the part geometry that promises a further improvement of folding patterns. More research is also needed with respect to the self-pierce riveting operation so that better joints can help to enhance overall part stability.

Table 5-3: *Compressed top-hat profiles*

Process chain	Sample 1	Sample 2	Sample 3
HF 7021			
WTF 7021			
HF-S 7021			

Table 5-3: *Compressed top-hat profiles*
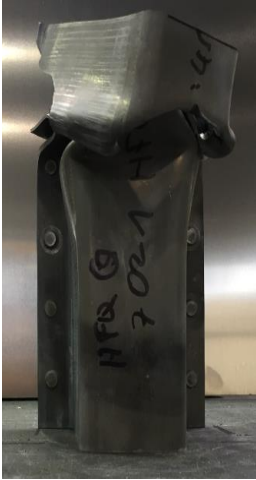
Process chain	Sample 1	Sample 2	Sample 3
PSF 7021			
HF 7075			
WTF 7075			
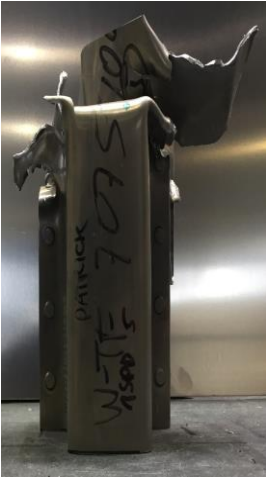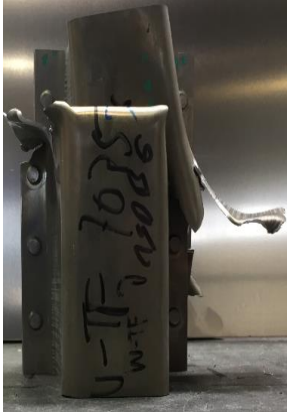
5.3.2 Quantitative crush worthiness assessment

The quantitative assessment of quasi-static crush worthiness was performed according to the characteristics commonly used for dynamic problems. Of course, deformation modes in dynamic crash situations might deviate considerably from the quasi-static case. Still, especially mean forces determined through quasi-static crush testing are believed to give a first hint on energy values that can potentially be absorbed under dynamic loading.

Force-length curves

Figure 5-26 shows the averaged force-length curves from quasi-static crush testing. The single measurements can be found in Appendix 5. In all curves, an initial force peak can be observed indicating the start of plastic deformation. This so-called trigger force is higher for the AW-7021 samples than for the AW-7075 samples (cf. Table 5-4), which is most likely linked to the higher yield strength values of the former after 1SPB.
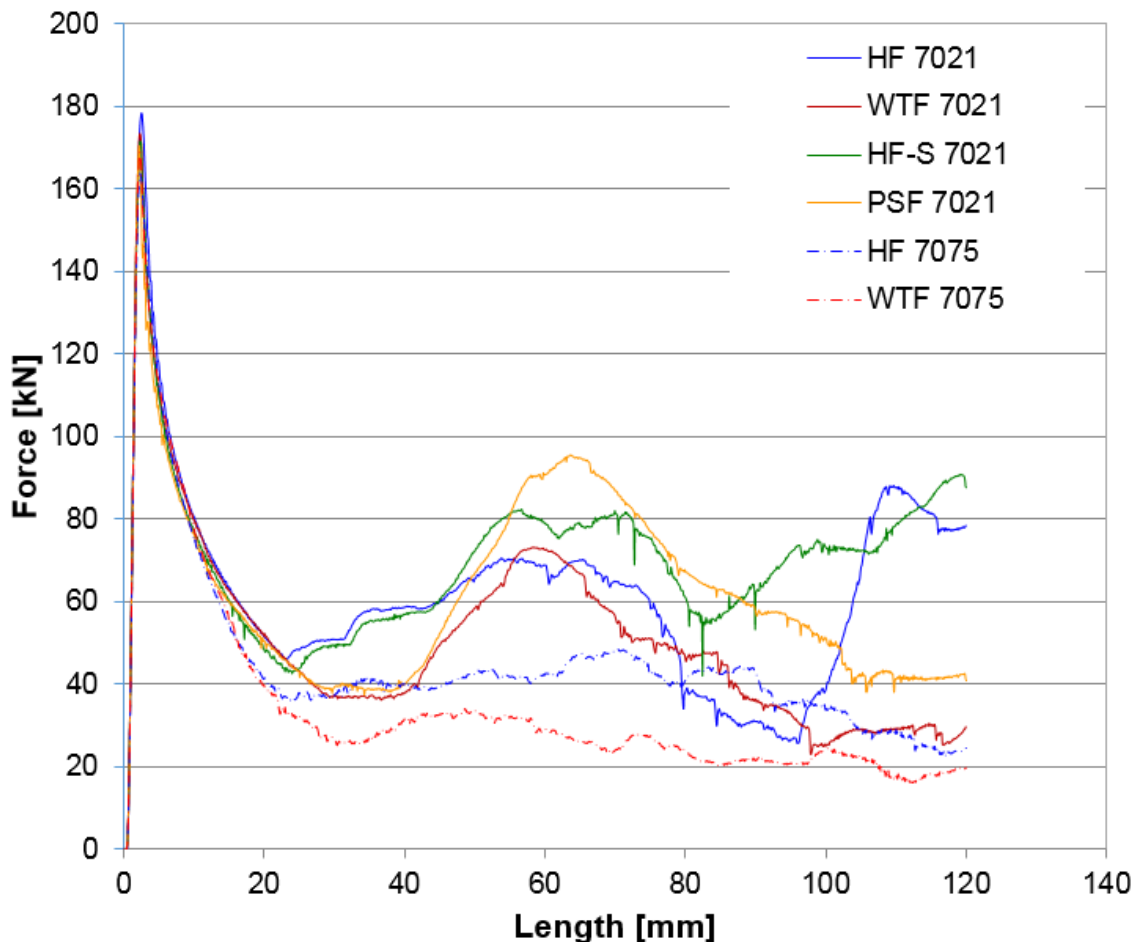
Figure 5-26: *Force-length curves from quasi-static crush testing*

After having reached the trigger point, a second increase in crush force occurs at approximately 25 mm for the HF-S 7021 and HF 7021 curves, while force levels of WTF 7021 and PSF 7021 curves start to rise again after approximately 45 mm. Parts

made from AW-7075 do not show a significant increase in crush force after having reached the major crush phase at 20 mm crush length. For HF 7075 and WTF 7075, crush force stays rather constant at a low level from that point on.

All AW-7021 process chains exhibit a second force peak at approximately 60 to 70 mm of crush length. Parts produced through hot forming (HF 7021, HF-S 7021) show a final increase in crush force after having reached the second force peak, while force levels of WTF 7021 and PSF 7021 samples continuously decrease thereafter. Interestingly enough, the second force peak is much more pronounced for the stabilised parts HF-S 7021 and PSF 7021 than for non-stabilised ones HF 7021 and WTF 7021. This reflects their better folding capability compared to the other process chains (cf. Section 5.3.1).

Energy-deformation curves

Energy absorption EA has been calculated from the force-length data through numerical integration according to Equation 2-4 in Section 2.6.3.

Figure 5-27 shows how the amount of energy absorbed increases with respect to the parts' relative deformation (punch displacement/ initial sample length). It becomes obvious from the diagram that alloy and process influence the gradient of the energy-deformation curves.
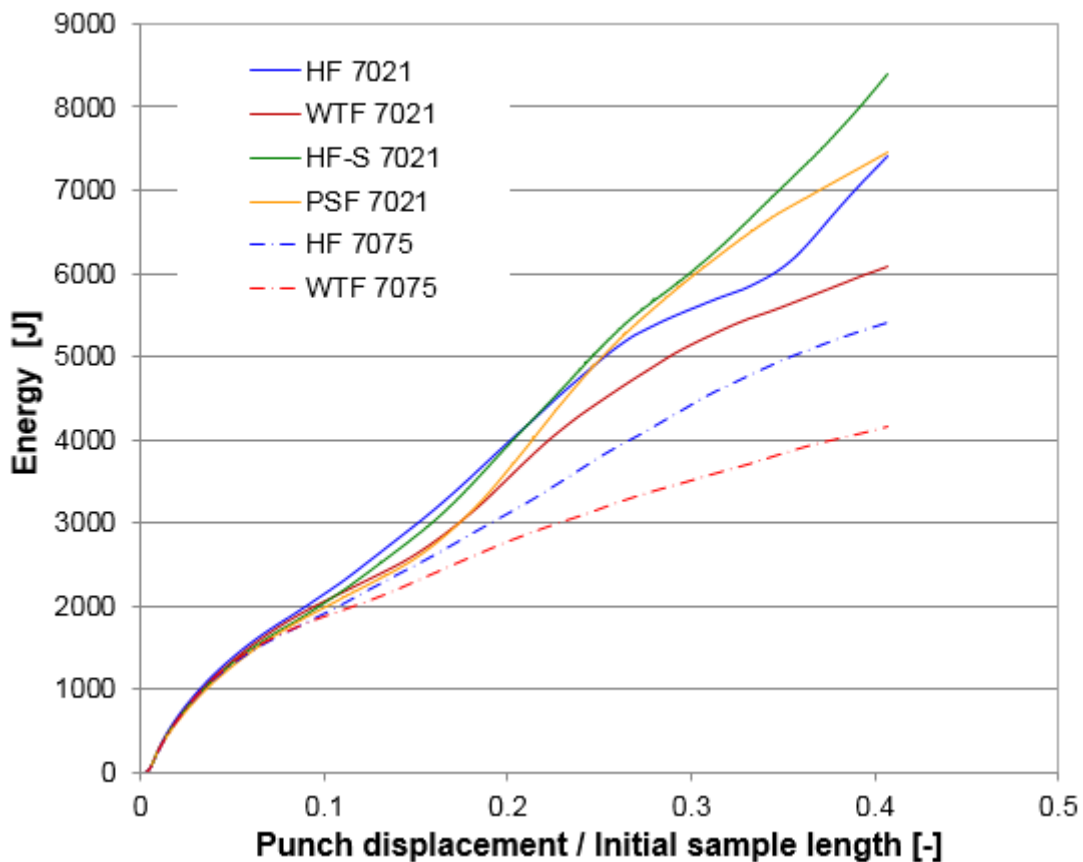
Figure 5-27: *Energy-deformation curves from quasi-static crush testing*

Generally speaking, higher gradients in energy-deformation curves can be attributed to higher mean crush force levels and an improved folding capability. In turn, higher mean crush force levels are in most cases directly related to higher part strength and an improved folding capability is due to better ductility. Tensile testing in Section 5.2.4 has shown that stabilised AW-7021 samples perform better in both, yield strength and elongation at fracture than non-stabilised samples from AW-7021 and samples from AW-7075. These findings are reinforced by the comparatively steep energy-deformation curve of HF-S 7021 from Figure 5-27. Contrarily, the rather flat curves of the parts made from the AW-7075 alloy indicate that they are much more brittle and part failure rather occurs through tearing than through folding.

Crush worthiness parameters

In Table 5-4, the averaged values from the determination of various crush worthiness parameters are compiled. A detailed description with respect to how these parameters are obtained and what they mean is given in Section 2.6.3.

Table 5-4: *Summary of averaged crushworthiness parameters*

Process chain	m [kg]	TF [kN]	MCF [kN]	CFE [%]	EA [J]	SEA [J/g]
HF 7021	0.65	178.73	62.27	34.84	7405.07	11.33
WTF 7021	0.65	173.73	40.04	23.06	6072.98	9.38
HF-S 7021	0.65	171.90	73.63	42.83	8392.27	12.82
PSF 7021	0.65	170.17	53.79	31.65	7445.10	11.37
HF 7075	0.65	164.10	35.20	21.44	5399.28	8.26
WTF 7075	0.65	169.2	24.25	14.34	4150.12	6.21

As expected, parts produced through the HF-S 7021 process chain perform best in terms of all mean crush force *(MCF)*, crush force efficiency *(CFE)* and specific energy absorption *(SEA)*. Parts from PSF 7021 and HF 7021 come in second place, with slightly higher SEA values for PSF 7021 but better results with respect to MCF and CFE for HF 7021. Profiles from the hot forming process chain HF 7021 perform better in all categories than their counterparts from the W-temper forming process chain WTF 7021. The same holds true for the AW-7075 alloy, although on a much lower level of crush worthiness of course.

A comparison of the results from this study with previous measurement data is difficult. This is partly because very little on the energy absorption behaviour of AW-7xxx aluminium structures has been published so far and partly because the test setup greatly varies with respect to part geometry, crush length, joining method or test speed in previous work. Still, a first estimation about the plausibility of the measured and calculated data can be obtained by having a look at the following two studies:

Estrada et al. [26] have performed finite element simulations to analyse the effect of mechanical discontinuities on the crushworthiness of AW-7108 T6 aluminium extrusions under dynamic loading. The extrusions were 400 mm in length, the dimension of the rectangular cross-section was 68 x 95 mm and sheet thickness was 2.5 mm. A striker mass of 500 kg would impact the parts with an initial velocity of 10 m/s at one end, the other end was placed in a rigid support. According to their models, the extrusions can absorb about 14.28 [J/g] at a relative deformation of about 0.4. Size and position of the mechanical discontinuities have already been optimised at that stage.

Kirov [27] has conducted quasi-static crush testing with structurally glued top-hat profiles from AW-5083 sheets. The profiles had a similar cross-section to the ones investigated within this work but were 400 mm in length. They were compressed for 200 mm at a constant speed of 10 mm/s, thus final relative deformation was at about 0.5. The profiles were able to produce four entire folds, however their cover plates were not included in the folding pattern but were rather sheared off. When reaching a relative deformation of 0.5, the parts had absorbed about 6200 J. Assuming a largely linear energy-deformation curve, this would correspond to approximately 4960 J at a relative deformation of 0.4.

5.4 Energy and material flow based system description

Conducting an additional stabilisation heat treatment directly after hot forming might be a particularly promising way of increasing resource efficiency in terms of product optimisation. As reported in Section 5.3.2, HF-S parts show the best potential for achieving high specific energy absorption values out of all process chains investigated within this work. From a process perspective, it is still questionable though how suitable hot-forming and especially the additional stabilisation heat treatment are in order to also lower resource consumption during production. For this reason, a qualitative, flow-oriented system description has been developed for the hot forming with subsequent stabilisation (HF-S) process chain. It builds upon the Black-Box thinking principle of energy and material flows presented in Section 4.11. By means of qualitatively discussing important system in- and outputs, a holistic view on production-relevant resource efficiency aspects of the HF-S process chain is given in the following.

Solution heat treatment

Just as for any of the other process chains investigated within this thesis, also parts produced through the HF-S chain need to be solution heat treated in the beginning (cf. Figure 5-28). Solution heat treatment is a very resource-intensive first process step in terms of energy and material flow. In larger industrial settings, it will usually occur in roller hearth furnaces consuming high amounts of electricity, natural gas and compressed air so as to achieve an even heating of the blanks with little temperature change during the hold time. The command variables of solution heat treatment temperature and time appear to be suitable levers to reduce the required amount of heat flow needed within this first process step. A blanket statement whether it is more resource-efficient to heat treat at higher temperatures for shorter time or vice versa cannot be given at this point. This issue must however be thought of when quantitatively assessing material and energy flow so as to prepare for optimisation.

Non-isothermal hot forming

During non-isothermal hot forming (cf. Figure 5-29), the solutionised sheets are quenched in the cold dies.

The material flow into this process step differs in two aspects from room temperature forming strategies. First, cooling water is needed so as to allow for sufficiently cold dies even if production volumes are high. This implies leakages and thus reduced sustainability. Second, high-performance lubricants capable of withstanding the elevated temperature levels have scarcely been developed so far [4]. Therefore, it is questionable whether the standards with respect to tribological aspects and lubricant consumption known from established cold forming processes can be met.

Energy consumption of a forming press is mainly governed by cycle time and required loads to form the sheets [6]. As shown in Section 5.1.3, blank strength considerably decreases at elevated temperatures. Considering blank strength as an important command variable for the hot forming step, it can be expected that required forming

loads will be significantly lower compared to room temperature forming strategies. At the same time though, cycle times will be a bit higher since the dies need to be kept closed even after forming has been completed. This is crucial so as to ensure sufficient quenching. The trade-off between reduced loads but slightly increased cycle times should be kept in mind when quantitatively evaluating press energy consumption.

Tool wear and therefore human support in terms of maintenance will be reduced due to lower press loads during non-isothermal hot forming [28]. In the long run, an increased tool-life due to less tool wear could positively affect the resource-efficiency balance of the HF-S process chain since it would reduce the number of tools that have to be machined. From an economic point of view, less maintenance effort could help to cut costs in terms of saving personnel hours.

Since plastic flow behaviour is much higher at elevated temperatures, it can be assumed that dimensional accuracy of hot formed parts is superior to other process chains. Higher dimensional accuracy means improved process stability and less scrap parts. In that sense, hot forming could help saving resources in terms of reducing material emissions.

Most important, non-isothermal hot forming saves an entire process step. Since the quenching step occurs simultaneously to the forming step, this makes it possible to save resources in terms of paring down additional handling operations. Also, the additional water consumption to cool the dies is eventually relativised therewith. For room temperature forming strategies, water or forced air is used to quench the sheets before they are formed.

Stabilisation heat treatment
The stabilisation heat treatment itself (cf. Figure 5-30) does only negatively affect the resource efficiency balance of the HF-S process chain. Additional effort in terms of material and energy is needed in order to perform this extra process step. The additional effort needs to be justified, either as a facilitation for subsequent process steps or due to increasing the quality of the final product.

Trimming
Having the parts in a substantially stable condition reduces the influence of the disturbance variable part hardness on the trimming process step (cf. Figure 5-31). In this context, command variables such as cutting line or trimming force can be met more precisely and process stability increases. Increased process stability does in turn reduce tool wear, lubricant consumption or the amount of scrap parts. This is because trimming machines can more precisely be adjusted to work under standardised conditions then. Undesired effects such as excessive cutting impact are reduced to a minimum.

Joining

For the joining step (cf. Figure 5-32), similar considerations as already discussed for the trimming step apply. It can be expected that stable material properties have the potential to facilitate the implementation of standardised operations. Against this background, especially material emissions such as scrap parts, rivet waste or consumed lubricant are believed to be lowered while rivet quality should rise at the same time. The latter is eventually important for improving overall part quality and thus ameliorate resource efficiency in use.

Paint bake heat treatment

The paint bake heat treatment (cf. Figure 5-33) marks the end of the process chain. From a resource-efficiency viewpoint, it is crucial to eventually obtain a final product with high artificial ageing response and good specific energy absorption behaviour here. For the HF-S process chain, the input into this last process step is a stabilised part. It can be expected that HF-S parts show improved part strength and ductility when leaving the paint bake furnace. In the sense of enabling weight reduction through high specific energy absorption, they might thus be promising candidates to save resources in use.

Following the general system description presented within this section, a quantification of all energy and material flows can take place during later stages of product and process development. Such a quantification could then serve as a basis for managing and optimising the process chain. Anyhow, creating a sound process description in the beginning seems to be central in order to achieve a resource-efficient process chain in the end. This is in accordance with the maxim set up by Peter Drucker:

> *"If you can't describe it, you can't measure it!*
> *If you can't measure it, you can't manage it!*
> *If you can't manage it, you can't optimise it!"*
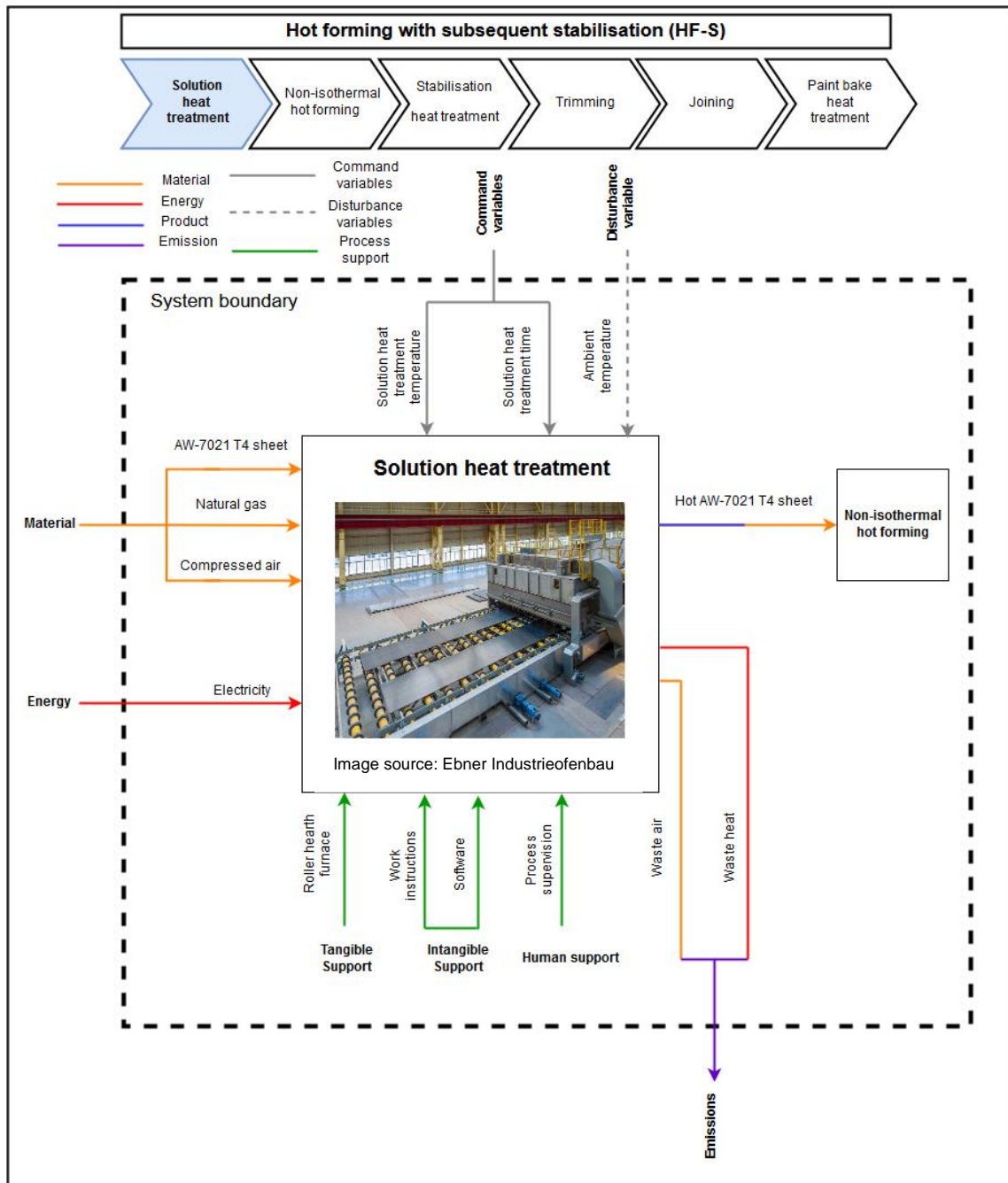
Figure 5-28: System description of the solution heat treatment step for the HF-S process chain
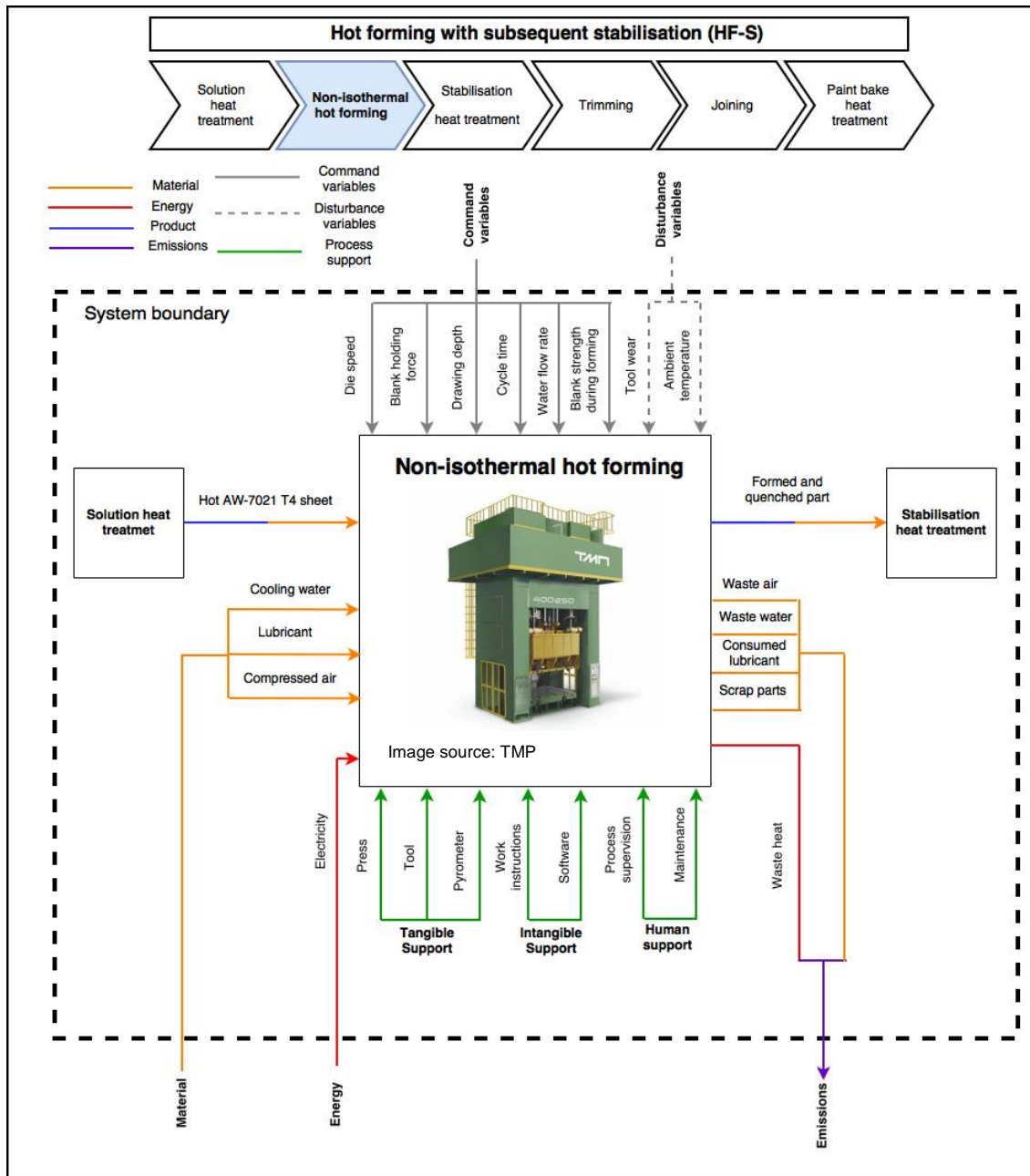
Figure 5-29: *System description of the non-isothermal hot forming step for the HF-S process chain*
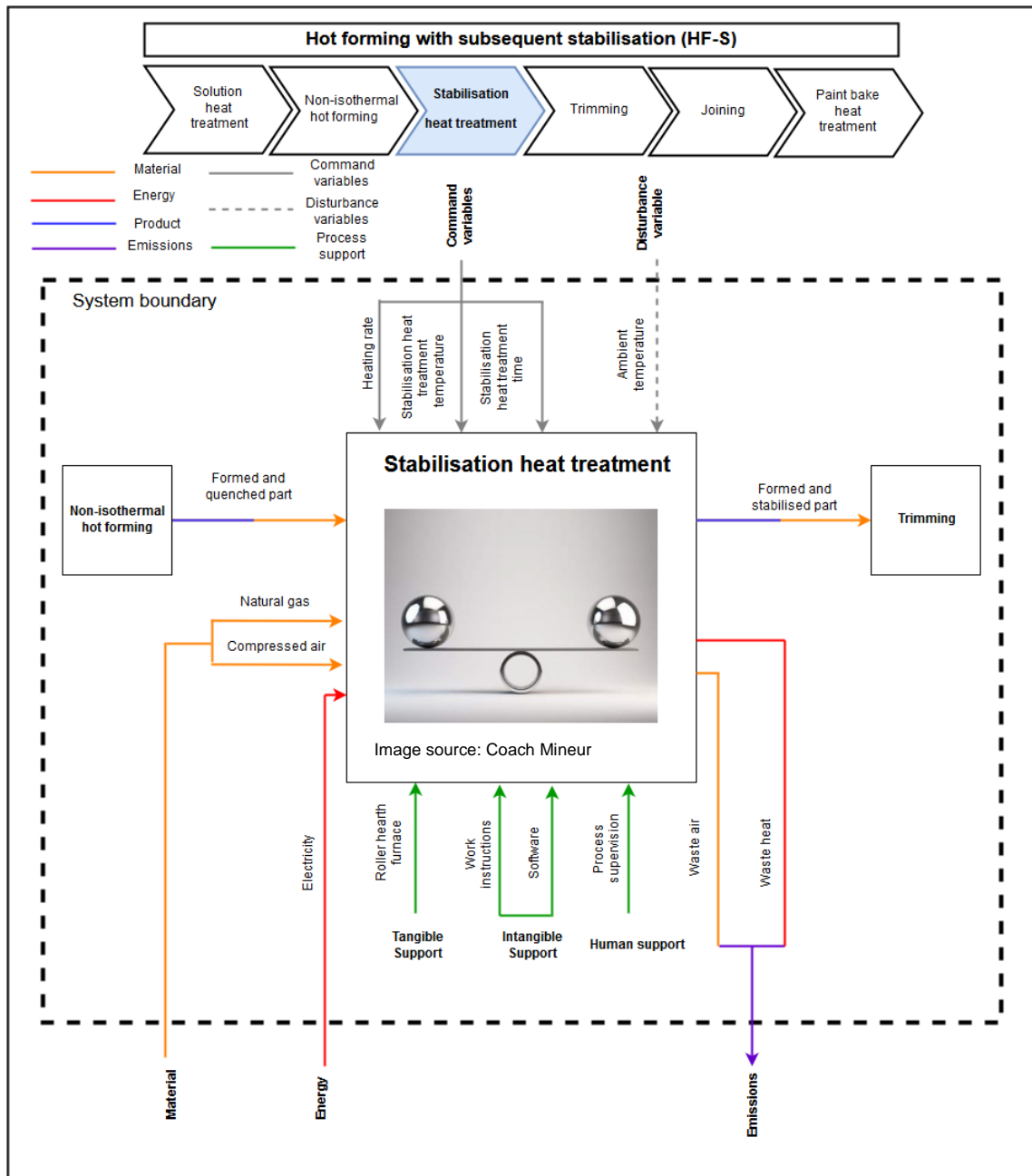
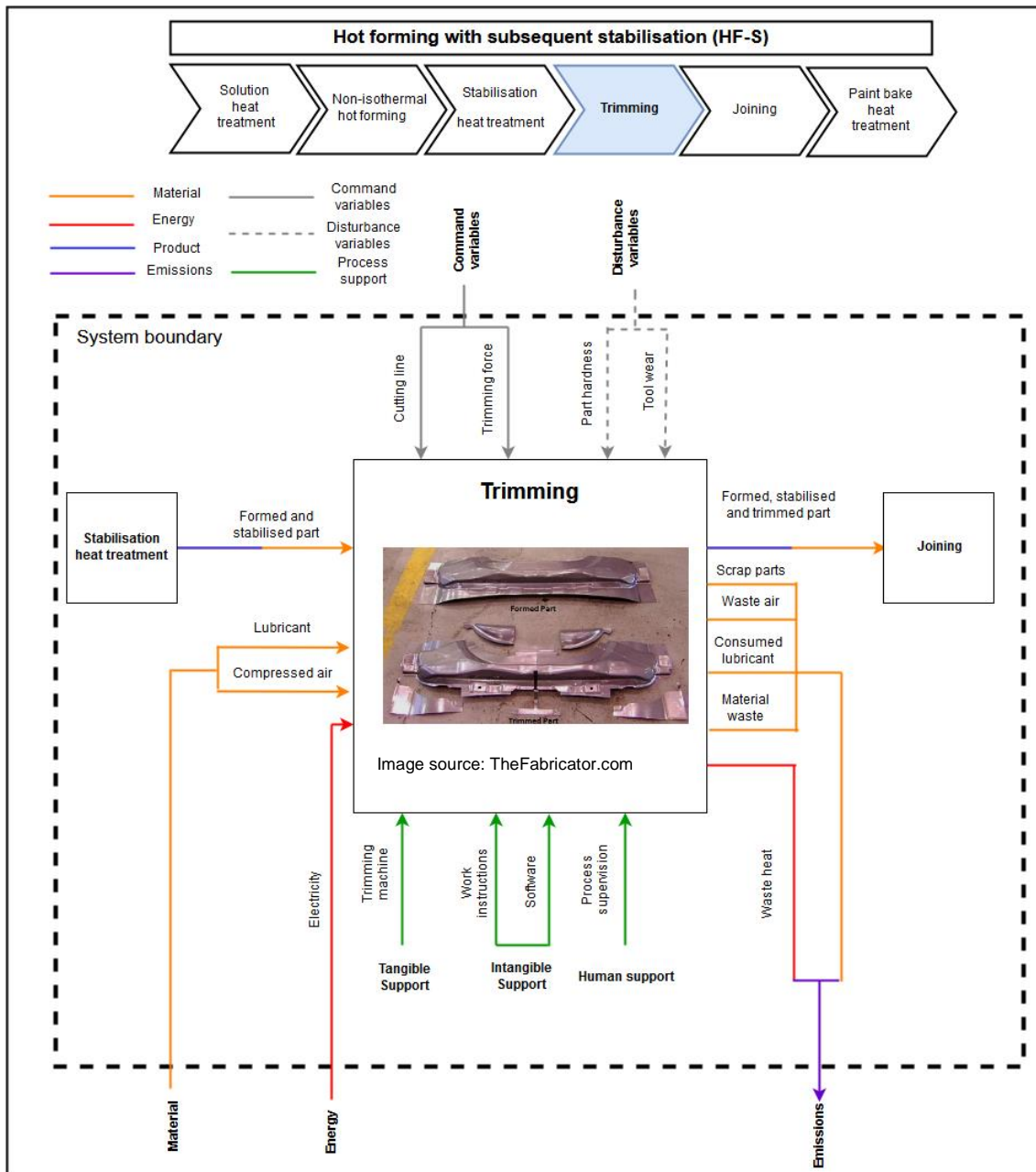**Figure 5-30:** *System description of the stabilisation heat treatment step for the HF-S process chain*

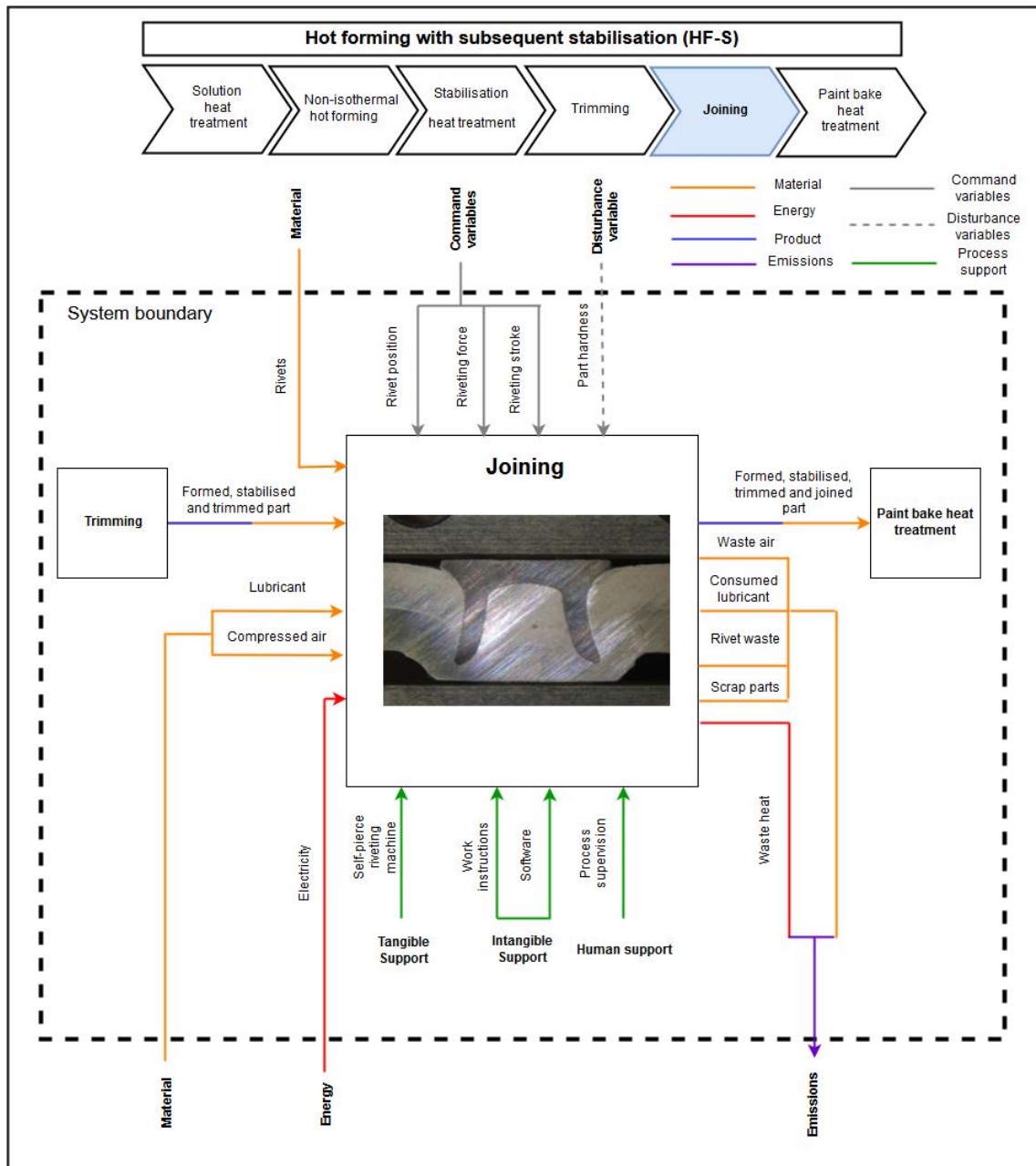***Figure 5-31:*** *System description of the trimming step for the HF-S process chain*

Figure 5-32: *System description of the joining step for the HF-S process chain*
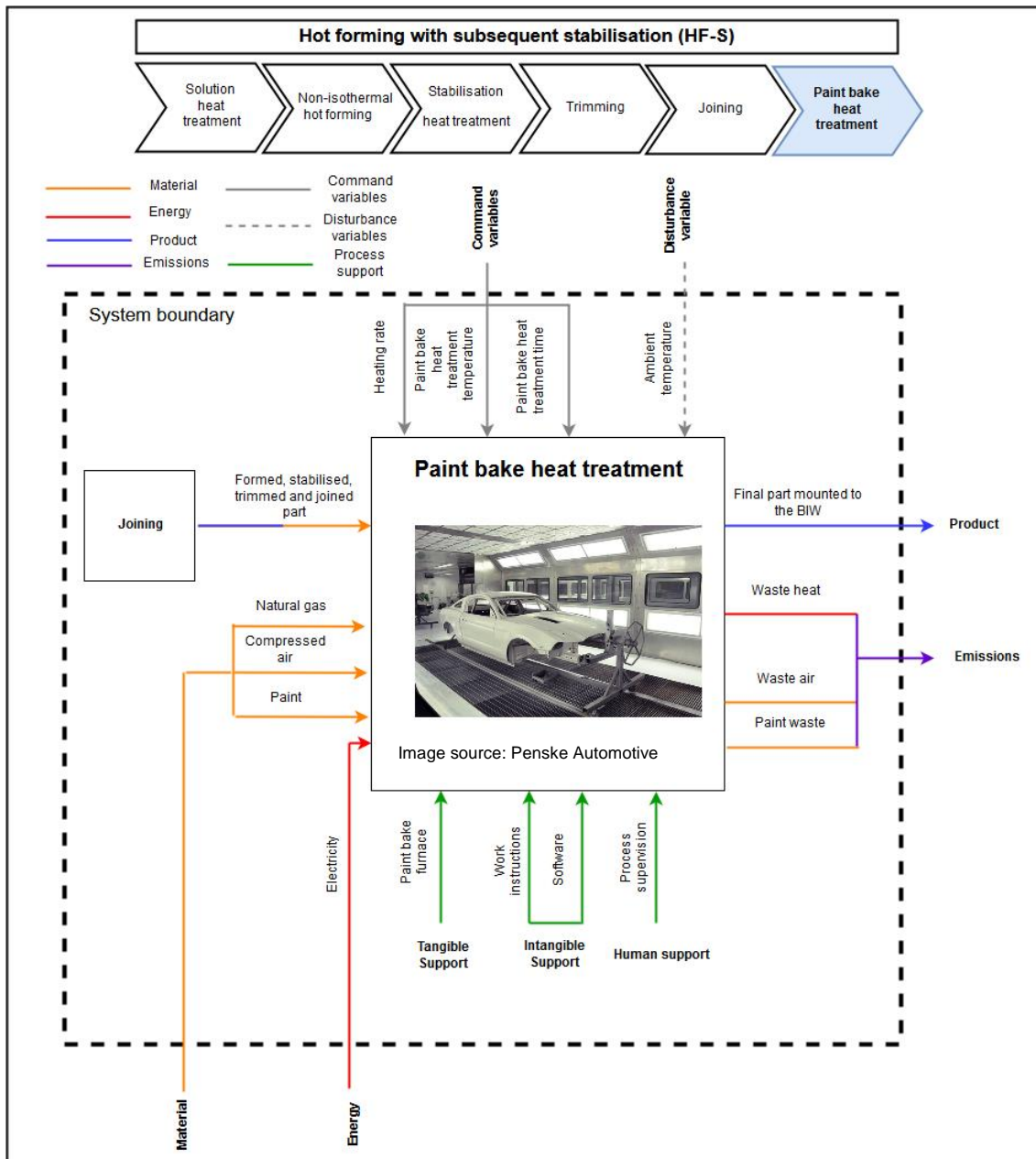
Figure 5-33: *System description of the paint bake heat treatment step for the HF-S process chain*

6 Conclusion

This work has characterised process chains for the production of automotive structural parts from AW-7021 and AW-7075 aluminium sheets. Due to their high specific strength, AW-7xxx aluminium alloys might be suitable materials for crash relevant parts. Their formability at room temperature is poor though. Therefore, alternative forming strategies and process routes are required. The variants studied within this thesis are hot forming (HF) and W-temper forming (WTF) respectively (cf. Section 2.5). Since post-forming material properties of AW-7xxx alloys are not stable throughout the process chains of HF and WTF, two further process modifications with respect to an additional stabilisation heat treatment have been investigated: Hot forming with subsequent stabilisation (HF-S) and post stabilisation forming (PSF) (cf. Section 2.5). The main findings with respect to the HF, WTF, HF-S and PSF process chains are presented in accordance with the research questions set up in Chapter 3.

(RQ 1) How do the alloys EN AW-7021 and EN AW-7075 perform in terms of **formability** *when being processed with the strategies of hot forming (HF), W-temper forming (WTF) and post stabilisation forming (PSF)? (Note: HF and HF-S do only differ after forming.)*

Hot forming (HF):

- Both, HF 7021 and HF 7075 seem to be suitable process variants to produce parts with high dimensional accuracy and low spring back.
- Both, HF 7021 and HF 7075 are sensitive to strain rate and temperature. Formability increases with increasing temperature and decreasing strain rates. This can be derived from strength and elongation at fracture values determined through tensile testing. On microstructure level, the reason for improved formability at elevated temperatures and low strain rates might be seen in more pronounced dynamic recovery.

W-temper forming (WTF):

- If forming is carried out immediately after quenching, WTF 7021 appears to be suitable to produce parts with high dimensional accuracy and low spring back. WTF 7075 is more likely to yield parts with low dimensional accuracy and extensive spring back.
- Both, WTF 7021 and WTF 7075 are not particularly strain-rate sensitive. Yield strength in the W state is approximately 200 MPa lower than in the as-delivered industrial T4 (AW-7021) or T6 (AW-7075) condition respectively. Elongation at fracture improves by about 15 % compared to the as-delivered industrial condition.

Post stabilisation forming (PSF):

- PSF 7021 is suitable to form simple geometries without fracture, even though dimensional accuracy might not be particularly good.
- PSF 7021 is not strain-rate sensitive. Compared to the as-delivered industrial T4 condition yield strength is about 60 MPa lower in the stabilised state.

(RQ 2) *How do* **material properties** *of the alloys EN AW-7021 and EN AW-7075* **change along the process chains** *of HF, HF-S, WTF and PSF?*

Natural ageing behaviour:

- Forming increases the hardness of the sheets. The hardness of parts formed at room temperature (WTF 7021, WTF 7075, PSF 7021) is higher than the hardness of parts produced through hot forming (HF 7021, HF 7075, HF-S 7021). This is due to reduced strain hardening of the HF process chains compared to the WTF and PSF process chains.
- HF 7021, HF 7075, WTF 7021 and WTF 7075 increase in hardness throughout a time span of 21 days after forming.
- HF-S 7021 and PSF 7021 do not vary significantly in hardness during an observation period of 21 days after forming. The hardness of parts produced through HF-S 7021 is lower than the hardness of parts produced through HF 7021 after 21 days.

Joinability:

- HF is more suitable for self-pierce riveting than WTF due to less strain hardening induced into the material during the forming operation. This applies for both alloys, AW-7021 and AW-7075 respectively.

Paint bake response:

- AW-7021 process chains (HF 7021, HF-S 7021, WTF 7021, PSF 7021) on average show slightly higher yield strength values than AW-7075 process chains (HF 7075, WTF 7075) after 21 days of natural ageing and 1SPB (185°C, 25 min).
- Conducting a stabilisation heat treatment prior to paint baking does not only increase paint bake response, it does at the same time also help the material retain some of its initial ductility. This behaviour is desired for crash relevant parts.

(RQ 3) *How do test crush elements from EN AW-7021 and EN AW-7075 that have been produced with the process routes of HF, HF-S, WTF and PSF differ with respect to their* **energy absorption behavior**?

Folding capability:

- Plasticity of unstabilised profiles (HF 7021, WTF 7021, HF 7075, WTF 7075) is not high enough to initiate a periodical deformation pattern.
- Some of the stabilised profiles (HF-S 7021, PSF 7021) were able to produce two entire folds and did not exhibit major cracks.

Energy absorption:

- Parts produced by AW-7021 process chains absorb considerably more energy than parts produced by AW-7075 process chains during quasi-static crush testing. Stabilised profiles (HF-S 7021, PSF 7021) outperform unstabilised profiles in terms of energy absorption.

*(RQ 4) How suitable is the process chain that promises highest resource efficiency during end use to also **save resources** during **production**?*

HF-S 7021 is the process chain that promises highest resource efficiency during end use due to comparatively high specific energy absorption values. Key considerations concerning its resource efficiency balance during production are:

- Hot forming might improve resource efficiency in terms of fewer scrap parts, less tool wear and lower press energy consumption.
- An additional stabilisation heat treatment represents an extra effort in terms of material and energy consumption.
- Higher specific energy absorption values and more stable operations might justify the additional effort of a stabilisation heat treatment.

The results show that the process route HF-S 7021 is most promising with respect to formability, post forming material properties, energy absorption behaviour and resource efficiency out of all variants investigated within this work. An additional stabilisation heat treatment does not only improve paint bake response and crushworthiness, it might at the same time also enhance process stability and could therefore be a suitable lever to facilitate logistics in the automotive industry. Altogether, this could lead to an increased use of high-strength AW-7xxx alloys for structural parts in the future.

In a follow-up project to this thesis, the dynamic energy absorption behaviour of similar parts will be examined. Based on the results from tensile testing, a material model for finite element forming and crash simulations will be built up. It is suggested that further investigations focus on the creation of forming limit diagrams for selected process routes and forming states. During later stages of product and process development, further research issues might also be seen in a quantification of material and energy flows throughout the production process. This could help to prepare for optimisation of selected process chains with respect to resource efficiency.

Bibliography

[1]   "European Aluminium Association," [Online]. Available: https://www.european-aluminium.eu/. [Accessed 11 11 2017].

[2]   F. Ostermann, Anwendungstechnologie Aluminium, Meckenheim: Springer Vieweg, 2014.

[3]   M. Lesemann and C. Sahr, "SuperLIGHT-CAR - the Multi-Material Car Body," LS-DYNA Anwenderforum, Bamberg, 2008.

[4]   M. Kumar, G. Kirov, F. Grabner and E. Mukeli, "Sheet forming porcesses for AW-7xxx Alloys: Relevant Process Parameters," *Materials Science Forum,* pp. 1036-1042, November 2016.

[5]   T. Grohmann, "Forming of AMAG 7xxx Series Aluminium Sheet," AMAG Austria Metall AG, Scientifc report, 2016.

[6]   C. Ingarao, R. Di Lorenzo and F. Micari, "Sustainability issues in sheet metal forming processes: an overview," *Journal of Cleaner Production,* pp. 337-347, October 2010.

[7]   "European Aluminium Association - Automotive Manual," [Online]. Available: https://www.european-aluminium.eu/resource-hub/aluminium-automotive-manual/. [Accessed 11 11 2017].

[8]   H.-J. Bargel and G. Schulze, Werkstoffkunde, Berlin: Springer Vieweg, 2012.

[9]   B. Milkereit, "Kontinuierliche Zeit-Temperatur-Ausscheidungs-Diagramme von Al-Mg-Si-Legierungen," Rostock University of Technology, Doctoral thesis, 2010.

[10]   "MakeItFrom.com - Material Properties Database," [Online]. Available: https://www.makeitfrom.com/. [Accessed 11 11 2017].

[11]   M. Beck, B. Milkereit and O. Kessler, "Ergebnisbericht Lösungsglühbedingungen, Erwärmexperimente und Kühlexperimente für die Legierugen EN AW-7021+V2 und EN AW-7075," Universtiät Rostock - Lehrstuhl für Werkstofftechnik, Scientific report, 2016.

[12]   V. Hansen, O. Karlsen, Y. Langsrud and J. Gjunnes, "Precipitates, zones and transitions during aging of Al-Zn-Mg-Zr 7000 series alloy," *Materials Science and Technology,* pp. 185-193, February 2004.

[13]   J. A. Oesterreicher, G. Kirov, E. Mukeli, F. Graber, M. Kumar and S. Gerstl, "Stabilization of 7xxx aluminium alloys," LKR Ranshofen, Scientific report, 2017.

[14]   A. Fallahiarezoodar, B. Aykas, D. Infante and T. Altan, "the fabricator.com," [Online]. Available: http://www.thefabricator.com/article/stamping/r-d-update-practical-methods-for-estimating-formability-of-sheet-materials. [Accessed 13 11 2017].

[15]   F. Hönsch, "Experimentelle Untersuchung und statistische Analyse wesentlicher

Prozessparameter beim Stanznieten von Aluminiumblechen," Technische Universität Graz, Master thesis, 2017.

[16] F. Garattoni, "Crashworthiness and composite materials: development of an experimental test method for he energy absorption determination and implementation of the relative numerical model," Universita di Bologna, Doctoral thesis, 2011.

[17] A. Göschel, A. Sterzing and J. Schönherr, "Systembetrachtungen von Prozessketten der Blechwarmumformung in Hinblick auf Energie- und Resourceneffizienz," Fraunhofer, Scientific report, 2010.

[18] NETZSCH-Gerätebau GmbH, "Differential Scanning Calorimetry DSC 204 F1 Phoenix," Netzsch Group, Product manual.

[19] J. Osten, B. Milkereit, C. Schick and O. Kessler, "Dissolution and Precipitation Behaviour during Continuous Heating of Al-Mg-Si Alloys in a Wide Range of Heating Rates," *Materials,* p. doi: 10.3390/ma8052830, May 2015.

[20] M. Zhou, Y. Lin, J. Deng and Y.-Q. Jiang, "Hot tensile deformation behaviors and constitutive model of an Al–Zn–Mg–Cu alloy," *Materials and Design,* pp. 141-150, March 2014.

[21] M. Kumar and N. Ross, "Investigations on the hot stamping of AW-7921-T4 alloy sheet," *Hindawi Publishing Corporation - Advances in Materials Science and Engineering,* p. Article ID 7679219, February 2017.

[22] R. Picu, "A mechanism for the negative strain-rate sensitivity of dilute solid solutions," *Acta Materialia,* pp. 232-246, April 2004.

[23] R. Picu, G. Vinczeb, F. Ozturka, J. Graciob, F. Barlatb and A. Maniattya, "Strain rate sensitivity of the commercial aluminum alloy AA5182-O," *Materials Science and Engineering,* pp. 334-343, August 2004.

[24] L. Hadjadj, R. Amira, D. Hamana and A. Mosbah, "Characterization of precipitation and phase transformations in Al–Zn–Mg alloy by the differential dilatometry," *Journal of Alloys and Compounds,* pp. 279-283, August 2007.

[25] X. Jiang, B. Noble, B. Holme, G. Waterloo and J. Tafto, "Differential Scanning Calorimetry and Electron Diffraction Investigation on Low-Temperature Aging in Al-Zn-Mg Alloys," *Metallurgical and materials transactions A,* pp. 339-348, February 2000.

[26] Q. Estrada, D. Szwedowicz, J. Silva-Aceves, T. Majewski, J. Vergara-Vazquez and A. Rodriguez-Mendez, "Crashworthiness behavior of aluminum profiles with holes considering damage criteria and damage evolution.," *International Journal of Mechanical Sciences,* pp. 776-791, October 2017.

[27] G. Kirov, "Numerische Betrachtungsmethoden für strukturell geklebte Bauteile," Fachhochschule Wels, Master thesis, 2013.

[28] J. Mendiguren, E. Saenz de Argandona and L. Galdos, "Hot stamping of AA7075 aluminium sheets," *Materials Science and Engineering,* pp. doi:10.1088/1757-

899X/159/1/012026, 2016.

[29] B. Milkereit, N. Wanderka, C. Schick and O. Kessler, "Continuous cooling precipitation diagrams of Al–Mg–Si alloys," *Materials Science and Engineering: A,* pp. 87-96, July 2012.

List of Figures

List of Tables

Abbreviations

Al	aluminium
AW	wrought aluminium alloy
A_0	initial cross section
°C	degree Celsius
CFE	crush force efficiency
c_p	excess specific heat capacity
Cr	alloying element chromium
Cu	alloying element copper
D	sphere diameter (hardness testing)
d	day
d	indentation diameter (hardness testing)
DSC	differential scanning calorimetry
EA	energy absorption
F	force
Fe	alloying element iron
FH	fast hardening
GP zone	precipitation state (cf. Section 2.4.4)
h	hour
HBW	hardness according to Brinell
HF	hot forming
HF-S	hot forming with subsequent stabilisation
HV	hardness according to Vickers
J	Joule
K	degree Kelvin
kN	kilo Newton

kp	kilopond
l	length
L_0	initial length
ΔL	elongation
m	mass
m_{SR}	strain rate sensitivity
MCF	mean crush force
Mg	alloying element magnesium
min	minute
mm	milimetre
MN	Mega Newton
Mn	alloying element manganese
MPa	Mega Pascal
Ni	alloying element nickel
PA	peak ageing
PSF	post stabilisation forming
$\dot{Q}$	heat flow
RF	retrogression forming
R_m	ultimate tensile strength
$R_{p0.2}$	yield strength
RQ	research question
RT	room temperature
S	sheet temper (cf. Section 2.3) - artificially aged to a obtain a stable condition
SEA	specific energy absorption
sec	second
Si	alloying element silicon
s_{rh}	rivet head end position

SSS	supersaturated solid solution state
T	temperature
TF	trigger force
Ti	alloying element titanium
T_m	melting temperature
T-phase	precipitation state (cf. Section 2.4.4)
t_r	residual wall thickness
T4	sheet temper (cf. Section 2.3) - naturally aged to a substantially stable condition
T6	sheet temper (cf. Section 2.3) - artificially aged to obtain maximum strength
UTS	ultimate tensile strength
u_i	undercut
W	sheet temper (cf. Section 2.3) - solution heat treated and water quenched
W&1d na	sheet temper (cf. Section 2.3) - solution heat treated, water quenched and 1 day naturally aged
WF	warm forming
WTF	W-temper forming
YS	yield strength
Zn	alloying element zinc
β	heating rate
ε	strain
$\dot{\varepsilon}$	strain rate
ε_f	elongation at fracture
ε_u	uniform elongation
η-phase	precipitation state (cf. Section 2.4.4)
η'-phase	precipitation state (cf. Section 2.4.4)

π   mathematical constant π

ρ   density

σ   stress

1SPB   1 step paint baking

Appendix

Appendix 1: Heat treatment curves
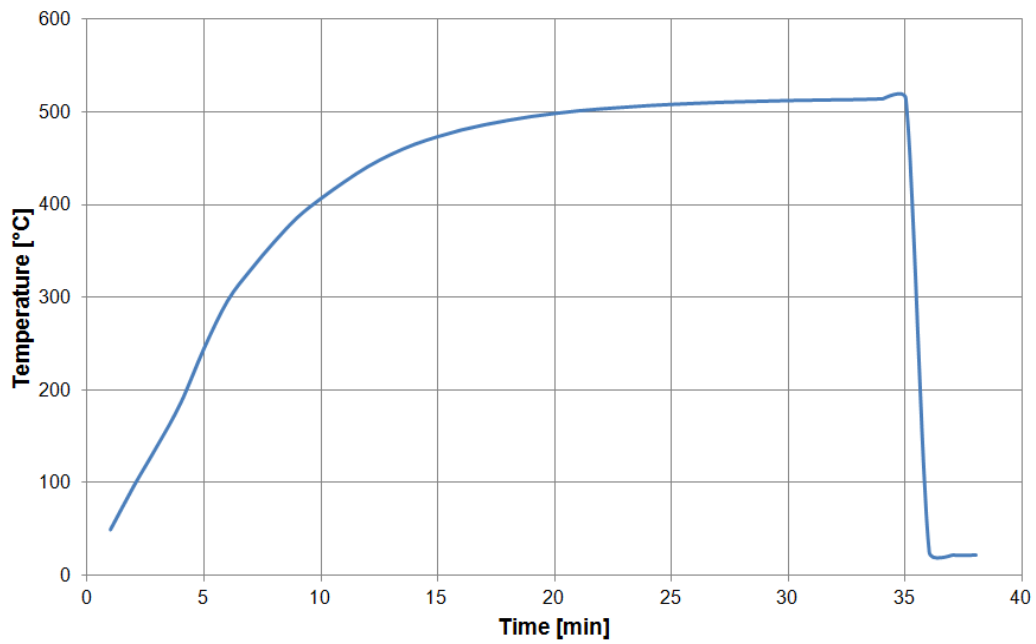
Figure A-1: *Solution heat treatment curve for AW-7021 (515°C / 5 min)*
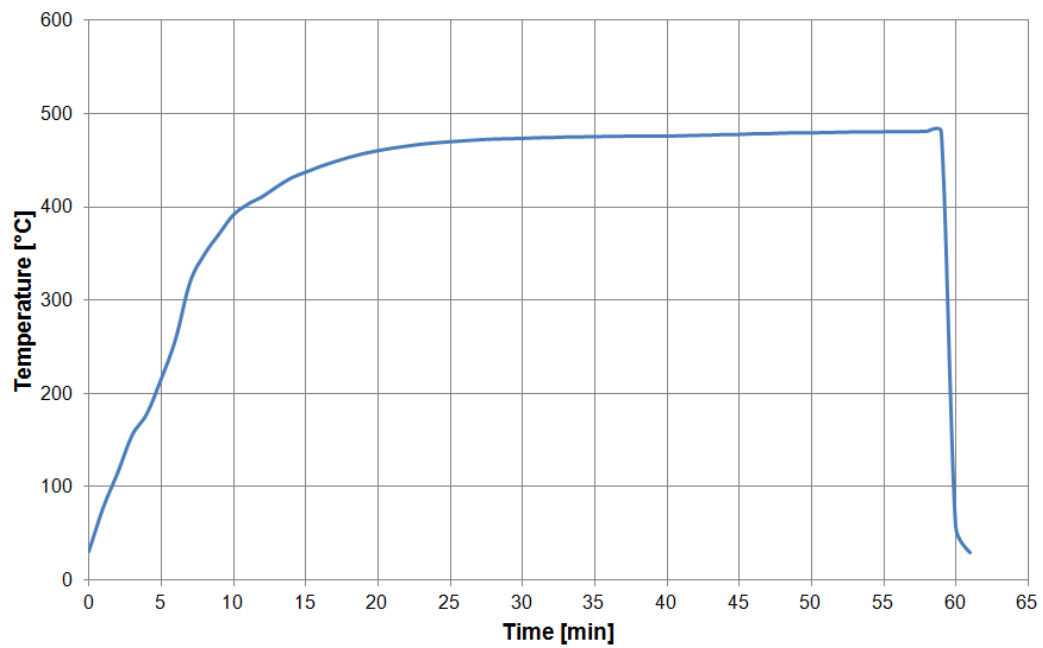
Figure A-2: *Solution heat treatment curve for AW-7075 (480°C / 15 min)*
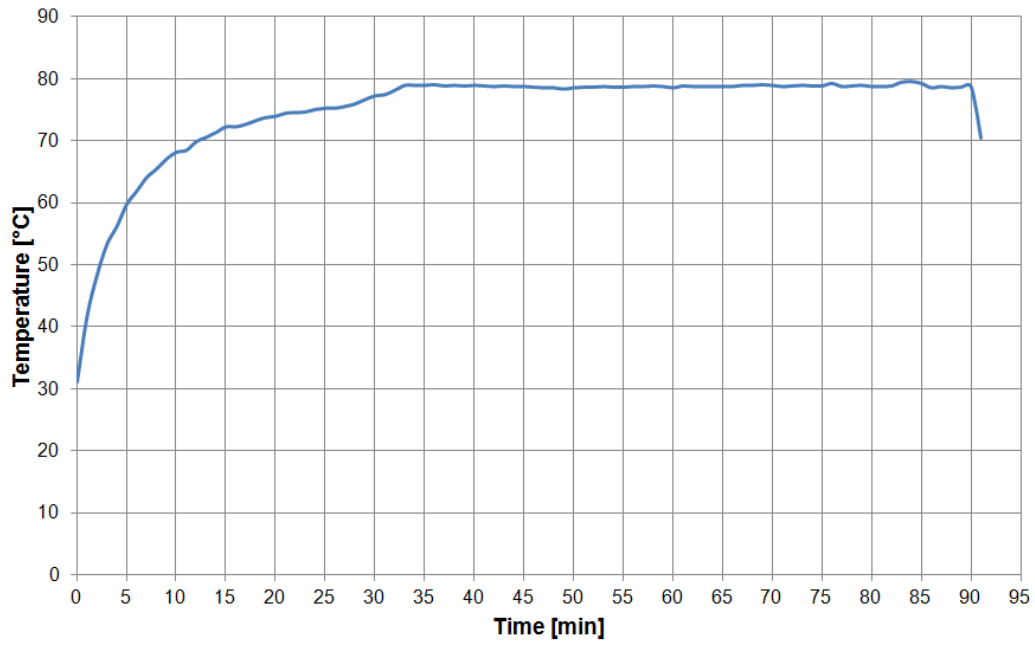
Figure A-3: Stabilisaton heat treatment curve for AW-7021 (80°C / 1h)
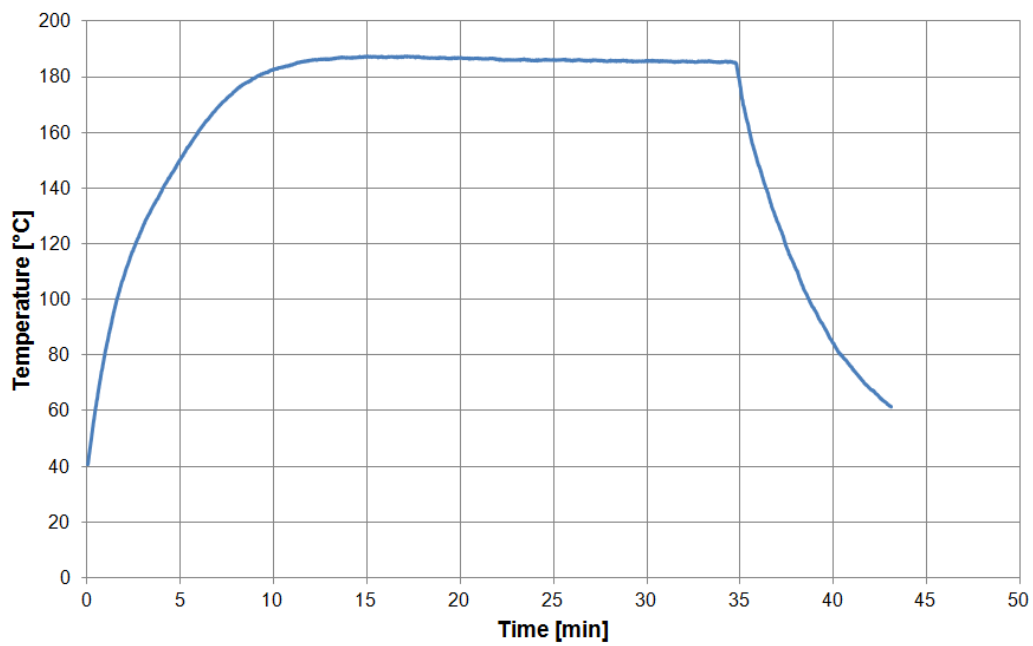
Figure A-4: Paint bake heat treatment (1SPB) curve (185°C / 25 min)
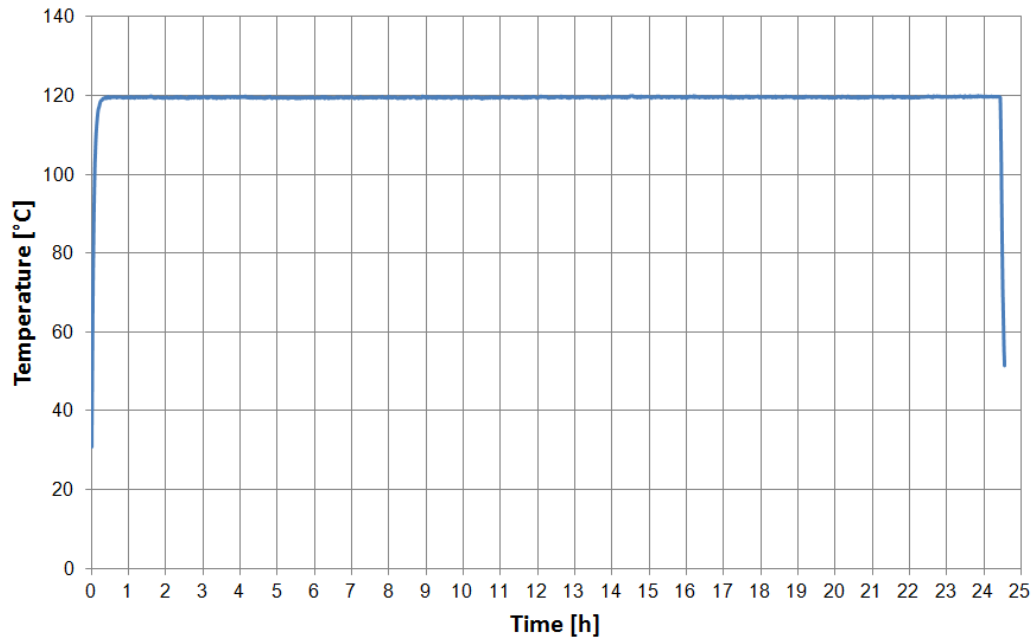
Figure A-5: *Peak ageing (PA) curve (120°C / 24h)*

Note: All heat treatments have been conducted measuring metal temperature. The tolerance margin during the holding phase was +/- 3°C.

Appendix 2: Measurement protocol for Section 5.1.3

Table A-1: Measurement protocol for tensile testing of hot forming states (AW-7021)

HF 7021 Formability		1 sec⁻¹				0.01 sec⁻¹			
		No. 1	No. 2	No. 3	**Average**	No. 1	No. 2	No. 3	**Average**
T4	$R_{p0.2}$ [MPa]	377.92	390.38	389.52	**385.94**	372.08	376.64	371.45	**373.39**
	R_m [MPa]	493.43	490.54	494.31	**492.76**	505.60	505.55	505.31	**505.49**
	ε_f [%]	18.52	18.20	17.69	**18.14**	19.32	19.86	19.82	**19.67**
140°C	$R_{p0.2}$ [MPa]	320.81	310.15	327.19	**319.38**	297.41	304.05	282.45	**294.63**
	R_m [MPa]	412.17	408.10	413.52	**411.26**	346.41	357.40	331.14	**344.98**
	ε_f [%]	12.96	11.95	12.25	**12.38**	17.15	18.05	11.17	**15.46**
240°C	$R_{p0.2}$ [MPa]	117.46	128.15	119.62	**121.74**	116.63	123.13	117.61	**119.13**
	R_m [MPa]	168.30	168.93	167.20	**168.14**	146.44	148.49	147.02	**147.32**
	ε_f [%]	30.27	31.10	30.73	**30.70**	34.59	33.51	34.11	**34.07**
340°C	$R_{p0.2}$ [MPa]	84.59	85.30	89.77	**86.55**	57.60	57.82	55.60	**57.01**
	R_m [MPa]	102.32	101.78	102.02	**102.04**	60.25	60.54	60.53	**60.44**
	ε_f [%]	45.96	46.04	45.99	**45.99**	41.32	40.98	41.28	**41.20**
440°C	$R_{p0.2}$ [MPa]	52.79	51.29	52.10	**52.06**	17.37	18.52	18.89	**18.26**
	R_m [MPa]	55.70	55.70	56.13	**55.84**	21.98	22.02	22.17	**22.06**
	ε_f [%]	66.73	67.16	66.81	**66.90**	64.77	62.60	62.97	**63.45**

Table A-2: *Measurement protocol for tensile testing of hot forming states (AW-7075)*

HF 7075 Formability		1 sec^{-1}				0.01 sec^{-1}			
		No. 1	No. 2	No. 3	Average	No. 1	No. 2	No. 3	Average
T6	$R_{p0.2}$ [MPa]	523.53	526.24	524.84	**524.87**	526.29	526.19	501.07	**526.24**
	R_m [MPa]	572.05	573.94	575.90	**573.97**	583.42	584.72	584.18	**584.11**
	ε_f [%]	10.05	9.72	9.75	**9.84**	13.91	13.96	14.10	**13.99**
120°C	$R_{p0.2}$ [MPa]	484.46	475.88	482.72	**481.02**	473.28	452.39	463.61	**463.09**
	R_m [MPa]	529.56	527.48	524.52	**527.19**	509.91	506.60	503.99	**506.83**
	ε_f [%]	12.05	11.39	10.85	**11.43**	14.08	13.29	13.35	**13.57**
220°C	$R_{p0.2}$ [MPa]	342.76	344.21	346.00	**344.32**	296.68	296.34	297.77	**296.93**
	R_m [MPa]	370.81	367.67	368.43	**368.97**	308.69	305.73	306.12	**306.85**
	ε_f [%]	17.40	17.88	17.66	**17.65**	20.93	25.50	25.30	**23.91**
320°C	$R_{p0.2}$ [MPa]	169.48	171.68	170.38	**170.51**	112.64	118.12	113.62	**114.79**
	R_m [MPa]	174.72	175.27	176.98	**175.66**	117.19	120.22	119.00	**118.80**
	ε_f [%]	28.65	28.08	29.13	**28.62**	33.79	33.49	32.48	**33.25**
420°C	$R_{p0.2}$ [MPa]	83.80	81.43	81.94	**82.39**	30.49	26.92	26.88	**28.09**
	R_m [MPa]	86.90	86.79	85.63	**86.44**	37.19	35.52	35.14	**35.95**
	ε_f [%]	67.39	67.91	68.68	**67.99**	68.64	81.52	77.37	**75.84**

Table A-3: *Measurement protocol for tensile testing of W-temper forming states (AW-7021)*

WTF 7021 Formability		1 sec⁻¹				0.01 sec⁻¹			
		No. 1	No. 2	No. 3	**Average**	No. 1	No. 2	No. 3	**Average**
T4	$R_{p0.2}$ [MPa]	377.92	390.38	389.52	**385.94**	372.08	376.64	371.45	**373.39**
	R_m [MPa]	493.43	490.54	494.31	**492.76**	505.60	505.55	505.31	**505.49**
	ε_f [%]	18.52	18.20	17.69	**18.14**	19.32	19.86	19.82	**19.67**
W	$R_{p0.2}$ [MPa]	113.22	115.63	113.69	**114.18**	114.31	113.07	113.13	**113.50**
	R_m [MPa]	230.97	232.09	232.66	**231.91**	261.07	257.76	256.61	**258.48**
	ε_f [%]	30.89	31.33	33.19	**31.80**	34.03	34.30	32.67	**33.67**
W & 1d na	$R_{p0.2}$ [MPa]	242.03	244.01	238.14	**241.39**	238.94	240.26	237.66	**238.95**
	R_m [MPa]	380.44	381.41	380.58	**380.81**	396.27	393.82	395.42	**395.17**
	ε_f [%]	24.11	23.65	23.52	**23.76**	24.87	23.60	25.60	**24.69**

Table A-4: *Measurement protocol for tensile testing of W-temper forming states (AW-7075)*

WTF 7075 Formability		1 sec⁻¹				0.01 sec⁻¹			
		No. 1	No. 2	No. 3	**Average**	No. 1	No. 2	No. 3	**Average**
T6	$R_{p0.2}$ [MPa]	523.53	526.24	524.84	**524.87**	526.29	526.19	501.07	**526.24**
	R_m [MPa]	572.05	573.94	575.90	**573.97**	583.42	584.72	584.18	**584.11**
	ε_f [%]	10.05	9.72	9.75	**9.84**	13.91	13.96	14.10	**13.99**
W	$R_{p0.2}$ [MPa]	191.09	186.47	191.82	**189.79**	190.38	191.42	193.51	**191.77**
	R_m [MPa]	349.93	352.23	353.47	**351.87**	387.08	385.36	385.98	**386.14**
	ε_f [%]	24.05	24.10	24.21	**24.12**	26.40	26.79	26.73	**26.64**
W & 1d na	$R_{p0.2}$ [MPa]	283.98	282.12	283.47	**283.19**	281.27	285.57	282.87	**283.24**
	R_m [MPa]	454.35	453.45	453.23	**453.67**	468.50	473.50	472.07	**471.36**
	ε_f [%]	20.74	20.52	21.12	**20.79**	22.80	23.92	23.13	**23.28**

Table A-5: *Measurement protocol for tensile testing of post stabilisation forming states (AW-7021)*

PSF 7021 Formability		1 sec^{-1}				0.01 sec^{-1}			
		No. 1	No. 2	No. 3	**Average**	No. 1	No. 2	No. 3	**Average**
T4	$R_{p0.2}$ [MPa]	377.92	390.38	389.52	**385.94**	372.08	376.64	371.45	**373.39**
	R_m [MPa]	493.43	490.54	494.31	**492.76**	505.60	505.55	505.31	**505.49**
	ε_f [%]	18.52	18.20	17.69	**18.14**	19.32	19.86	19.82	**19.67**
S	$R_{p0.2}$ [MPa]	325.83	322.55	315.66	**321.35**	319.04	314.69	313.99	**315.91**
	R_m [MPa]	451.59	452.31	453.76	**452.55**	465.37	464.85	464.49	**464.91**
	ε_f [%]	21.73	21.54	21.61	**21.63**	23.10	23.13	23.02	**23.08**

Note: All samples have been taken from undeformed sheets with the longitudinal sample axis being parallel to 0° rolling direction.

Appendix 3: Measurement protocol for Section 5.2.1

Table A-6: *Measurement protocol for the assessment of post-forming natural ageing behaviour through hardness testing*

HF 7021 – Natural ageing behaviour					
Natural ageing state		No.1 [HBW 2.5/62.5]	No.2 [HBW 2.5/62.5]	No.3 [HBW 2.5/62.5]	**Average [HBW 2.5/62.5]**
1 h	60 min	85	88	89	**87**
4 h	240 min	95	97	97	**96**
1 d	1440 min	114	114	114	**114**
7 d	10080 min	123	123	123	**123**
14 d	20160 min	127	126	127	**127**
21 d	30240 min	127	127	129	**128**
HF-S 7021 – Natural ageing behaviour					
Natural ageing state		No.1 [HBW 2.5/62.5]	No.2 [HBW 2.5/62.5]	No.3 [HBW 2.5/62.5]	**Average [HBW 2.5/62.5]**
1 h	60 min	124	123	124	**124**
4 h	240 min	124	123	124	**124**
1 d	1440 min	126	123	126	**125**
7 d	10080 min	128	127	128	**128**
14 d	20160 min	129	131	127	**129**
21 d	30240 min	126	125	128	**126**
WTF 7021 – Natural ageing behaviour					
Natural ageing state		No.1 [HBW 2.5/62.5]	No.2 [HBW 2.5/62.5]	No.3 [HBW 2.5/62.5]	**Average [HBW 2.5/62.5]**
1 h	60 min	88	84	84	**85**
4 h	240 min	100	102	104	**102**
1 d	1440 min	118	115	117	**117**
7 d	10080 min	130	130	127	**129**
14 d	20160 min	132	135	135	**134**
21 d	30240 min	135	136	139	**137**

PSF 7021 – Natural ageing behaviour				
Natural ageing state		No.1 [HBW 2.5/62.5]	No.2 [HBW 2.5/62.5]	No.3 [HBW 2.5/62.5]	Average [HBW 2.5/62.5]
1 h	60 min	134	134	138	**135**
4 h	240 min	134	134	138	**135**
1 d	1440 min	134	135	141	**137**
7 d	10080 min	138	137	141	**139**
14 d	20160 min	141	143	144	**143**
21 d	30240 min	143	140	139	**141**

HF 7075 – Natural ageing behaviour				
Natural ageing state		No.1 [HBW 2.5/62.5]	No.2 [HBW 2.5/62.5]	No.3 [HBW 2.5/62.5]	Average [HBW 2.5/62.5]
1 h	60 min	116	116	116	**116**
4 h	240 min	125	123	124	**124**
1 d	1440 min	138	141	138	**139**
7 d	10080 min	147	148	144	**146**
14 d	20160 min	149	148	148	**148**
21 d	30240 min	155	154	152	**154**

WTF 7075 – Natural ageing behaviour				
Natural ageing state		No.1 [HBW 2.5/62.5]	No.2 [HBW 2.5/62.5]	No.3 [HBW 2.5/62.5]	Average [HBW 2.5/62.5]
1 h	60 min	125	123	122	**123**
4 h	240 min	135	135	135	**135**
1 d	1440 min	153	156	156	**155**
7 d	10080 min	159	158	156	**158**
14 d	20160 min	158	159	160	**159**
21 d	30240 min	159	160	161	**160**

7021 W – Natural ageing behaviour				
Natural ageing state		No.1 [HBW 2.5/62.5]	No.2 [HBW 2.5/62.5]	No.3 [HBW 2.5/62.5]	**Average [HBW 2.5/62.5]**
1 h	60 min	81	82	81	**81**
4 h	240 min	88	88	89	**88**
1 d	1440 min	101	103	102	**102**
7 d	10080 min	116	119	118	**118**
14 d	20160 min	122	122	123	**122**
21 d	30240 min	124	123	125	**124**
7021 S (80°C / 1h) – Natural ageing behaviour				
Natural ageing state		No.1 [HBW 2.5/62.5]	No.2 [HBW 2.5/62.5]	No.3 [HBW 2.5/62.5]	**Average [HBW 2.5/62.5]**
1 h	60 min	114	114	114	**114**
4 h	240 min	106	109	108	**108**
1 d	1440 min	107	109	110	**109**
7 d	10080 min	115	115	115	**115**
14 d	20160 min	119	118	120	**119**
21 d	30240 min	119	119	120	**119**
7075 W– Natural ageing behaviour				
Natural ageing state		No.1 [HBW 2.5/62.5]	No.2 [HBW 2.5/62.5]	No.3 [HBW 2.5/62.5]	**Average [HBW 2.5/62.5]**
1 h	60 min	101	102	100	**101**
4 h	240 min	112	112	112	**112**
1 d	1440 min	125	128	126	**126**
7 d	10080 min	139	141	140	**140**
14 d	20160 min	144	144	141	**143**
21 d	30240 min	142	143	143	**143**

Note: Samples for HF 7021, HF-S 7021, WTF 7021, PSF 7021, HF 7075 and WTF 7075 have been taken from the side-wall section of heat treated and formed parts. Samples for 7021 W, 7021 S and 7075 W have been taken from heat treated and undeformed sheets.

Table A-7: *Measurement protocol for the assessment of post-forming artificial ageing behaviour through hardness testing*

HF 7021 – Artificial ageing behaviour			
Artificial ageing state	No.1 [HBW 2.5/62.5]	No.2 [HBW 2.5/62.5]	No.3 [HBW 2.5/62.5]	**Average [HBW 2.5/62.5]**
1 SPB	150	152	153	**152**
PA	168	167	165	**167**
WTF 7021 – Artificial ageing behaviour			
Artificial ageing state	No.1 [HBW 2.5/62.5]	No.2 [HBW 2.5/62.5]	No.3 [HBW 2.5/62.5]	**Average [HBW 2.5/62.5]**
1 SPB	155	156	154	**155**
PA	171	173	171	**172**
HF-S 7021 – Artificial ageing behaviour			
Artificial ageing state	No.1 [HBW 2.5/62.5]	No.2 [HBW 2.5/62.5]	No.3 [HBW 2.5/62.5]	**Average [HBW 2.5/62.5]**
1 SPB	155	153	153	**154**
PA	168	170	171	**170**
PSF 7021 – Artificial ageing behaviour			
Artificial ageing state	No.1 [HBW 2.5/62.5]	No.2 [HBW 2.5/62.5]	No.3 [HBW 2.5/62.5]	**Average [HBW 2.5/62.5]**
1 SPB	157	154	157	**156**
PA	176	174	179	**176**
HF 7021 – Artificial ageing behaviour			
Artificial ageing state	No.1 [HBW 2.5/62.5]	No.2 [HBW 2.5/62.5]	No.3 [HBW 2.5/62.5]	**Average [HBW 2.5/62.5]**
1 SPB	160	163	165	**163**
PA	179	177	182	**179**
WTF 7021 – Artificial ageing behaviour			
Artificial ageing state	No.1 [HBW 2.5/62.5]	No.2 [HBW 2.5/62.5]	No.3 [HBW 2.5/62.5]	**Average [HBW 2.5/62.5]**
1 SPB	166	164	165	**165**
PA	185	185	185	**185**

Note: Samples for HF 7021, HF-S 7021, WTF 7021, PSF 7021, HF 7075 and WTF 7075 have been taken from the side-wall section of heat treated and formed parts.

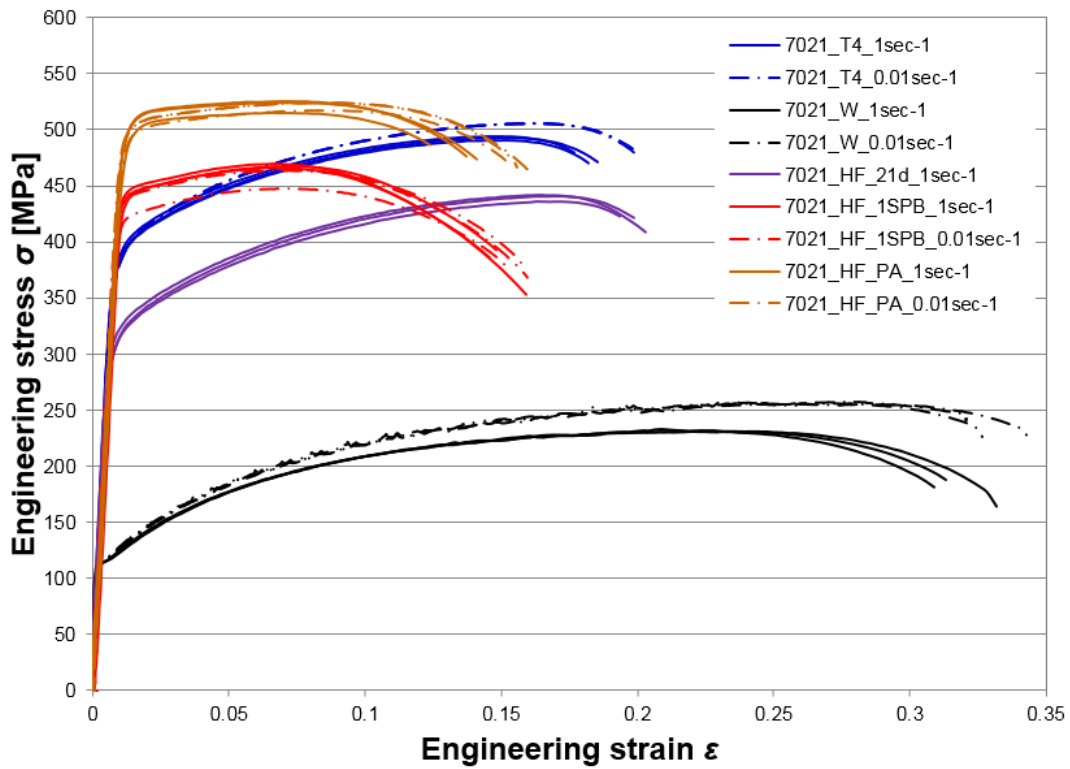## **Appendix 4:** Measurement protocol for Section 5.2.4

Figure A-6: Post-forming tensile testing curves of HF 7021

HF 7021 **Post-forming material properties**		**1 sec⁻¹**				**0.01 sec⁻¹**			
		No. 1	No. 2	No. 3	**Average**	No. 1	No. 2	No. 3	**Average**
21 d	$R_{p0.2}$ [MPa]	305.36	307.71	313.90	**308.99**				
	R_m [MPa]	435.74	441.20	442.05	**439.67**				
	ε_f [%]	19.37	19.86	20.32	**19.85**				
1SPB	$R_{p0.2}$ [MPa]	447.11	424.12	440.35	**437.20**	433.30	436.35	413.48	**427.71**
	R_m [MPa]	467.28	466.16	469.62	**467.69**	464.20	465.13	447.57	**458.97**
	ε_f [%]	14.81	14.60	15.91	**15.10**	15.73	15.98	15.23	**15.64**
PA	$R_{p0.2}$ [MPa]	482.58	498.30	503.49	**494.79**	486.26	489.35	475.59	**483.73**
	R_m [MPa]	515.51	524.76	524.96	**521.74**	517.65	524.59	524.04	**522.10**
	ε_f [%]	12.41	14.08	13.72	**13.40**	15.17	16.10	15.56	**15.61**

Table A-8: Measurement protocol for post-forming tensile testing of HF 7021
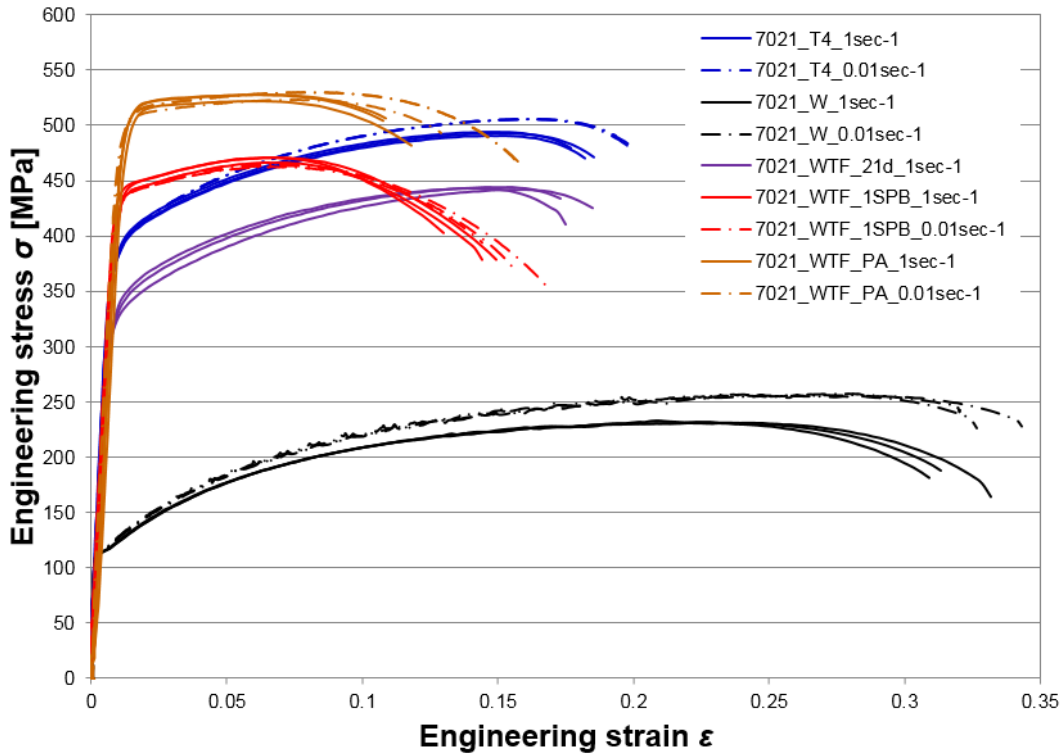
Figure A-7: *Post-forming tensile testing curves of WTF 7021*

WTF 7021 Post-forming material properties		1 sec^{-1}				0.01 sec^{-1}			
		No. 1	No. 2	No. 3	**Average**	No. 1	No. 2	No. 3	**Average**
21 d	$R_{p0.2}$ [MPa]	313.87	325.50	318.07	**319.15**				
	R_m [MPa]	442.19	442.46	444.61	**443.09**				
	ε_f [%]	18.50	17.50	17.32	**17.77**				
1SPB	$R_{p0.2}$ [MPa]	416.72	426.92	437.31	**426.98**	429.70	421.42	434.59	**428.57**
	R_m [MPa]	465.86	470.71	471.30	**469.29**	463.21	464.46	464.79	**464.15**
	ε_f [%]	14.42	13.01	14.93	**14.12**	14.92	16.90	15.50	**15.77**
PA	$R_{p0.2}$ [MPa]	462.71	491.05	485.11	**479.62**	487.63	463.66	472.79	**474.69**
	R_m [MPa]	521.50	527.95	527.76	**525.74**	523.34	530.22	530.04	**527.87**
	ε_f [%]	11.79	10.75	10.85	**11.13**	12.89	15.83	15.58	**14.77**

Table A-9: *Measurement protocol for post-forming tensile testing of WTF 7021*
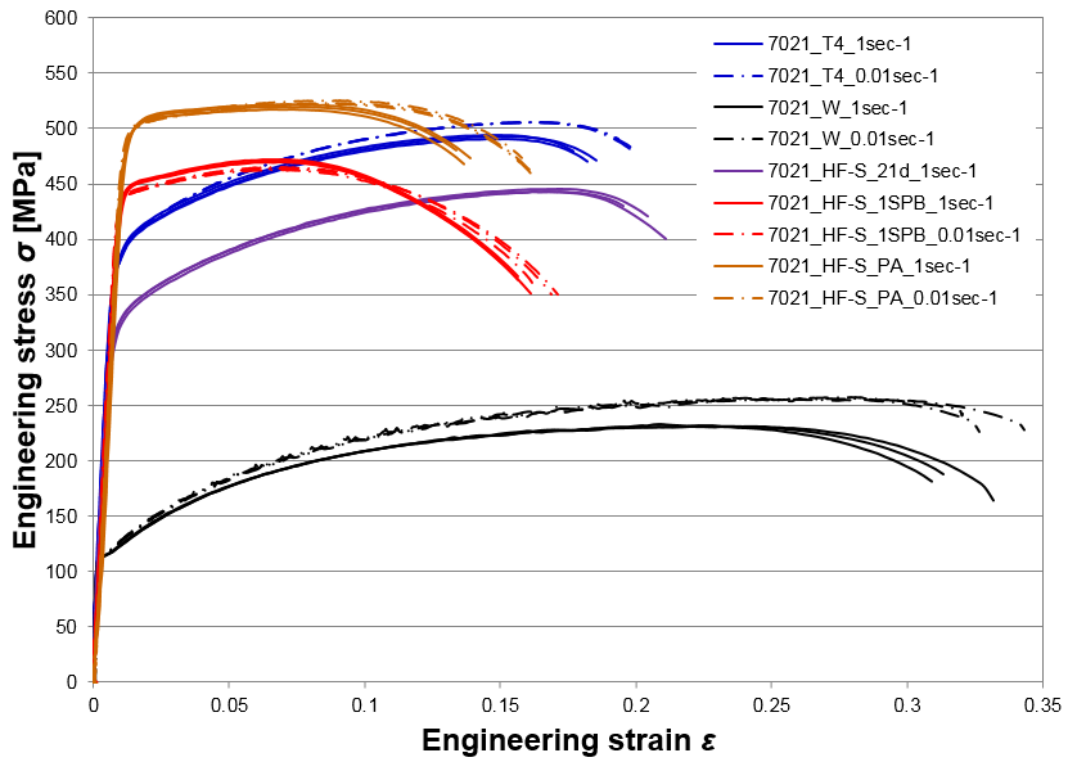
Figure A-8: *Post-forming tensile testing curves of HF-S 7021*

HF-S 7021 Post-forming material properties		1 sec⁻¹				0.01 sec⁻¹			
		No. 1	No. 2	No. 3	**Average**	No. 1	No. 2	No. 3	**Average**
21 d	$R_{p0.2}$ [MPa]	322.77	322.66	321.92	**322.45**				
	R_m [MPa]	443.09	443.36	445.12	**443.86**				
	ε_f [%]	21.12	19.51	20.45	**20.36**				
1SPB	$R_{p0.2}$ [MPa]	429.33	439.09	457.50	**441.97**	431.54	433.18	437.97	**434.23**
	R_m [MPa]	471.05	469.24	472.48	**470.92**	463.77	462.85	465.61	**464.08**
	ε_f [%]	15.65	16.11	15.78	**15.84**	17.09	16.15	16.87	**16.70**
PA	$R_{p0.2}$ [MPa]	479.92	495.71	484.00	**486.54**	477.50	481.96	484.09	**481.18**
	R_m [MPa]	516.89	521.59	520.02	**519.50**	523.17	526.04	521.62	**523.61**
	ε_f [%]	13.65	13.90	13.38	**13.64**	16.17	15.77	16.13	**16.03**

Table A-10: *Measurement protocol for post-forming tensile testing of HF-S 7021*
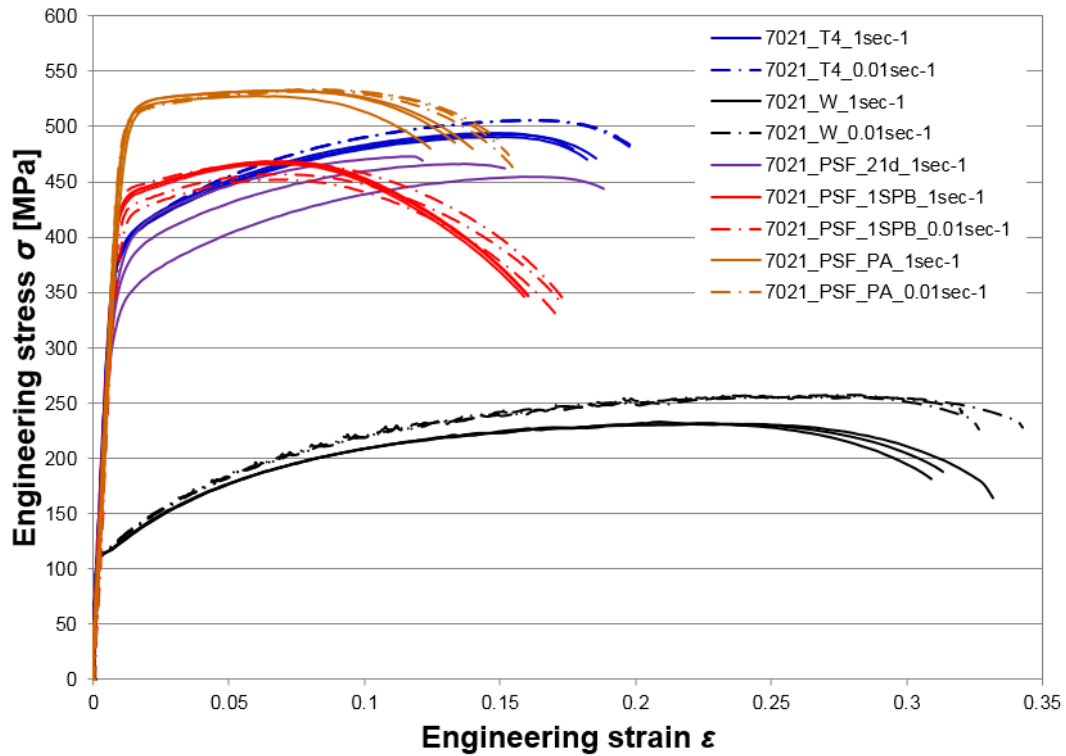
Figure A-9: *Post-forming tensile testing curves of PSF 7021*

PSF 7021 Post-forming material properties		1 sec⁻¹				0.01 sec⁻¹			
		No. 1	No. 2	No. 3	Average	No. 1	No. 2	No. 3	Average
21 d	$R_{p0.2}$ [MPa]	370.08	321.15	360.81	**350.68**				
	R_m [MPa]	472.54	454.37	466.87	**464.59**				
	ε_f [%]	12.13	18.81	15.16	**15.36**				
1SPB	$R_{p0.2}$ [MPa]	431.84	428.71	432.43	**430.99**	354.84	406.06	426.27	**416.16**
	R_m [MPa]	469.00	469.08	466.99	**468.35**	452.12	457.49	467.17	**462.33**
	ε_f [%]	15.49	16.02	16.02	**15.84**	17.11	17.16	17.36	**17.26**
PA	$R_{p0.2}$ [MPa]	493.41	491.11	486.56	**490.36**	474.34	461.82	496.24	**477.47**
	R_m [MPa]	532.41	532.98	528.22	**531.20**	532.52	532.58	533.89	**533.00**
	ε_f [%]	13.34	13.99	12.43	**13.25**	15.02	15.47	15.31	**15.27**

Table A-11: *Measurement protocol for post-forming tensile testing of PSF 7021*
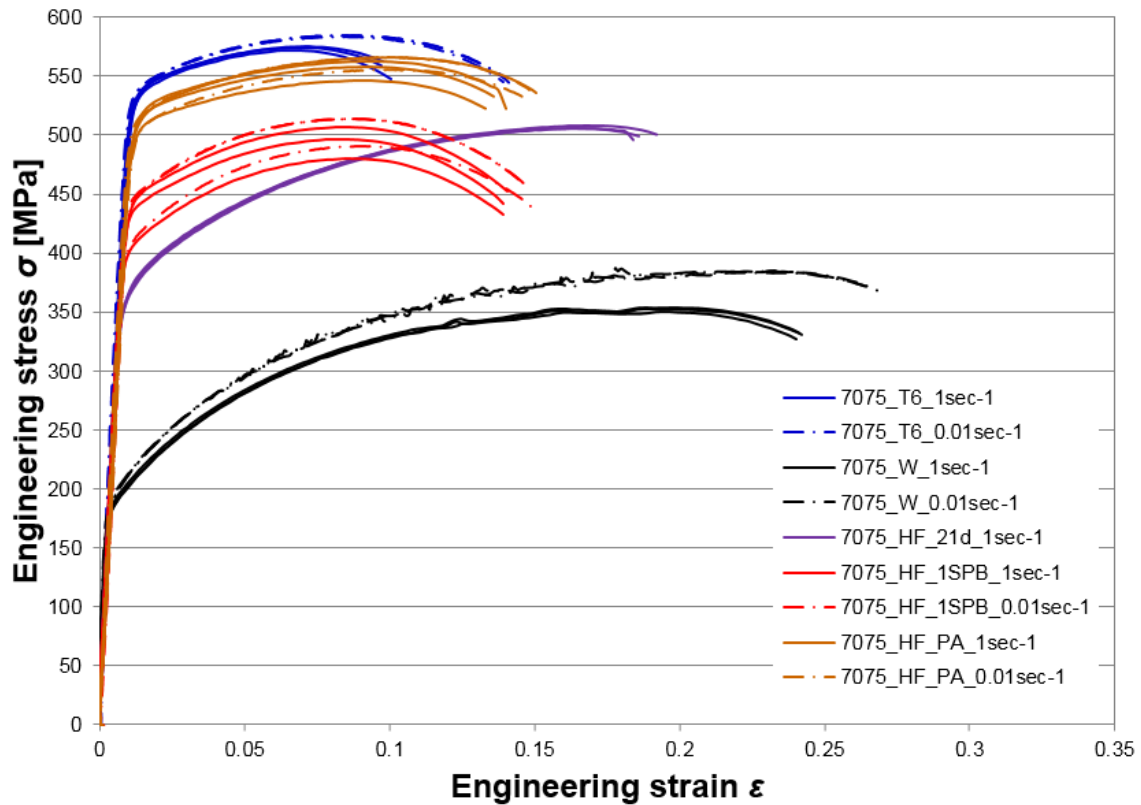
Figure A-10: *Post-forming tensile testing curves of HF 7075*

HF 7075 Post-forming material properties		1 sec⁻¹				0.01 sec⁻¹			
		No. 1	No. 2	No. 3	**Average**	No. 1	No. 2	No. 3	**Average**
21 d	$R_{p0.2}$ [MPa]	359.47	362.26	362.87	**361.53**				
	R_m [MPa]	506.23	508.37	506.20	**506.93**				
	ε_f [%]	18.43	19.23	18.58	**18.75**				
1SPB	$R_{p0.2}$ [MPa]	435.80	395.82	424.36	**418.66**	442.44	402.41	436.85	**427.23**
	R_m [MPa]	496.09	479.91	507.34	**494.45**	514.26	491.07	513.46	**506.26**
	ε_f [%]	13.92	13.90	14.08	**13.97**	14.64	14.89	14.42	**14.65**
PA	$R_{p0.2}$ [MPa]	506.83	494.02	485.84	**495.56**	500.96	493.01	510.95	**501.64**
	R_m [MPa]	562.32	557.52	546.50	**555.45**	555.85	565.99	565.72	**562.52**
	ε_f [%]	14.01	13.57	13.31	**13.63**	14.66	14.79	15.07	**14.84**

Table A-12: *Measurement protocol for post-forming tensile testing of HF 7075*
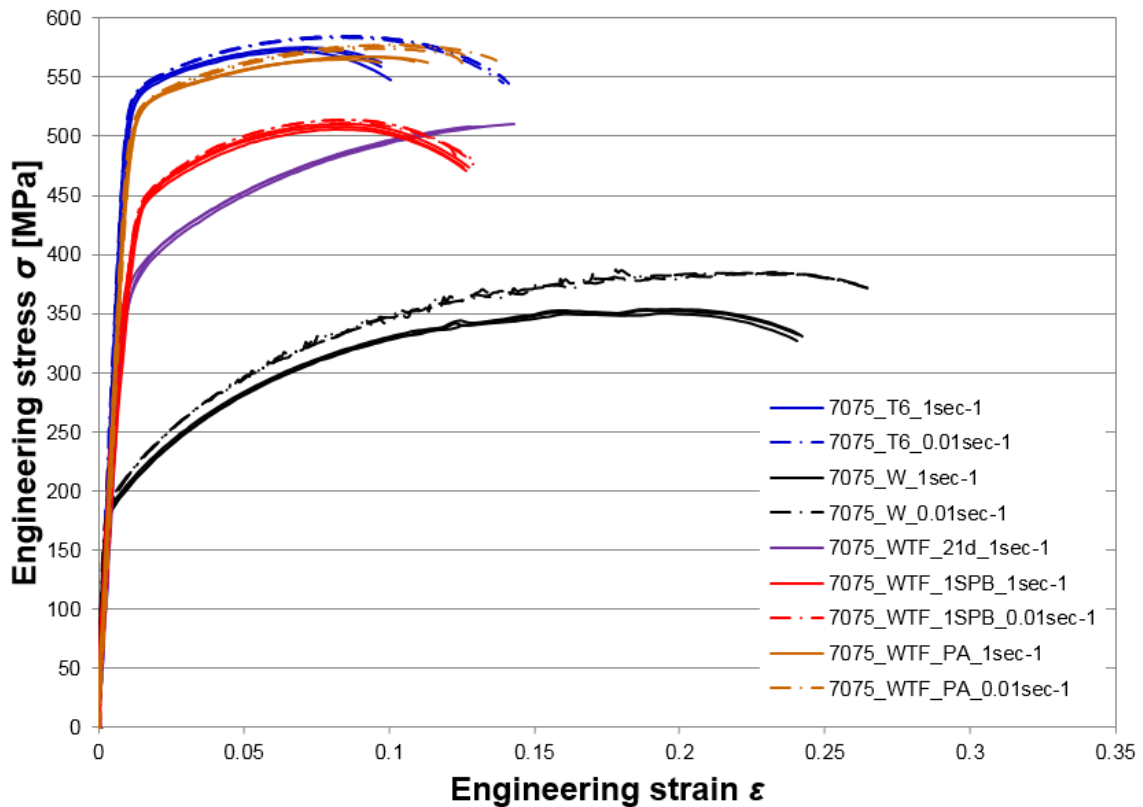
Figure A-11: *Post-forming tensile testing curves of WTF 7075*

WTF 7075 Post-forming material properties		1 sec⁻¹				0.01 sec⁻¹			
		No. 1	No. 2	No. 3	**Average**	No. 1	No. 2	No. 3	**Average**
21 d	$R_{p0.2}$ [MPa]	362.69	357.04	352.87	**357.53**				
	R_m [MPa]	507.99	507.78	510.65	**508.81**				
	ε_f [%]	13.19	12.79	14.29	**13.42**				
1SPB	$R_{p0.2}$ [MPa]	415.73	415.99	410.29	**414.00**	404.11	429.64	432.11	**421.95**
	R_m [MPa]	505.39	510.21	508.31	**507.97**	513.82	514.36	512.08	**513.42**
	ε_f [%]	12.64	12.73	12.56	**12.64**	12.37	12.93	12.93	**12.74**
PA	$R_{p0.2}$ [MPa]	513.96	503.49	504.03	**507.16**	500.71	502.10	498.69	**500.50**
	R_m [MPa]	564.64	567.41	567.52	**566.52**	12.53	12.89	12.66	**12.69**
	ε_f [%]	9.70	10.88	11.35	**10.64**	574.68	574.44	576.03	**575.05**

Table A-13: *Measurement protocol for post-forming tensile testing of WTF 7075*

Note: All samples have been taken from the side-wall section of heat treated and formed parts with the longitudinal sample axis being parallel to 0° rolling direction.

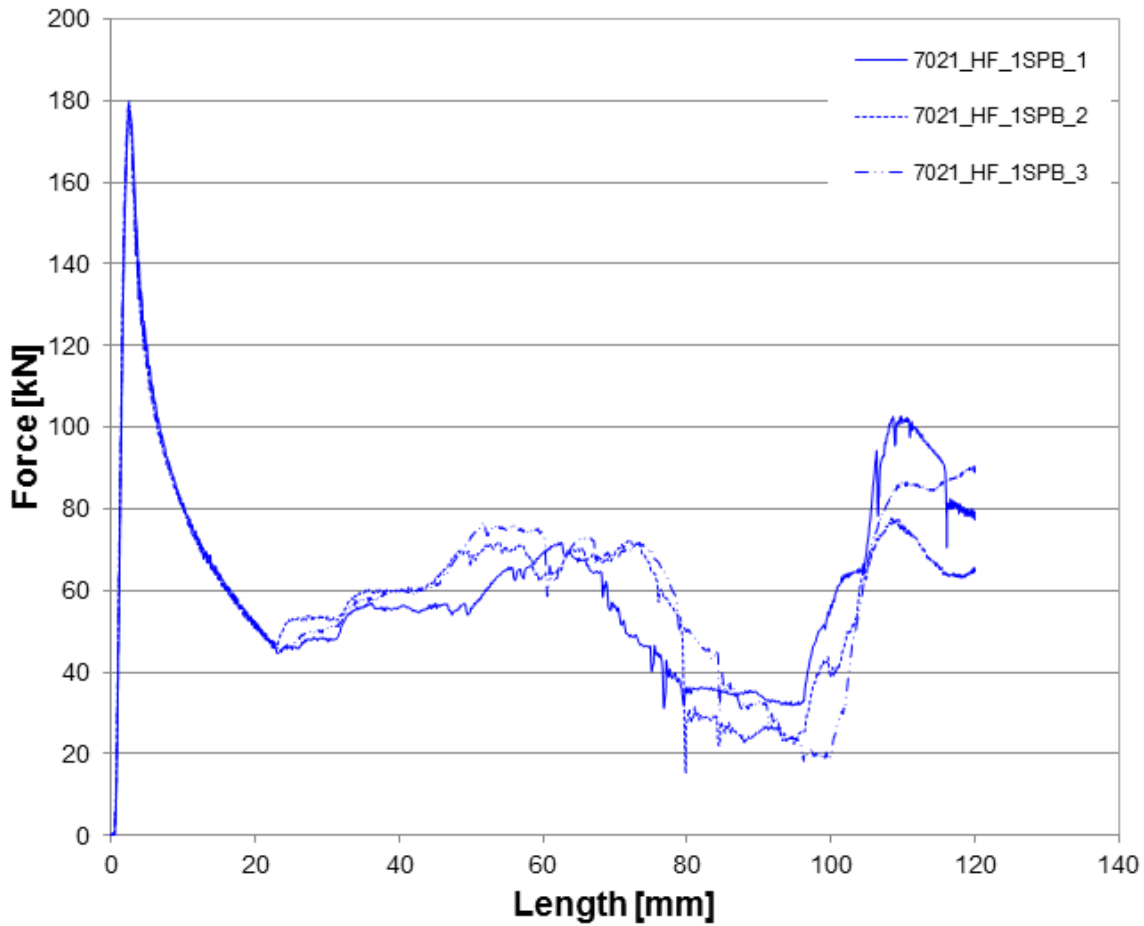## Appendix 5: Measurement protocol for Section 5.3.2

Figure A-12: *Quasi static crush testing curves of HF 7021*

HF 7021						
Sample	**m [kg]**	**TF [kN]**	**MCF [kN]**	**CFE [%]**	**EA [J]**	**SEA [J/g]**
No. 1	0.65	177.50	63.63	35.85	7415.82	11.34
No. 2	0.65	178.80	57.59	32.21	7238.38	11.10
No. 3	0.65	179.90	65.59	36.46	7561.01	11.56
Average	**0.65**	**178.73**	**62.27**	**34.84**	**7405.07**	**11.33**

Table A-14: *Measurement protocol for quasi static crush testing of HF 7021*
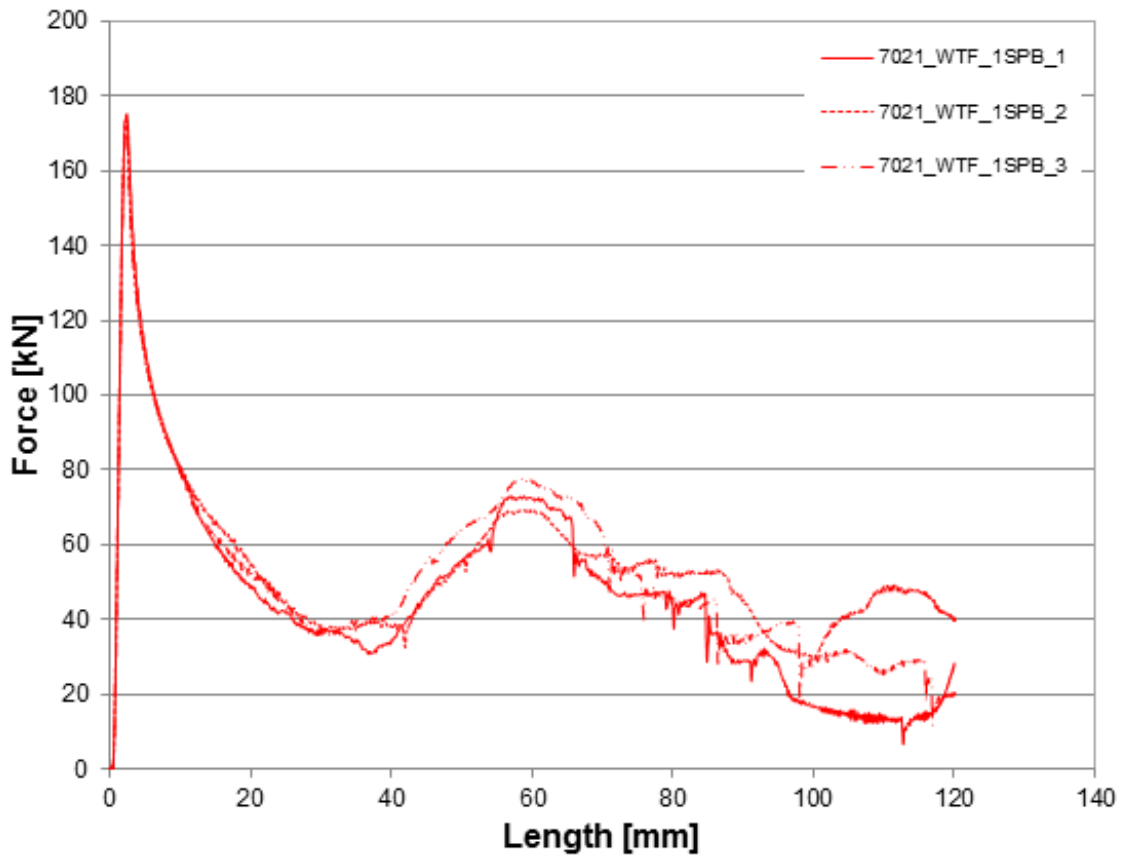
Figure A-13: *Quasi static crush testing curves of WTF 7021*

WTF 7021						
Sample	**m [kg]**	**TF [kN]**	**MCF [kN]**	**CFE [%]**	**EA [J]**	**SEA [J/g]**
No. 1	0.65	175.20	33.99	19.40	5531.38	8.54
No. 2	0.65	173.40	46.29	26.70	6466.65	9.98
No. 3	0.65	172.60	39.85	23.09	6220.90	9.63
Average	**0.65**	**173.73**	**40.04**	**23.06**	**6072.98**	**9.38**

Table A-15: *Measurement protocol for quasi static crush testing of WTF 7021*
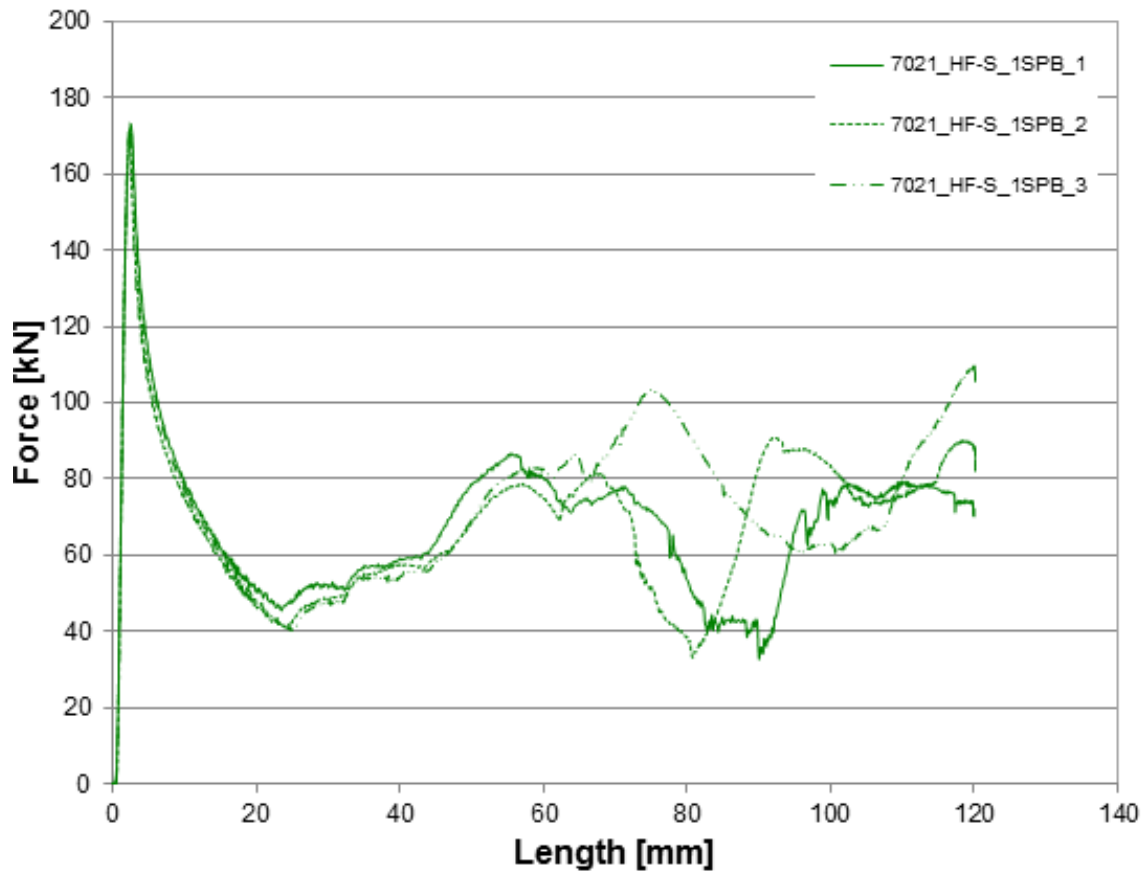
Figure A-14: *Quasi static crush testing curves of HF-S 7021*

| HF-S 7021						
Sample	**m [kg]**	**TF [kN]**	**MCF [kN]**	**CFE [%]**	**EA [J]**	**SEA [J/g]**
No. 1	0.65	173.00	67.17	38.83	8176.49	12.46
No. 2	0.65	168.90	73.12	43.29	8168.61	12.49
No. 3	0.65	173.80	80.60	46.37	8831.70	13.50
Average	**0.65**	**171.90**	**73.63**	**42.83**	**8392.27**	**12.82**

Table A-16: *Measurement protocol for quasi static crush testing of HF-S 7021*
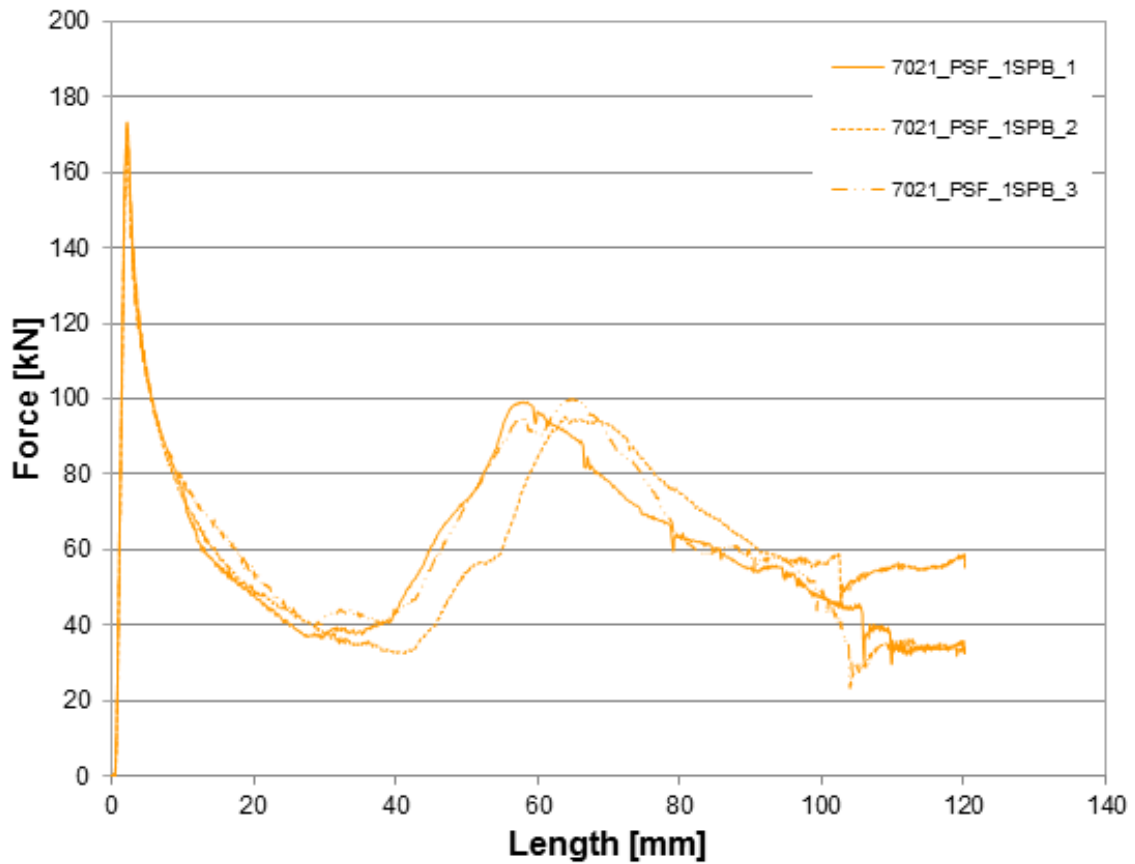
Figure A-15: *Quasi static crush testing curves of PSF 7021*

| PSF 7021						
Sample	**m [kg]**	**TF [kN]**	**MCF [kN]**	**CFE [%]**	**EA [J]**	**SEA [J/g]**
No. 1	0.65	173.30	51.27	29.59	7299.73	11.27
No. 2	0.65	166.90	58.46	35.03	7528.60	11.48
No. 3	0.65	170.30	51.65	30.33	7506.97	11.37
Average	**0.65**	**170.17**	**53.79**	**31.65**	**7445.10**	**11.37**

Table A-17: *Measurement protocol for quasi static crush testing of PSF 7021*
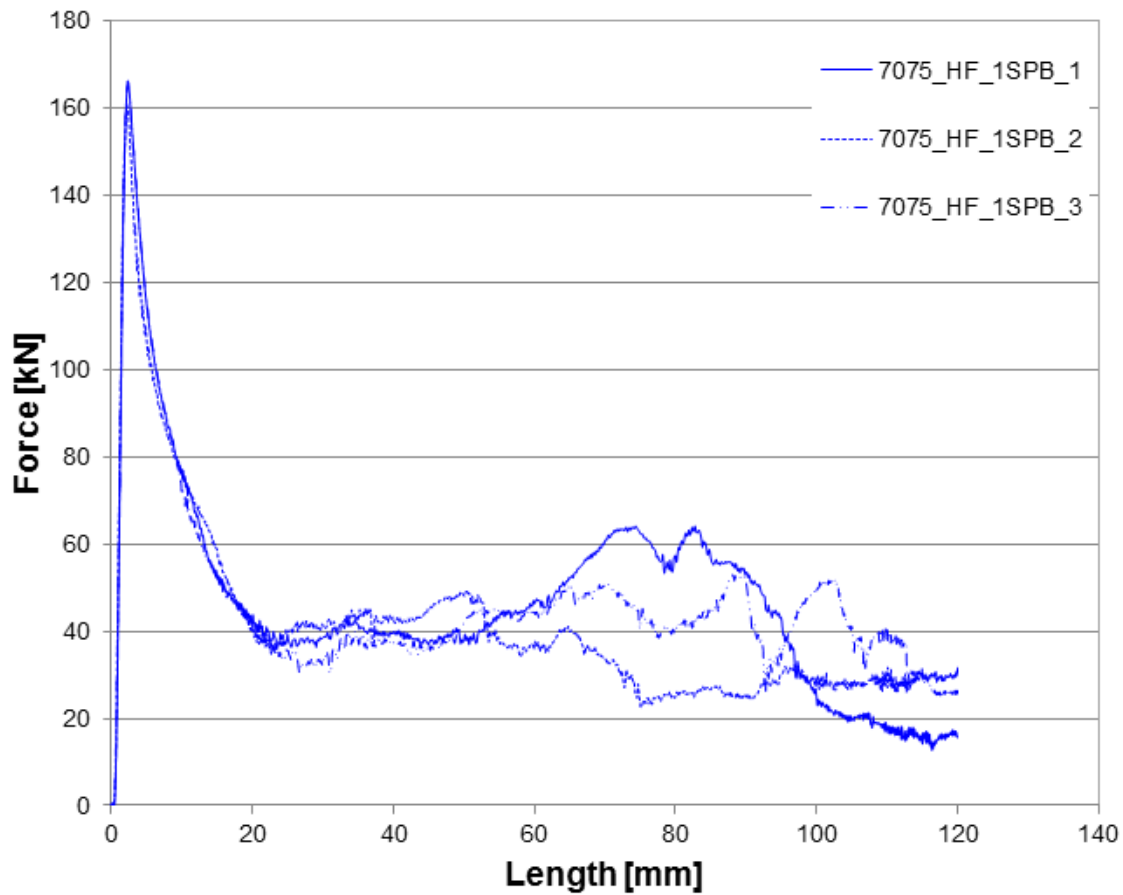
Figure A-16: *Quasi static crush testing curves of HF 7075*

HF 7075						
Sample	**m [kg]**	**TF [kN]**	**MCF [kN]**	**CFE [%]**	**EA [J]**	**SEA [J/g]**
No. 1	0.65	166.20	34.87	20.98	5631.33	8.61
No. 2	0.65	160.90	33.15	20.60	4980.80	7.64
No. 3	0.65	165.20	37.57	22.74	5585.71	8.54
Average	**0.65**	**164.10**	**35.20**	**21.44**	**5399.28**	**8.26**

Table A-18: *Measurement protocol for quasi static crush testing of HF 7075*
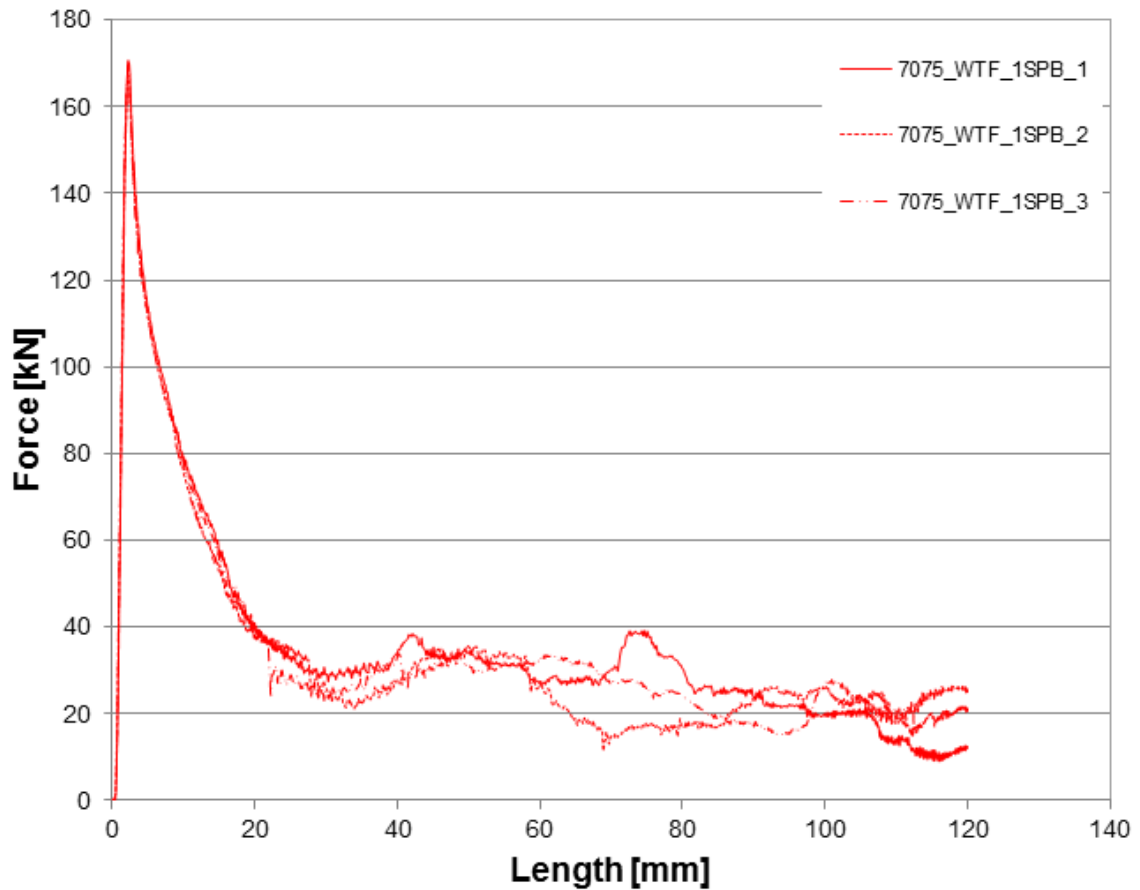
Figure A-17: *Quasi static crush testing curves of WTF 7075*

WTF 7075						
Sample	**m [kg]**	**TF [kN]**	**MCF [kN]**	**CFE [%]**	**EA [J]**	**SEA [J/g]**
No. 1	0.65	170.70	23.51	13.77	4288.51	6.15
No. 2	0.65	167.20	23.67	14.16	3983.18	6.47
No. 3	0.65	169.70	25.58	15.08	4178.66	6.01
Average	**0.65**	**169.20**	**24.25**	**14.34**	**4150.12**	**6.21**

Table A-19: *Measurement protocol for quasi static crush testing of WTF 7075*